UNIVERSITÀ
POLITECNICA
DELLE MARCHE

Facoltà di Ingegneria
Corso di Laurea in Ingegneria Meccanica

Development of mathematical models for pressure drop calculation in Gas Turbine intake systems

Sviluppo di modelli matematici per il calcolo delle perdite di carico nei sistemi di aspirazione di Turbine a Gas

Candidate:
Stefano Gargiulo

Advisor:
Prof. Andrea Crivellini

Coadvisor:
Ing. Giacomo Calza

Academic Year 2025-2026

Università Politecnica delle Marche
Facoltà di Ingegneria
Corso di Laurea in Ingegneria Meccanica
Via Brecce Bianche – 60131 Ancona (AN), Italy

Abstract

This thesis investigates pressure drop in gas turbine intake systems. A methodology is defined to develop mathematical models capable of estimating these losses as a function of the geometric and construction features of intake components. The aim is to describe the broadest possible range of intake duct configurations that assume different sizes and geometries while they are built for Heavy Duty, Industrial or Aero-derivative Gas Turbines. The developed models are then implemented in an automated, user-friendly Excel tool. The research was carried out in cooperation with Baker Hughes – Nuovo Pignone, at the Porto Recanati office, within the "Air Duct and Ventilation" division.

The proposed methodology is based on the comparison between operational or experimental data and numerical results. The experimental data were collected from literature sources or from running turbine data, while the numerical results were generated through Computational Fluid Dynamics (CFD) simulations. The CFD analyses were performed to study typical intake duct fittings including parallel baffle silencers, transitions and elbows, both as individual components and in coupled configurations where mutual interaction is significant. The geometric and construction parameters of these components and their effect on pressure drop were investigated and the numerical data were post-processed to define predictive mathematical correlations.

The goal of this research is to avoid time-consuming CFD simulations during the early stages of the design process while still providing accurate pressure drop predictions. Indeed, the results demonstrate that only a deviation below 10% was detected between numerical and experimental data. In addition, the proposed tool significantly reduces pressure drop calculation time because no 3D models or meshing processes are required anymore.

These findings provide engineers not only with a valuable tool for the pressure losses estimation, but also with useful insights for gas turbine intake systems design. In particular, the analyses of component interaction suggest which are the most efficient and compact configurations. Future work will focus on expanding the fittings database and extending the proposed workflow to gas turbine exhaust systems.

Sommario

L'obiettivo di questa tesi è lo studio delle perdite di carico nel sistema di aspirazione di turbine a gas. A tale scopo, viene definito un metodo per sviluppare modelli matematici in grado di stimare tali perdite in funzione delle caratteristiche geometriche e costruttive dei componenti. Descrivere le perdite per un'ampia gamma di configurazioni dei sistemi di aspirazione è un aspetto di fondamentale importanza, in quanto i sistemi assumono dimensioni e forme diverse a seconda del tipo di turbina che devono servire. Infatti, le configurazioni mutano a seconda delle portate che sono diverse tra turbine Heavy Duty, Aero-derivative o Industriali. Inoltre, la tesi descrive l'implementazione dei modelli sviluppati in un tool che consiste in un foglio Excel automatizzato. Il tool permette di calcolare le perdite di carico eliminando la dipendenza da simulazioni fluidodinamiche nelle prime fasi di progetto, così da permettere un notevole risparmio in termini di tempo. L'intera ricerca è stata sviluppata in collaborazione con Baker Hughes – Nuovo Pignone, in particolare con la sede di Porto Recanati e l'ufficio di "Air Ducts and Ventilation".

Le perdite di carico nei sistemi di aspirazione delle turbomacchine sono un aspetto di fondamentale importanza. Infatti, questo è uno dei parametri che influenza l'efficienza complessiva del ciclo Brayton. I parametri fondamentali che influenzano l'efficienza sono il rapporto di compressione garantito dal compressore assiale e la temperatura di ingresso in turbina. Però, anche le perdite di carico all'ingresso della macchina hanno un'influenza non trascurabile sulla potenza meccanica in uscita. In effetti, queste perdite dal punto di vista fisico sono una conversione irreversibile di energia meccanica in termica e comportano una minore portata massica di aria disponibile per la combustione. In questa trattazione, le perdite di carico vengono modellate tramite un coefficiente adimensionale di perdita che verrà indicato con K_{loss}. In accordo con la letteratura, si definisce tale coefficiente per ognuno dei componenti facenti parte del sistema di aspirazione. Tale coefficiente, moltiplicato per la pressione dinamica in uscita da un componente, fornisce il valore della sua perdita di carico.

Per la definizione di K_{loss} sono state utilizzate simulazioni CFD parametriche. In primis sono stati studiati i disegni tecnici dei sistemi di aspirazione con il fine di individuare le geometrie ricorrenti e il range di dimensione entro il quale variano. Successivamente, sono stati sviluppati in SpaceClaim dei modelli CAD parametrici di questi componenti, sui quali sono stati definiti sia mesh che setup di simulazione opportuni. Completate le simulazioni in ANSYS Fluent, i dati sono stati processati in Octave e in Excel proprio con il fine di calcolare il coefficiente K_{loss}.

I componenti analizzati comprendono curve, convergenti e silenziatori a pannelli paralleli. Inoltre, vengono definiti sempre mediante simulazioni CFD parametriche dei coefficienti correttivi $K_{\text{interdependence}}$, utili qualora il flusso in ingresso ad un item del sistema di aspirazione non risultasse uniforme. I coefficienti correttivi servono per definire quantitativamente come peggiorano le performance aerodinamiche dei componenti. In particolare, si è studiato il modo in cui le curve, che generano forte separazione del flusso, influenzano le perdite di carico dei silenziatori posizionati dopo di esse.

Definiti i modelli matematici che esprimono K_{loss} e $K_{\text{interdependence}}$, questi ultimi sono stati implementati all'interno di un tool Excel automatizzato. Una prima validazione dei modelli viene effettuata tramite un confronto tra i risultati numerici e quelli presenti in letteratura. Nell'analisi di questi risultati si deve necessariamente tenere in considerazione il fatto che il numero di Reynolds è molto maggiore nei sistemi di aspirazione di Turbine a Gas rispetto ai dati trovati in letteratura. Una seconda validazione, sicuramente più significativa, è stata ottenuta confrontando il valore di perdita di carico ottenuto dal tool con i valori sperimentali letti da un software che monitora le turbine operative. Questo confronto mostra su diverse configurazioni un errore percentuale inferiore al 10% tra valori numerici e sperimentali, validando così il tool.

Avere uno strumento che permette di calcolare le perdite di carico, senza richiedere l'uso di simulazioni CFD, determina un elevato risparmio di tempo. Inoltre, come già discusso, questo strumento è in grado di fornire previsioni accurate in modo da semplificare le prime fasi di progettazione, e andare ad effettuare eventuali analisi fluidodinamiche solo in una fase finale. Inoltre, durante l'intera fase di sviluppo del tool sono stati raccolti dati utili per stabilire buone norme di progettazione dei sistemi, in particolare, per quanto riguarda l'interdipendenza tra i componenti. Infatti, questa mole di dati può essere usata per progettare sistemi più compatti e quindi più economici con maggiore consapevolezza.

L'approccio mostrato in questa ricerca risulta facilmente estensibile a nuovi componenti del sistema di aspirazione. Inoltre, facendo le opportune considerazioni, lo stesso procedimento può essere applicato anche ai condotti di scarico. Risulta però necessario studiare l'andamento della temperatura dei gas all'interno del sistema, perché da questo aspetto dipendono tanti parametri come la densità, la portata volumetrica e il numero di Reynolds. Infine, queste eventuali aggiunte garantirebbero la possibilità di validare i modelli su un più ampio numero di configurazioni, assicurando una maggiore robustezza statistica e una più fedele aderenza alla realtà dei modelli sviluppati.

Contents

List of Figures

List of Tables

Chapter 1

Pressure drop in gas turbine intake systems

1.1 Gas turbine power plants

A gas turbine power plant is a thermal energy conversion system designed to generate electrical power by exploiting the expansion of high-temperature gases produced through fuel combustion. It runs according to the Brayton cycle, in which ambient air is first drawn into the plant through an intake system, where it is filtered and conditioned to ensure the appropriate quality and flow characteristics. The air is then compressed to high pressure within the compressor before being directed into the combustion chamber, where it is mixed with fuel and ignited. The resulting high-temperature and high-pressure combustion gases expand through the turbine, producing mechanical work that is used to drive both the compressor and an electrical generator.

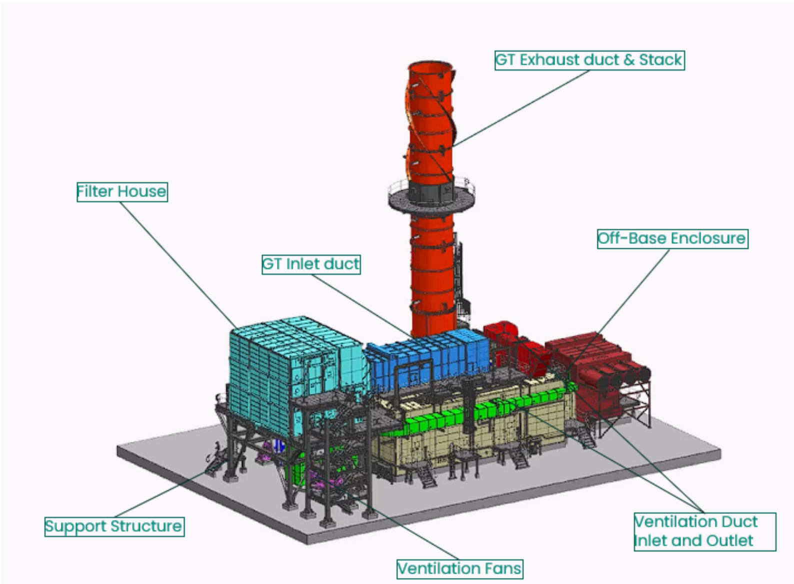

Figure 1.1: Gas turbine simple-cycle power plant. ©Copyright 2026 Baker Hughes Company. All rights reserved.

Beyond the core components, a gas turbine power plant includes several auxiliary subsystems essential for its safe and efficient operation. The air intake system ensures a continuous supply of clean air, preventing contaminants from entering the compressor, and maintaining stable operating conditions. The ventilation system plays a critical role in regulating temperature within the turbine enclosure and associated equipment compartments, removing excess heat, and preventing the accumulation of hazardous gases. In addition, the exhaust system is responsible for directing hot gases that leave the turbine safely into the atmosphere, often incorporating silencers and diffusers to reduce noise and thermal impact.

In some configurations, the exhaust system also enables heat recovery for improved overall efficiency, as in combined-cycle plants. The utilisation of gas turbine exhaust gases for steam generation or in the use of cooling or heating buildings greatly affects the overall efficiency of power plants. This is shown in the following histogram [1] that underlines the efficiencies of Simple Cycle Gas Turbine (SCGT) with firing temperatures of 1315 $^\circ$C, Recuperative Gas Turbine (RGT), the Steam Turbine Plant (ST), the Combined Cycle Power Plant (CCPP), the Advanced Combined Cycle Power Plants (ACCP) such as combined cycle power plants using Advanced Gas Turbine Cycles, and finally the Hybrid Power Plants (HPP).

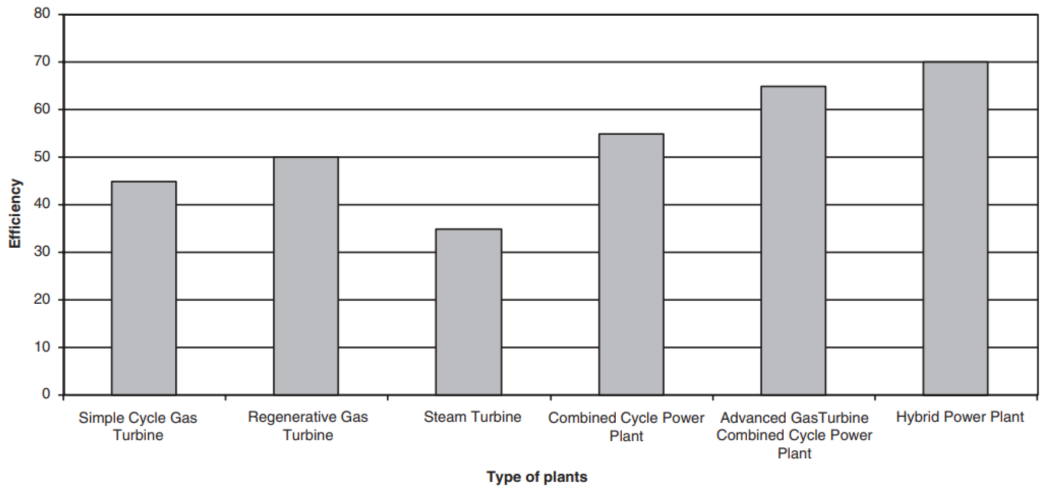

Figure 1.2: Average efficiency comparison across different plant types

In the area of performance, the steam turbine power plants have an efficiency of about 35%, as compared to combined cycle power plants, which have an efficiency of about 55%. However, it is worth noting that the increase in efficiency does not lead to a decrease in availability. Indeed, many analyses show that a 1% drop in the availability needs about a 2–3% increase in efficiency to offset that loss. Therefore, as long as natural gas or diesel fuel are available the choice of combined cycle power plants is obvious.

1.2 Parameters affecting gas turbine efficiency

In this discussion we mainly focus on some of the parameters that affects the overall efficiency of gas turbine power plants.

First, the discussed parameters are the ones that directly affects the performances of the gas turbines belonging to the following groups:

1. Frame Type Heavy-Duty Gas Turbines: the frame units are the large power generation units ranging from 3 MW to 480 MW in a simple cycle configuration, with efficiencies ranging from 30–46%.

2. Aircraft-Derivative Gas Turbines (Aero-derivative): as the name indicates, these are power generation units, which originated in the aerospace industry as the prime mover of aircraft. These units have been adapted to the electrical generation industry by removing the bypass fans and adding a power turbine at their exhaust. These units range in power from 2.5 MW to about 50 MW. The efficiencies of these units can range from 35–45%.

3. Industrial Type-Gas Turbines: these vary in range from about 2.5 MW–15 MW. This type of turbine is used extensively in many petrochemical plants for compressor drive trains. The efficiencies of these units are in the range from 30–35%.

Especially, the effect of the compressor pressure ratio and the turbine firing temperature is discussed, since their impact is determinant on the overall efficiency.

In a second moment, the effect of the auxiliary systems design on the overall efficiency is discussed [1]. In particular, pressure losses in intake and exhaust ducts and their role on the overall cycle efficiency is described, since a correct assessment of these losses is the main topic of this thesis.

1.2.1 Compressor pressure ratio and turbine firing temperature

The aerospace engines have been the leaders in most of the technology in the gas turbine. The design criteria for these engines were high reliability, high performance, with many starts and flexible operation throughout the flight envelope. The engine life of about 3500 hours between major overhauls was considered good. The aerospace engine performance has always been rated primarily on its thrust/weight ratio. Increase in engine thrust/weight ratio is achieved by the development of high-aspect ratio blades in the compressor as well as optimizing the pressure ratio and firing temperature of the turbine for maximum work output per unit flow.

The Industrial Gas Turbine has always emphasized long life, and this conservative approach has resulted in the Industrial Gas Turbine in many aspects giving up high performance for rugged operation. The Industrial Gas Turbine has been conservative in the pressure ratio and the firing temperatures. This has all changed in the 1990s, when spurred on by the introduction of the “Aero-Derivative Gas Turbine” the industrial gas turbine has dramatically improved its performance in all operational aspects. This has resulted in dramatically reducing the performance gap between these two types of gas turbines.

Figures 1.3a and 1.3b show the growth of the Pressure Ratio and Firing Temperature. The growth of both the Pressure Ratio and Firing Temperature parallel each other, as both growths are necessary to achieving the optimum thermal efficiency.

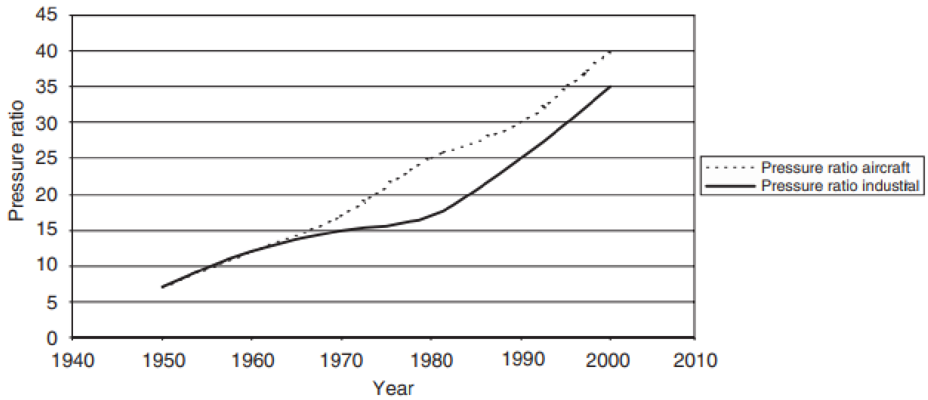

(a) Pressure ratio development through the years

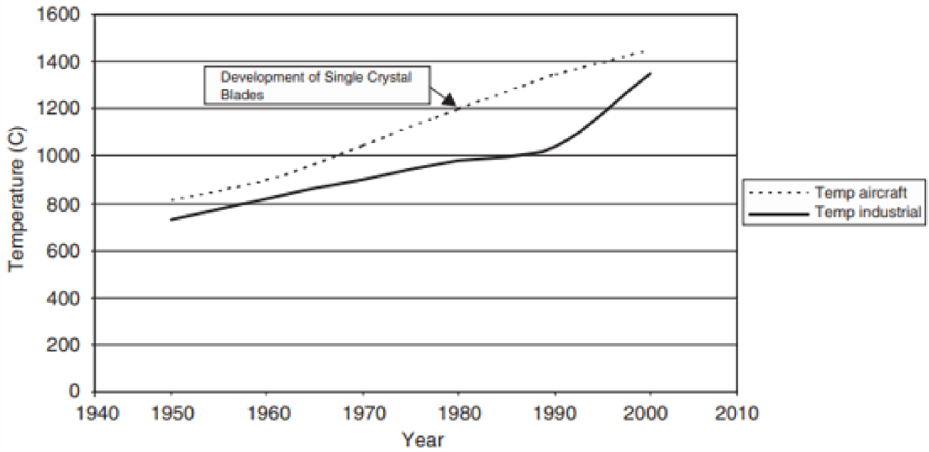

(b) Firing temperature development through the years

Figure 1.3: Evolution of key gas turbine efficiency parameters over the years

Figure 1.4 shows the effect on the overall cycle efficiency of the increasing pressure ratio and the firing temperature. The increase in the pressure ratio increases the overall efficiency at a given temperature, however increasing the pressure ratio beyond a certain value at any given firing temperature can result in lowering the overall cycle efficiency.

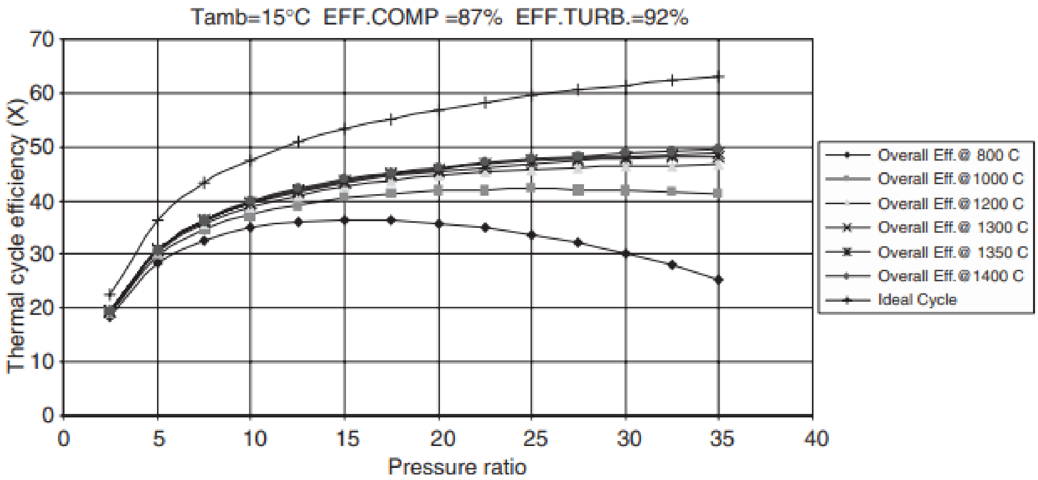

Figure 1.4: Overall thermal efficiency as a function of pressure ratio and turbine firing temperature

The limiting factor for most gas turbines has been the turbine inlet temperature. With new schemes of cooling using steam or conditioned air, and breakthroughs in blade metallurgy, higher turbine temperatures have been achieved. The new gas turbines have fired inlet temperatures as high as 1427 $\circ$C, and pressure ratios of 40:1 with efficiencies of 45% and above.

1.2.2 Pressure drop in gas turbine intake systems

This section is dedicated to the effect of intake system design on the overall efficiency of the simple-cycle power plants. Indeed, these systems need to be properly designed to guarantee many different aspects that are generally conflicting with each other. The following aspects need to be guaranteed:

- The requested filtration grade, that ensure the correct operation of the turbine and the compressor;
- The contractual noise levels;
- The contractual output shaft power and fuel consumption, therefore the contractual pressure drop value;
- The flow uniformity at the compressor inlet, that ensure the nominal fluid dynamics operation of it;
- Availability and reliability levels comparable to the other plant components;

Before clarifying how the overall cycle efficiency is affected by intake systems pressure drop is useful to briefly present the components that characterize it. In figure 1.5 there is a schematic representation of an intake arrangement:

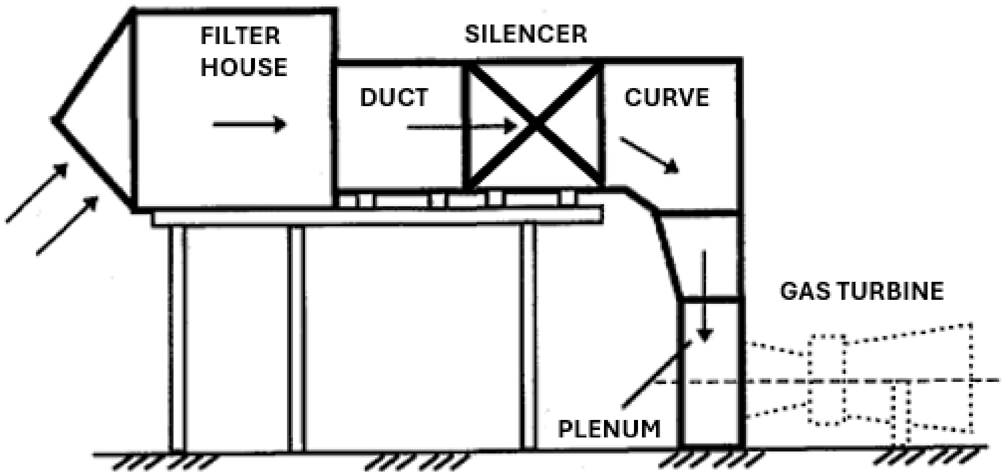

Figure 1.5: Schematic representation of gas turbine intake system

The components that constitute the intake system are:

- Filter house: is a large housing where multi-stage air filtration is performed. The cross-section area of the filter house is very high to ensure low velocities and low pressure drop inside the different filtration stage.

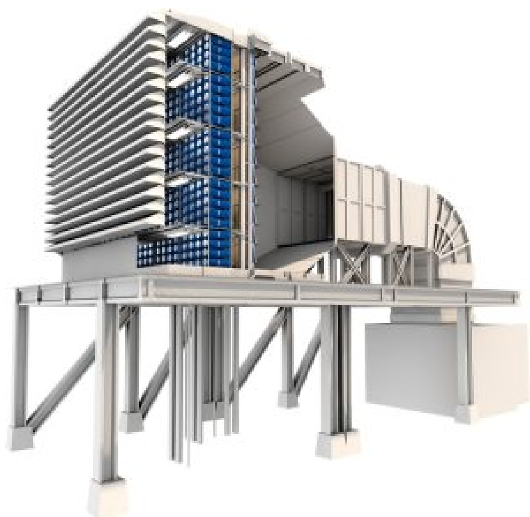

Figure 1.6: Static filter house

It is necessary to filter intake air because gas turbines and compressors must be protected wherever there are dust, heavy rain, storms, mist, and constantly high humidity. Filtered air permits to these rotatory machines to work non-stop for long periods and avoid shutdowns that can be costly, no matter how brief they are. Maximum availability and optimum efficiency don't have to be mutually exclusive – but they require an uncompromising air filtration system. Especially offshore oil and gas production facilities as well as coastal gas-fired power plants often experience challenging weather conditions.

Insufficient filtration levels could bring to damages for turbine or compressor blade such as corrosion or pitting or even foreign object damage (FOD).

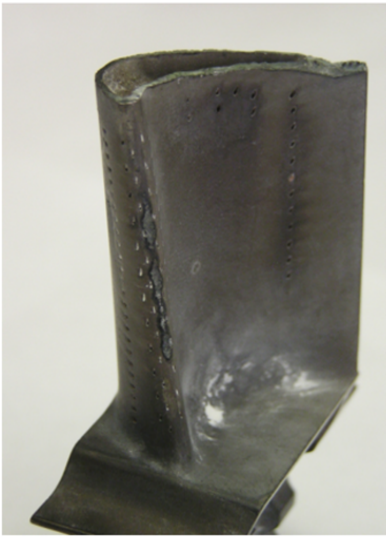

(a) Erosion of the leading edge of a gas turbine blade

(b) Foreign object damage (FOD) on a gas turbine

Figure 1.7: Examples of damages related to poor filtration grade of combustion air

- Ducts, transitions and curves: these are the components used to guide the flow from the filter house outlet to the inlet plenum. Transitions are used to reduce the gas path cross-section from that of the filter house to the one of the inlet plenum, Additionally, the flow is typically redirected from horizontal to vertical, as the filter house is usually located at an elevated position.

- Parallel baffle silencers: consist of a duct and a series of internal sound-absorbing panels, called baffles. The panels are made of are made of an outer casing in perforated sheet metal, which may be stainless steel, marine-grade aluminium, or galvanized steel, containing mats of rock wool or other sound-absorbing materials. The silencer design depends on the noise level specified in the contract, both in the near field and at the far field. It is also worth to underline that high acoustic performances imply high pressure drops, so a compromise between the acoustic and aerodynamic performances is needed.

Figure 1.8: Industrial parallel baffle silencer

- Inlet plenum: it is the final section of the intake system before the air enters the axial compressor. The geometry of the plenum is extremely important from a fluid dynamic point of view, as this component must guarantee a uniform flow at the compressor inlet to avoid surge or stall of the compressor. The materials used and the construction of the walls are entirely similar to those of the other sections of the intake system.

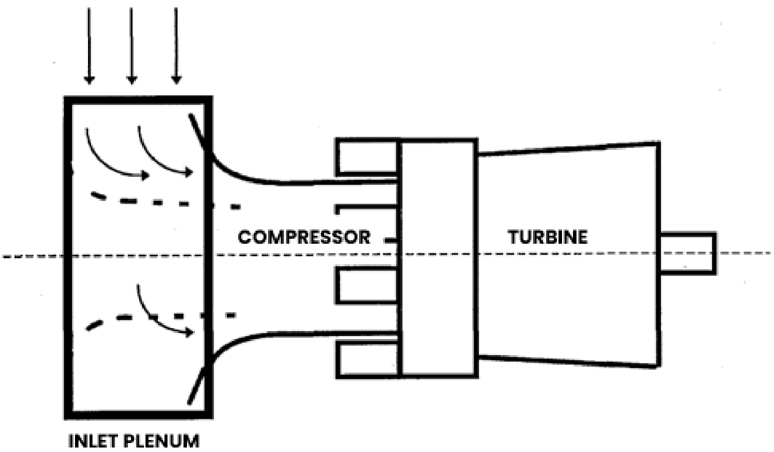

Figure 1.9: Schematic representation of the inlet plenum

Clearly while the combustion airflow passes all these components, it experiences flow separation and friction losses which reduce the total pressure and consequently the density of the combustion intake air. These pressure losses or density losses lead to a decrease in the total mass inflow in the turbine. As a consequence of a lower air mass flow, there are both a reduction of the output shaft power and an increase in specific fuel consumption.

In a similar way even exhaust pressure losses cause a drop in the overall efficiency. The exhaust system may include one or more silencers, bends, heat recovery boilers (in combined cycle or cogeneration applications), diverters, dampers, and other elements, up to the discharge to the atmosphere. As exhaust gases pass through the system, they undergo friction losses and flow separations which increase the back pressure compared to atmospheric pressure. Having a higher counter pressure at the turbine outlet implies a reduction of the expansion ratio of the turbine, since the expansion process culminate at a pressure level that is higher than the reference atmospheric pressure. The result is a reduction in useful power and an increase in specific consumption.

Table 1.1 provides typical values describing performance variations as a function of pressure losses at the inlet and exhaust. For the reasons discussed, these effects scale linearly with the magnitude of the pressure losses.

Table 1.1: Effects of intake and exhaust pressure drop on gas turbine efficiency

For every 100 mmH_2O at the intake	For every 100 mmH_2O at the exhaust
$1.3 \div 1.6\%$ of power loss	$1 \div 0.6\%$ of power loss
$1 \div 0.5\%$ of increment in Heat Rate	$1 \div 0.5\%$ of increment in Heat Rate

Investigating pressure losses in intake arrangements is not only related to a better overall efficiency of the power plant. Indeed, an accurate pressure drop prediction of each component is useful to develop new design ideas finalized to the development of compact intake arrangements reducing the overall footprint of the power plant.

The intake component interdependence analysis performed in this thesis are focused in studying how the distance between different transitions and silencers affects the overall pressure drop of the systems. A better understanding of this aspect can lead to design and build more compact intake systems that require less stainless steel for their construction leading to lower plant prices and footprints.

1.3 Pressure drop physical understanding and modelling

This section is dedicated to the fundamental theoretical basis needed to understand the thesis topic [2] [3]. The main goal is to explain what pressure losses are, starting from the physical phenomena that generates it, and then, adding more information on how pressure drop is modelled from the mathematical point of view. Especially the focus is on the Bernoulli equation modified for real flows, that is the theory used to define the K_{loss} coefficient. In a second moment the interest moves on how Computational Fluid Dynamics (CFD) codes model the pressure losses, since they are the tool used in this thesis to calculate the K_{loss} coefficient.

1.3.1 Pressure drop foundation and physical meaning

Pressure drop (ΔP) is defined as the difference in total pressure between two points of a fluid carrying network. Pressure drop occurs in real viscous flows because a portion of the total energy is expended to overcome the resistance forces that a flow has to face while flowing through pipes or ducts. This loss of energy is due to irreversible conversion of mechanical energy into heat.

The conversion of mechanical energy into heat happens due to turbulence, that in industrial applications is the most common flow regime. In internal flow, turbulence is a phenomenon which is considered desirable in one situation and undesirable in another, for instance it is responsible for most of the pressure losses, but it also makes heat transfer, mass transfer and combustion processes economically possible.

Turbulence consists of three dimensional and irregular eddies with length scale ranging from the dimension of the flow path down to eddies whose Reynolds numbers, based upon the vortex diameter, are of the order of unity. Even these eddies are very large compared to molecular length scales, so turbulence takes place in a continuum. Close to the boundaries there is a region known as the viscous sub-layer. The thickness of this sub-layer is related to the smallest turbulent eddies that can exist without viscosity almost instantly transforming their kinetic energy into heat. In the steep velocity gradient region outside the viscous sub-layer, the shear stresses tear the fluid into small and energetic eddies. Away from the walls, in the region of low shear stresses, eddies are larger and elongated.

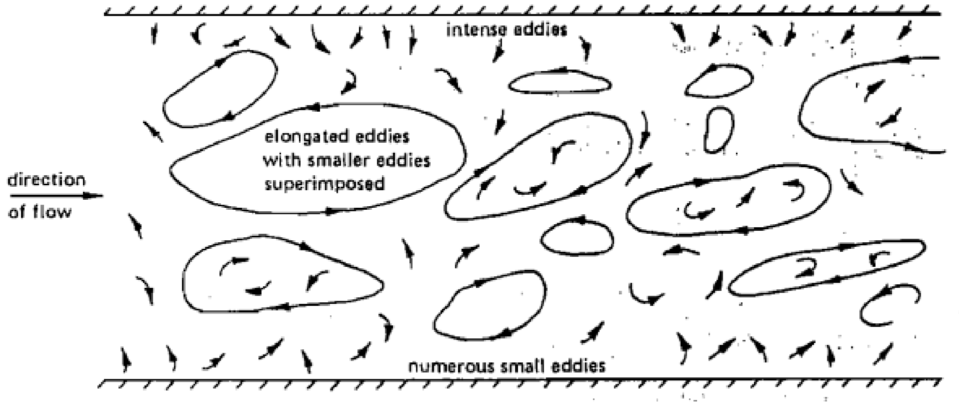

Figure 1.10: Turbulence in pipes and passages as seen by an observer moving at the mean flow velocity

Turbulence needs a continual supply of energy, or it decays rapidly and this energy is provided by shear forces at the expenses of the total flow energy. Part of the energy transferred into turbulence is immediately dissipated, particularly in regions close to boundaries and along edges of discontinuity that causes wakes and flow separation. The remaining amount of energy is transferred to large eddies and cascaded down to smaller ones. Then, at the Kolmogorov scales, very small eddies get converted into internal energy due to molecular viscosity.

Flows are usually turbulent inside straight ducts if the Reynolds number exceeds 2000, that is equivalent to a water velocity of 0.002 [m/s] in a 1 [m] diameter pipe. This helps understanding that turbulent flow is the most common flow regime in industrial applications and that, considering ducts dimensions in gas turbine intake arrangements, turbulence is the rule in this field too.

Things change a whenever there is a variation of the cross-section area. Indeed, following a smooth contraction the flow may still be laminar even though the Reynolds number is well above 2000. This happen because during acceleration the static pressure is converted to dynamic pressure, which is a stable and a low energy dissipation process. Differently, in components where velocities are reduced, intense turbulence is generated as dynamic pressure is converted to static pressure. The term "adverse pressure gradient" is used to denote a region where the static pressure rises in the direction of flow. The reason for the non reversibility lies in the non uniformity of velocity in parallel flow against the uniformity of static pressure. As shown in figure 1.11 there is a clear energy deficiency in the near-wall zone.

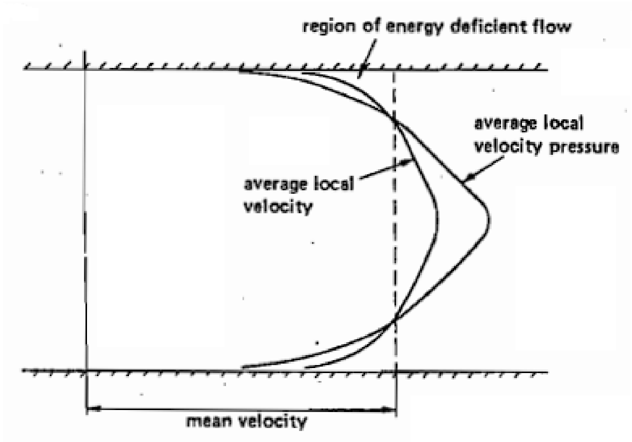

Figure 1.11: Velocity and velocity pressure distribution for developed pipe flow

When the energy deficient flow enters a region of rising static pressure, involving a conversion of velocity pressure to static pressure, it either must be supplied with energy from the higher energy fluid away from the walls, or else it progressively gives up its velocity energy and comes to rest. If part of the low is brought to rest the flow is said have stalled or separated from the boundary. When separation takes place, the main flow usually contracts for some distance downstream of the separation point and an area of reversed flow forms as shown in figure 1.12.

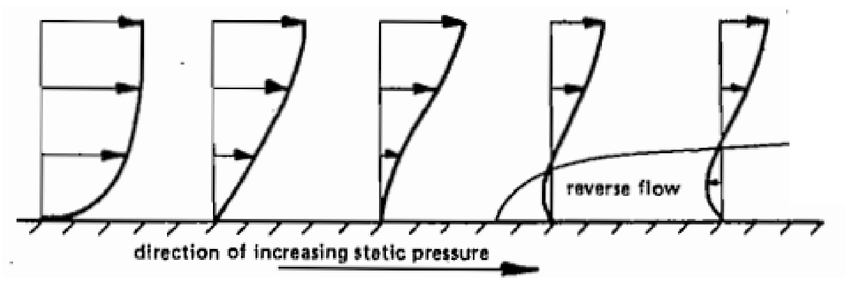

Figure 1.12: Change in near wall velocity profile in an adverse pressure gradient

Downstream of the separation point, large scale mixing spreads through the main flow balancing the energy distribution at the expense of a drop in total pressure, then flow re-attachment follows.

The same thing happens when flow is turned. When the fluid flows across elbows pressure gradients are set up across the flow. In this situation the possibility exists for low energy fluid entering a high static pressure region to escape towards regions of lower static pressure. The result is that secondary flows superimposed upon the main flow are generated. The presence of these secondary flows are additional losses due to mixing in the turning section and in the flow region upstream of it.

1.3.2 Turbulence and losses modelling in CFD codes

In this section the way turbulence and losses are modelled in CFD software is detailed [4]. Turbulence, which is the physical phenomenon responsible for most pressure losses, is a non-linear process described by the Navier–Stokes equations. As is well known, these equations cannot be solved in closed form except for very simple flows. There are three main approaches to solving fluid dynamics problems: analytical solutions (available only for simplified cases), experimental methods such as wind tunnel testing, and numerical methods, in particular Computational Fluid Dynamics (CFD). In this research, as in the most of industrial applications, CFD simulations are the instrument used to calculate the pressure losses inside the gas turbine intake systems.

Turbulent flows are characterized by fluctuating velocity fields, and these fluctuations are characterized by small scale and high frequency, therefore they are too computationally expensive to be directly simulated. However, the instantaneous (exact) governing equations can be time-averaged resulting in a modified set of equations that are computationally less expensive named as Reynolds Averaged Navier-Stokes equations (RANS).

RANS equations contain additional unknown variables, so it is necessary to introduce additional terms in the governing equations that need to be modelled to achieve "closure" (same number of governing equations and unknown variables). This set of equations represent transport equations for the mean flow quantities only, with all the scales of the turbulence being modelled. The approach of permitting a solution for the mean flow variables greatly reduces the computational effort. The Reynolds averaged approach is generally adopted for practical engineering calculations, and uses models such as Spalart-Allmaras, k-ϵ and its variants, k-ω and its variants, and the Reynolds Stress Models (RSM). In Reynolds averaging, the solution variables in the instantaneous (exact) Navier-Stokes equations are decomposed into the mean (ensemble-averaged or time-averaged) and fluctuating components. For the velocity components:

$$u_i = \bar{u}_i + u_i' \tag{1.1}$$

where $\bar{u}_i$ is the mean velocity and u_i' is the fluctuating velocity.

In the same way, for pressure and other scalar quantities:

$$\phi_i = \bar{\phi}_i + \phi_i' \tag{1.2}$$

where ϕ denotes a scalar such as pressure, energy, or species concentration.

Substituting expressions of this form for the flow variables into the instantaneous continuity and momentum Navier-Stokes equations, taking a time average and dropping the overbar on the mean velocity yields the ensemble-averaged momentum equations. They can be written in Cartesian tensor form as:

$$\frac{\partial \rho}{\partial t} + \frac{\partial}{\partial x_i}(\rho u_i) = 0 \tag{1.3}$$

$$\frac{\partial}{\partial t}(\rho u_i) + \frac{\partial}{\partial x_j}(\rho u_i u_j) = -\frac{\partial p}{\partial x_i} + \frac{\partial}{\partial x_j}\left[\mu\left(\frac{\partial u_i}{\partial x_j} + \frac{\partial u_j}{\partial x_i} - \frac{2}{3}\delta_{ij}\frac{\partial u_\ell}{\partial x_\ell}\right)\right] + \frac{\partial}{\partial x_j}\left(-\rho\,\overline{u_i' u_j'}\right) \tag{1.4}$$

Equations (1.5) and (1.4) have the same general form as the instantaneous Navier-Stokes equations, with the velocities and other solution variables now representing ensemble-averaged (or time-averaged) values. Additional terms now appear that represent the effects of turbulence. These Reynolds stresses $-\rho\,\overline{u_i' u_j'}$, must be modelled to close Reynolds Averaged Navier-Stokes equation.

The Reynolds-averaged approach to turbulence modelling requires that the Reynolds stresses in equations (1.5) and (1.4) to be properly modelled. A common method to model the Reynolds stresses employs the Boussinesq hypothesis to relate the Reynolds stresses to the mean velocity gradients: The hypothesis models the Reynolds Stresses as follows:

$$-\rho\,\overline{u_i' u_j'} = \mu_t\left(\frac{\partial u_i}{\partial x_j} + \frac{\partial u_j}{\partial x_i}\right) - \frac{2}{3}\left(\rho k + \mu_t\frac{\partial u_i}{\partial x_i}\right)\delta_{ij} \tag{1.5}$$

The Boussinesq hypothesis is used in the Spalart-Allmaras model, the k-ϵ models, and the k-ω models. The advantage of this approach is the relatively low computational cost associated with the computation of the turbulent viscosity, μ_t. In the case of the Spalart-Allmaras model, only one additional transport equation (representing turbulent viscosity) is solved. In the case of the k-ϵ and k-ω models, two additional transport equations (for the turbulence kinetic energy, k, and either the turbulence dissipation rate, ϵ, or the specific dissipation rate, ω) are solved, and μ_t is computed as a function of k and ϵ. It is worth to underline the fact that the turbulence dissipation at the Kolmogorov scales, that is responsible for the conversion of mechanical energy into thermal energy that was streamlined in the previous section, is modelled using ϵ and ω variables.

The disadvantage of the Boussinesq hypothesis as presented is that it assumes μ_t is an isotropic scalar quantity, which is not strictly true. The alternative approach, embodied in the RSM, is to solve transport equations for each of the terms in the Reynolds stress tensor. An additional scale-determining equation for ϵ or ω is also required. This means that five additional transport equations are required in 2D flows and seven additional transport equations must be solved in 3D. In many cases, models based on the Boussinesq hypothesis perform very well, and the additional computational expense of the Reynolds stress model is not justified. However, the RSM is clearly superior for situations in which the anisotropy of turbulence has a dominant effect on the mean flow such cases including highly swirling flows and stress driven secondary flows.

Stress driven secondary flows are common at the square ducts edges as shown in figure 1.13.

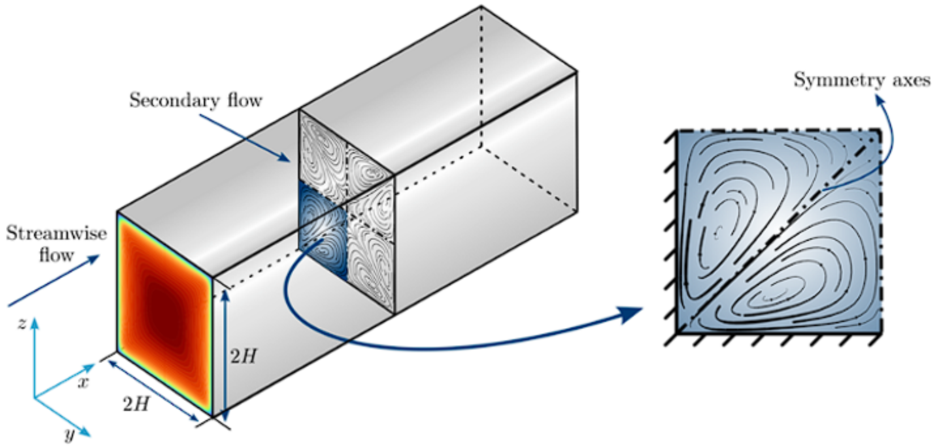

Figure 1.13: Secondary flows schematic representation in a square duct

Since the velocities involved in this phenomenon are low if compared to the velocity in the main flow direction, the overall effect on pressure drop of secondary flows is negligible. The quantitative effect is not documented in this thesis, but the simulations suggest that the pressure drop is slightly higher when using Reynolds Stress Models (RSM) than the values obtained on the same condition while using isotropic turbulence models.

In summary, turbulence is the primary contributor to pressure losses, as discussed in the analysis of the physics behind pressure drop. Now, it is also clear how turbulence and consequently pressure losses are modelled in CFD codes using the average fluctuating velocity components.

1.3.3 Bernoulli equation extended to real flows and pressure loss coefficient K_{loss} definition

Using Computational Fluid Dynamics allows to find the pressure losses of each desired fitting. Then, the calculated data needs to be post-processed to create mathematical models. To understand how the data are post processed and what is meant by the term "total pressure losses" or "total energy losses", the following mathematical formulation is introduced [5]. Firstly, is important to recall the Bernoulli Equation, which can be developed by equating the forces on an element of a stream tube in a frictionless fluid flow to the rate of momentum change. On integrating this relationship for steady flow, the following expression results:

$$\frac{v^2}{2} + \int \frac{dP_s}{\rho} + gz = \text{constant} \quad [\text{Nm/kg}] \tag{1.6}$$

where:

- v is the streamline velocity $[m/s]$;

- P_s is the static pressure in $[Pa]$;
- v is density in $[kg/m^3]$;
- g is the acceleration due to gravity $[m^2/s]$;
- v is the elevation $[m]$;

Assuming constant fluid density within the system, equation 1.6 reduces to:

$$\frac{v^2}{2} + \frac{P_s}{\rho} + gz = \text{constant} \quad [\text{Nm/kg}] \tag{1.7}$$

Although equation 1.7 was derived for steady, ideal frictionless flow along a stream tube, it can be extended to analyse flow through ducts in real systems. In terms of pressure, the relationship for fluid resistance between two sections associated to the subscripts 1 and 2 is:

$$\frac{\rho_1 V_1^2}{2} + P_1 + g\rho_1 z_1 = \frac{\rho_2 V_2^2}{2} + P_2 + g\rho_2 z_2 + \Delta P_{1,2} \tag{1.8}$$

where:

- V = average duct velocity in [m/s]
- $\Delta P_{1,2}$ = total pressure loss due to friction and dynamic losses between sections 1 and 2 in [Pa]

In Equation 1.8, V (section average velocity) replaces v (streamline velocity) because experimentally determined loss coefficients allow for errors in calculating ρv^2 (velocity pressure) across streamlines.

On the left side of Equation 1.8, add and subtract $P_{z,1}$; on the right side, add and subtract $P_{z,2}$, where $P_{z,1}$ and $P_{z,2}$ are the values of atmospheric air at heights z_1 and z_2. Thus, the following formulation is explained:

$$\frac{\rho_1 V_1^2}{2} + P_1 + (P_{z,1} - p_{z,1}) + gP_1 z_1 = \frac{\rho_2 V_2^2}{2} + P_2 + (P_{z,2} - P_{z,2}) + gP_2 z_2 + \Delta P_{1,2} \tag{1.9}$$

The atmospheric pressure at any elevation ($P_{z,1}$ and $P_{z,2}$) expressed in terms of the atmospheric pressure P_a at the same datum elevation is given by

$$P_{z,1} = P_a - gP_a z_1 \tag{1.10}$$

$$P_{z,2} = P_a - gP_a z_2 \tag{1.11}$$

Substituting these last two equations into equation 1.9 and simplifying brings to an expression of the total pressure variation between sections 1 and 2. Assume no variation in temperature between sections 1 and 2 (no heat exchanger within the section); therefore, $\rho_1 = \rho_2$. When a heat exchanger is located within the section, the average of the inlet and outlet temperatures is generally used. Let $p = p_1 - p_{z,1}$ $(p_1 - p_{z,1})$ and $(p_2 - p_{z,2})$ are gauge pressures at elevations z_1 and z_2.

$$\Delta P_{t,1,2} = \left(P_{s,1} + \frac{\rho V_1^2}{2}\right) - \left(P_{s,2} + \frac{\rho V_2^2}{2}\right) + g(\rho_a - \rho)(z_2 - z_1) \tag{1.12}$$

$$\Delta P_{t,1,2} = \Delta P_t + \Delta P_{se} \tag{1.13}$$

$$\Delta P_t = \Delta P_{t,1,2} - \Delta P_{se} \tag{1.14}$$

where

- $P_{s,1}$ = static pressure, gage at elevation z_1 in [Pa]
- $P_{s,2}$ = static pressure, gage at elevation z_2 in [Pa]
- V_1 = average velocity at section 1 in [m/s]
- V_2 = average velocity at section 2 in [m/s]
- ρ_a = density of ambient air in [kg/m^3]
- ρ = density of air or gas within duct in [kg/m^3]
- ΔP_{se} = thermal gravity effect in [Pa]
- ΔP_t = total pressure variation between sections 1 and 2 in [Pa]
- $\Delta P_{t,1,2}$ = total pressure loss due to friction and dynamic losses between sections 1 and 2 in [Pa]

Since the temperature differences are negligible inside gas turbine intake ducts (the domain of interest in this thesis does not comprehend chiller coils), it is possible to assume that the total pressure variation between two sections is equal to the total pressure losses due to friction and dynamic losses: $\Delta p_t = \Delta p_{t,1,2}$. On the other hand, the same assumption is not valid for exhaust ducts where the thermal gravity effect ΔP_{se} is an important contribution.

The pressure difference between two section is the result obtained through CFD simulations but to be implemented on the tool the result must be post-processed to calculate the K_{loss} coefficient. Indeed, the pressure drop is assumed to be proportional to dynamic pressure, and can be expressed as:

$$\Delta P_{1,2} = \frac{1}{2} K_{\text{loss}} \rho V^2 \tag{1.15}$$

So, the value of the K_{loss} coefficient is calculated starting from equation 1.15 as:

$$K_{\text{loss}} = \frac{2 \cdot \Delta P}{\rho V^2} \tag{1.16}$$

Each different intake component will be addressed by a different value of K_{loss}.

It is worth noting that in the K_{loss} coefficient also the friction losses through the component walls are considered. Anyway, the friction losses are negligible since they are inversely proportional to the hydraulic diameter that is very high if compared to length. These is even more clear if the Darcy-Weisbach equation is presented:

$$\Delta P = f \cdot \left(\frac{L}{D_h}\right)\left(\frac{\rho v^2}{2}\right) \tag{1.17}$$

where:

- f is the Darcy friction factor that is generally inversely proportional to the Reynolds number (Re) for $Re < 10^6$ and it stabilizes for $Re > 10^6$;
- L is the pipe length [m];
- D_h is the hydraulic diameter [m];
- v is the mean flow velocity [m/s];
- g is the gravity acceleration [m/s^2]

Chapter 2

Thesis workflow and methodology

2.1 Workflow overview

The entire work has been divided in four different phases as it is described in this chapter. The development of the pressure drop mathematical models on which the calculation tool relies has not been a straight-forward process, but an iterative one. The division in four different phases is necessary to clarify the method used for this research, but it has not to be intended as the 4 phases were strictly developed in chronological order.

The first phase is dedicated to collect geometric and experimental data. The geometric data were collected by studying technical drawings. The experimental data, such as pressure drop, air temperature and mass airflow, were collected from a software tool used to monitor the installed turbines.

The second step of the work is based on parametric CFD simulations, that were performed to assess how the pressure drop of each single component is related to the constructive geometric parameters of the component itself.

The third part of the work is centred on the development of mathematical models based on the large quantity of numerical data gained through the simulations. These mathematical models had to express the pressure loss coefficient K_{loss} as a function of the key geometric parameters for each fitting. Then, all the mathematical models were implemented in an automated Excel file that is the pressure drop calculation tool.

The last phase is focused on the tool validation that was performed through the comparison between the experimental data taken from the software tool and the numerical data obtained through the mathematical models developed. Clearly, this validation process was performed only on some specific arrangements.

In the next sections these 4 phases are described in detail to provide a general explanation of the approach used to develop the study. Only general information is provided in this chapter as other additional ones are provided when specifically speaking about the analyses.

2.2 1st Phase: Geometric and Experimental data collection

2.2.1 Geometric data collection

When referring to intake systems or arrangements, the structured set of components that constitute them is implied. An example of intake arrangement could be the one constituted by a transition, a curve and a silencer.

As input for the research, several intake arrangements of interest were selected. The goal of the entire study is to create mathematical models capable of predicting the pressure drop for these specific intake arrangements. Being able to assess the pressure drop for an intake arrangement means that the models need to be validated to all the different gas path dimensions for that arrangement. Indeed, the typical gas path dimension and the hydraulic diameters of the intake ducts, transitions, elbows and filter houses vary a lot considering gas turbine of different nature and dimensions such as Frame Type, Aero-derivative and Industrial ones.

Therefore, as already said above, for each possible arrangement many different installations exists and the geometric dimensions vary a lot from an installation to another one. This is because the same intake arrangement could be used for gas turbine of different size.

So, to create general mathematical models that predict the pressure drop is important to understand how losses vary as a function of the geometric parameters that characterize the fittings. The geometric parameters of interest for each fitting were inspected through an analysis of the technical drawings. The key parameters mainly consists of:

- Inlet gas path dimensions;
- Outlet gas path dimensions;
- Length of the component in the flow direction;
- Radius of the fillet at inlet;

Apart from the parameters detailed above, for silencers other important geometric parameters are:

- Number of parallel panels (baffles);
- Width of the panels;
- Panels shape;

The typical sizes of the parameters of interest were collected in this first phase and were crucial to set the bounds of the parametric studies that are detailed in the section 3. Indeed, the most important output of the technical drawing studies are the minimum and maximum dimensions of the constructive parameters for each fitting. These data are then imposed as bounds of the parametric studies.

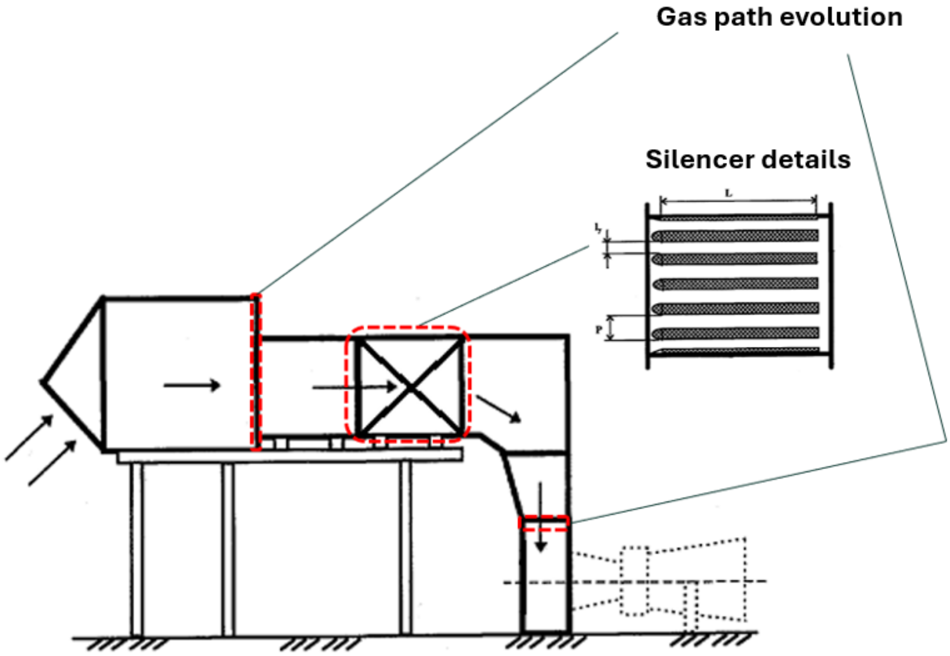

Figure 2.1: Overview of the key geometric parameters for a gas turbine intake system

2.2.2 Experimental data collection

Other fundamental data are the experimental ones that were collected from a software tool used for diagnostic and real-time monitoring on the running gas turbines. The acquired data are related to pressure drop and the parameters that affects it, such as air temperature and mass airflow at the axial compressor inlet. Clearly, the data collection was performed on gas turbine intake arrangements equivalent to the one studied on the technical drawings.

As the overall work has the intent to develop a tool with reasonable pressure drop results, the acquired data are used to validate the analytical models. The goal of the study is to inspect the domain that goes from the plane downstream the filter house to a plane positioned at the plenum inlet. Therefore, the pressure drop assessment is not made on the entire gas turbine intake system, since the filter house is excluded from the study. The reason why the filters are excluded is that pressure drop assessment for these devices is made by the companies that develop them through experimental testing. The domain of interest in this research is clarified in figure 2.2.

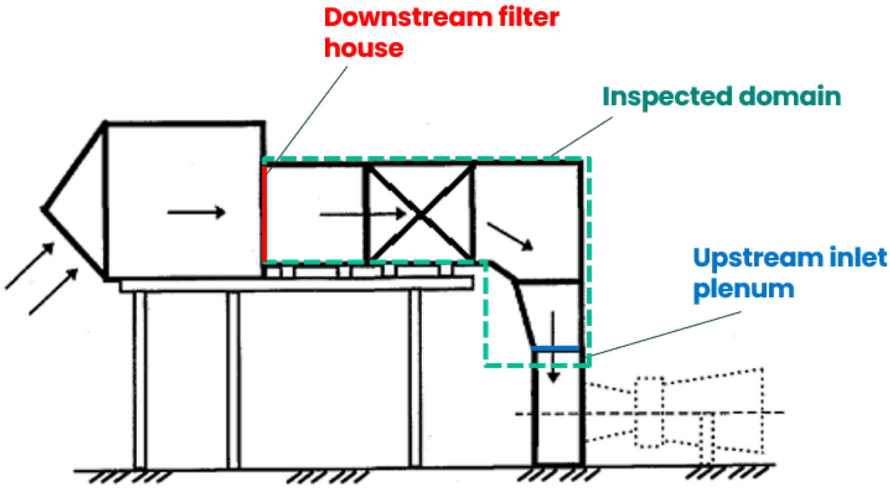

Figure 2.2: Overview of the inspected gas turbine intake domain

The only intake arrangements that were inspected in the monitoring application are the ones with static pressure ports or Pitot tubes placed on the boundaries of the inspected domain. Not all the arrangements have pressure ports in the desired spots, so only a small number of machines could be used for the validation. Indeed, most of the arrangements have static pressure ports or even Pitot tubes near the plenum inlet for safety reasons, but only a fraction of them have pressure ports downstream of the filter house.

The other important data collected from the software tool are the mass air flow and the air temperature, since from these 2 parameters density is derived. Density is fundamental since the pressure drop data depends on it. In figure 2.3 an example of the acquired data for one specific machine is presented and shows that the four parameters were recorded at the same time.

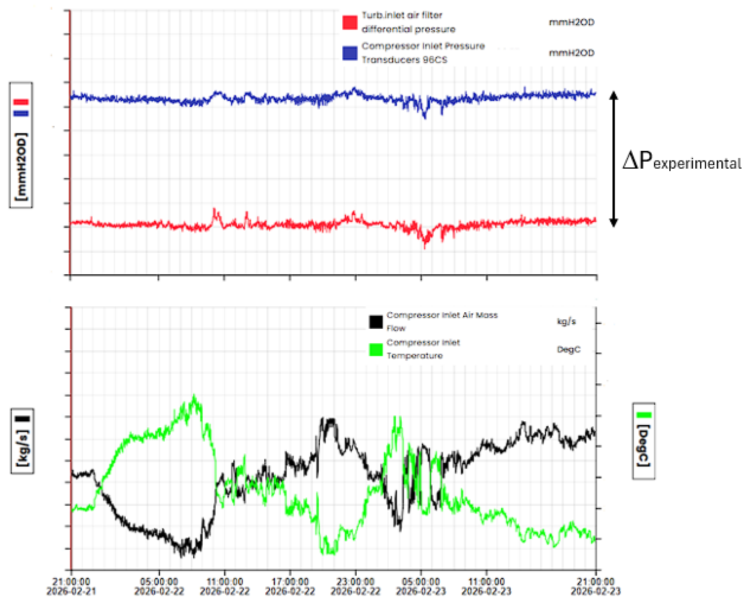

Figure 2.3: Physical parameters acquired as experimental data from the monitoring application.

2.3 2nd Phase: Parametric Computational Fluid Dynamics simulations

In this section the entire workflow inherent to the CFD simulations is described. Starting from the development of the parametric CAD models, through the meshing workflow till the simulation setup and results post-processing. Most of the workflow was managed through ANSYS Workbench.

2.3.1 General CAD model development

The parametric CAD models were developed using ANSYS SpaceClaim scripting, as the goal was to manage CAD models with many parameters.

First, the parameters that directly affects the pressure losses of each single fitting need to be determined. To achieve this, a literature review was conducted to study pre-existing mathematical formulations. Generally, the number of parameters that plays a role on affecting the pressure drop is large, therefore some parameters were ignored. The decision to limit the number of parameters for each study to three was taken to simplify the procedure of writing the mathematical laws and reducing the overall number of design points to simulate.

Once the geometric parameters were determined and the bounds of the parametric study were fixed, the design points of the study could be established. Each design point corresponds to a different CAD model and a different simulation.

Table of Design Points

	A	B	C	D	E	F	G	H	I
1	Name	Update Order	P1 - gaspath	P2 - first_vane	P3 - nose_radius	P4 - baffle_lenght	P5 - baffle_number	P6 - pitch	P7 - Tr
2	Units		mm	mm	mm	mm		mm	
3	DP 0	1	2000	75	83.75	1500	8	72.857	1
4	DP 1	2	2000	75	83.75	1700	8	72.857	1
5	DP 2	3	2000	75	83.75	1900	8	72.857	1
6	DP 3	4	2000	75	83.75	2100	8	72.857	1
7	DP 4	5	2000	75	83.75	2300	8	72.857	1
8	DP 5	6	2000	75	83.75	2500	8	72.857	1
9	DP 6	7	2000	75	83.75	2700	8	72.857	1
10	DP 7	8	2000	75	83.75	2900	8	72.857	1

Figure 2.4: Design points and corresponding parameter sets ANSYS Workbench table

It is also worth adding that in the CAD models the inlet and the outlet were extruded to prevent reverse flow at the boundaries, as this has an impact on the solution convergence.

In addition, in many simulations only half of the model was used, and in those cases symmetry was applied in the calculation setup. Assuming symmetric behaviour was not a simplification, since both the geometry and the boundary conditions are symmetric.

2.3.2 Turbulence Models used: K-ω SST, BSL Reynolds Stress Model and standard K-ϵ model

During the entire research, three different RANS turbulence models were used, and the reasons are explained in the following paragraph.

1. K-ω SST: this model was used for all the 2D simulations and most of the 3D simulations. Compared to the standard K-ϵ model, it provides better performance in the presence of flow separation and behaves more accurately under adverse pressure gradient conditions. However, it is natively a wall-resolved model, which makes it computationally more expensive since the mesh in the near-wall regions needs to be fine enough to directly solve the boundary layer.

2. BSL Reynolds Stress Model: this model is one of the Reynolds Stress Models available in ANSYS Fluent. BSL stands for baseline and indicates that the formulation on which it relies was designed to improve the robustness and accuracy of the original Reynolds Stress Model. While traditional RSM were originally developed to be used with wall functions, this formulation is based on an ω approach, and it therefore uses a wall-resolved treatment. It was employed only in a limited number of simulations to achieve higher accuracy. The reason why it was used only in few cases lies on the fact that it is extremely computationally demanding for a parametric study. Indeed, it directly models the full Reynolds stress tensor instead of relying on the eddy viscosity hypothesis, thus it uses seven additional transport equations. In addition to that, this BSL version is wall-resolved entailing a larger number of cells is required. These aspects have limited its use.

3. Standard K-ϵ: this model was used exclusively for the interdependence analyses where silencers and other fittings were simulated together to study how they interact. These analyses are characterized by 3D computational domains, so a large number of cells would have been necessary for a wall-resolved treatment. Therefore, standard K-ϵ model was chosen for its reduced computational cost enabled using wall functions, which is particularly beneficial in this case. Furthermore, given the way the interdependence was implemented in the computational tool, a lower level of accuracy was considered acceptable.

Clearly, the differences in the pressure drop results among the models are limited and are not the object of this thesis.

2.3.3 General Meshing Setup

In this paragraph the general meshing setup is explained to give info about the analyses that are discussed in the next chapters. During the parametric analyses performed in ANSYS Workbench, only the meshing workflow of the first design point needs to be defined. The mesh on other design points of the same parametric study is automatically generated using the same workflow.

In order to generate a good quality mesh, the following parameters and precautions need to be considered:

- Mesh element type: quadrilateral elements to mesh 2D computational domains and polyhedral elements to mesh 3D computational domains. Naturally, with a few exceptions;
- Free flow mesh dimension: fine enough to guarantee mesh independence;
- Inflation layers number: 25-35 elements for wall-resolved approach and 7-15 elements for wall functions;
- First layer thickness: calculated starting from y^+ and defined as follows:

$$y = 2y^+ \cdot \frac{\nu}{\rho \cdot \mu_t} \tag{2.1}$$

  where:
  - $y^+ = 1$ for wall-resolved treatment and $y^+ = 30 \div 100$ for wall functions treatment;
  - ν is the kinematic viscosity;
  - ρ is the flow density;
  - $\mu_t = \sqrt{\frac{\tau_\omega}{\rho}}$ where τ_ω is the wall shear stress;
- Provide a finer mesh, with a growth ratio of 1.15, at flow discontinuities or in regions with steeper velocity gradients, such as sharp edges or silencer baffles;

With the workflow described above, the meshing parameters are fixed for all the design points belonging to the same parametric study. The meshing parameters were tuned to guarantee good mesh quality for all the design points, consisting of the right y^+ value, low skewness and high orthogonal quality. Even though meshing parameters can be used as design point parameters, the flow regime differences were negligible between the different design points, thus, this was not necessary.

ANSYS Fluent Meshing with the "Watertight Geometry Workflow" was used for 3D computational domains and ANSYS Mechanical meshing was used for 2D computational domains. Meshing examples are provided in figure 2.5:

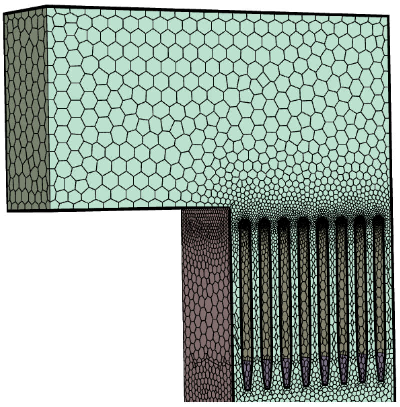

(a) Example of polyhedral mesh used in a 3D interdependence analysis

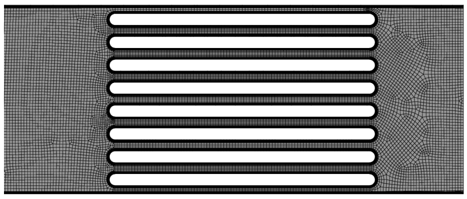

(b) Example of quadrilateral mesh used for silencer 2D analysis

Figure 2.5: Meshing examples for 2D and 3D computational domains

2.3.4 CFD Simulation Setup and Results

In this paragraph all the settings of the CFD simulations are detailed, apart from the turbulence models that were discussed above.

The simulation were performed using ANSYS Fluent. The pressure-based solver was adopted since the condition $Ma < 0.3$ is always verified in gas turbine intake ducts. In addition, pseudo-transient simulations were performed without considering the gravity effects. This assumption is valid since air density has a negligible effect on the flow. A conservative Courant-Friedrichs-Lewy number (CFL) was provided to guarantee convergent behaviour for all the design points.

The boundary conditions chosen were:

- Mass flow at inlet in [kg/s]: it is the combustion mass flow of the gas turbine. It is worth noting that the mass flow that must be specified is the half of the real mass flow if the symmetric boundary condition is used;
- Pressure outlet in [Pa]: the pressure value was fixed at 0 [Pa];

A large iteration number was specified to reach good convergence for all the design points and no convergence condition on the residuals was added.

The outputs of the single CFD simulation are:

- Mass imbalance: it is the absolute value of the difference between the mass flow at the inlet and the mass flow at the outlet, calculated as follows:

$$\text{Mass imbalance} = |\dot{m}_{\text{inlet}} - \dot{m}_{\text{outlet}}| \tag{2.2}$$

  This parameter is useful to assess convergence without requiring an evaluation of the residual trends or the trends of the physical values;

- Pressure drop: in some simulations is calculated as the difference between the total pressure at the inlet and the total pressure at the outlet:

$$\Delta P = P_{\text{t inlet}} - P_{\text{t outlet}} = \left(p_{\text{s inlet}} + \frac{1}{2}\rho v_{\text{inlet}}^2\right) - \left(p_{\text{s outlet}} + \frac{1}{2}\rho v_{\text{outlet}}^2\right) \quad (2.3)$$

  In some cases, the total pressure evolution through the computational domain is the output of the analysis. This result is then post-processed to calculate the pressure drop at a specific distance from the inspected component. The total pressure evolution is obtained by calculating the mass-flow-averaged total pressure on different planes, equally spaced apart.

2.4 3rd Phase: Mathematical Model Development

Once the CFD simulations were performed, the numerical data obtained as output needs to be post-processed to develop mathematical models. So, pressure drop is used to calculate the K_{loss} coefficient through the following mathematical formulation:

$$K_{\text{loss}} = \frac{\Delta P}{\frac{1}{2}\rho v_{\text{outlet}}^2} \tag{2.4}$$

It is important to underline that the dynamic pressure at the component outlet is used to compute the K_{loss} coefficient. Instead, if the dynamic pressure at the component inlet is used the K_{loss} coefficient value would have been different.

The mathematical models developed in this research can be divided in two different groups:

- Single variable models: these models are the easiest ones and were developed using Excel trend-line function;
- Multi-variable models: these models were developed using Octave and consists of scalar function on two variables, so their behaviour is still easy to predict;

Two different parameters were used to assess the accuracy of the developed models:

- Determination coefficient (R^2) that is calculated as:

$$R^2 = 1 - \frac{\sum_{i=1}^{n} (y_i - \hat{y}_i)^2}{\sum_{i=1}^{n} (y_i - \bar{y})^2} \tag{2.5}$$

- RMSE (Root Mean Squared Error) that is calculated as:

$$\text{RMSE} = \sqrt{\frac{1}{n}\sum_{i=1}^{n} (y_i - \hat{y}_i)^2} \tag{2.6}$$

where y_i represents the observed (true) value, $\hat{y}_i$ denotes the predicted value obtained from the model, and $\bar{y}$ indicates the mean of the observed values over all n samples.

2.5 4th Phase: Results Analysis and Comparison between Numerical and Experimental Data

Once the mathematical models were developed, they were validated. Therefore, the experimental data collected from literature and from the software tool were compared with the numerical results.

Some components, similar to gas turbine intake fittings, were largely tested in the past, so their K_{loss} coefficients are tabulated. In particular, this is valid for fittings like transitions and elbows for which a direct comparison between the mathematical models and the existing literature data was possible.

For other components, such parallel baffle silencers, no tabulated data exists and a dedicated study was developed in this thesis.

The only way to validate the silencer models was to compare the numerical results to the software tool data. But, as explained before, software data express the pressure drop of the entire inspected domain that always comprehend many fittings. Indeed, gas turbine intake systems generally comprise a transition followed by an elbow and a silencer and the experimental pressure drop values are characterized by all these contributions. The only way to calculate experimental silencer pressure drop consists of isolating the contribution starting from the total pressure drop, as it is explained in the following equation:

$$\Delta P_{\text{silencer}} = \Delta P_{\text{total}} - \Delta P_{\text{transition}} - \Delta P_{\text{elbow}} \tag{2.7}$$

However, using this method without having the correct experimental values of $\Delta P_{\text{transition}}$ and ΔP_{elbows} entails that the calculated $\Delta P_{\text{silencer}}$ value is not perfectly accurate.

Therefore, the mathematical model validation was performed by comparing the pressure drop collected from the monitoring application to the sum of the numerical pressure drop value of each single fitting. The numerical value of the pressure drop was calculated as follows:

$$\Delta P_{\text{num total}} = \Delta P_{\text{num silencer}} + \Delta P_{\text{num transition}} + \Delta P_{\text{num elbow}} \tag{2.8}$$

The percentage error was calculated as:

$$\%\text{error} = \left| \frac{\Delta P_{\text{num total}} - \Delta P_{\text{software}}}{\Delta P_{\text{software}}} \right| \cdot 100 \tag{2.9}$$

The maximum %error value accepted in this research is the 10%.

Chapter 3

Gas turbine intake fittings

3.1 Importance of studying K_{loss} coefficient of key intake system fittings

In literature, many books and papers based on experimental evidence were developed to assess how the K_{loss} coefficient of different fittings varies as a function of geometric parameters. However, typical gas turbine intake duct dimensions are out of range if compared with the components found on literature data. This difference in dimensions is a good reason to perform parametric studies even though literature data exist.

Indeed, different dimensions of intake ducts imply different flow conditions, especially different Reynolds numbers. To underline the importance of doing CFD parametric studies, even though data exist, it is worth to show how the Reynolds number affects pressure drop. To do so, a study on a $90°C$ degree elbow has been made.

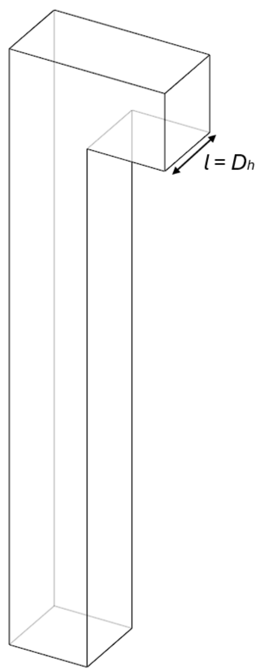

Figure 3.1: 90° elbow

In this study the goal is to compare the K_{loss} coefficient of the same fitting but with different hydraulic diameter D_h, that for square ducts is equal to the edge length l.

Two different computational domains were tested, one characterized by typical gas turbine intake duct dimensions ($D_h = 3000$ [mm]) and the other with dimensions scaled according to the maximum Reynolds number found in literature for $90°C$ degree elbows. All the setup details related to these simulations are expressed in table 3.1:

Table 3.1: Flow parameters and Reynolds numbers for literature cases and gas turbine reference conditions

Simulation	ρ [kg/m^3]	D_h [m]	μ [kg/(m s)]	$\dot{m}$ [kg/s]	v [m/s]	Re
Gas turbine	1.225	3.000	1.78×10^{-5}	90.0	8.16	1.69×10^{6}
Literature data	1.225	0.2492	1.78×10^{-5}	0.621	8.16	1.40×10^{5}

Clearly, the pressure drop value is strictly dependent to the distance from the curve outlet. Thus, to compare these two cases a dimensionless distance was considered. Consequently, the K_{loss} coefficient value is calculated for a distance equivalent to three hydraulic diameters D_h. The mathematical trend of the K_{loss} coefficient as a function of the distance, always measured as the number of hydraulic diameters D_h is shown in figure 3.2.

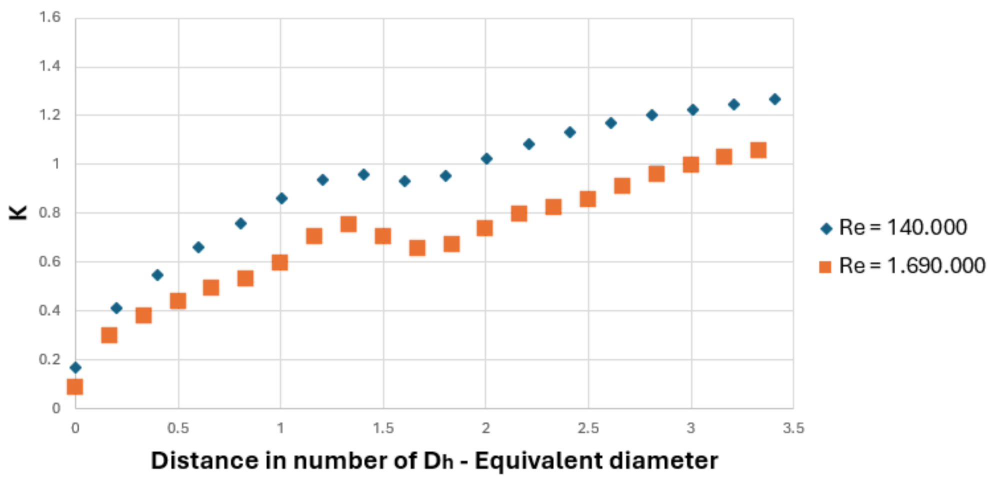

Figure 3.2: K_{loss} expressed as a function of the distance specified as number of hydraulic diameters D_h

This figure is obtained by sampling with planes at increasing distance from the curve outlet and calculating the mass averaged total pressure at each sampling plane. The scatters represent the K_{loss} coefficient calculated from the pressure drop value at each plane.

The results are summarized in table 3.2:

Table 3.2: K_{loss} coefficient for literature cases and gas turbine reference conditions

Re	ΔP [Pa]	K
1.69×10^6	43	0.99
1.40×10^5	53	1.23

So, it is evident that the results obtained for different Reynolds numbers have a significant deviation one from another. Therefore, blindly using the literature K_{loss} coefficients can lead to large mistakes. In particular, using literature values can lead to overestimate the overall pressure drop.

There are also other reasons why is important to study the different fittings that characterize gas turbine intake systems. Hence, in literature there are no data related to some of the fittings used in gas turbine intake arrangements, and the K_{loss} value cannot be derived as linear superposition from known fittings. For example, the convergent elbow transitions described in section 3.2 are a typical fitting in gas turbine intake systems, but they are not listed in the existing literature databases.

To give further explanation of this phenomenon, some consideration on Darcy-Weisbach equation are necessary. As explained in chapter 1, this equation shows that friction losses are inversely proportional to hydraulic diameter D_h. Therefore, friction contribution in gas turbine intake systems is almost negligible. On the other hand, the friction contribution has a significant effect for fittings characterized by a lower value of D_h.

3.2 Elbow ducts analysis

The first fitting analysed in detail through a parametric study is elbow duct, which is a common junction element in intake systems. A parametric analysis was necessary to achieve higher accuracy in predicting its pressure drop. In fact, as previously shown, literature data are not directly applicable to gas turbine fittings due to differences in Reynolds number.

3.2.1 Investigated Parameters and Design Points

A literature review was conducted to detect the parameters that has strong impact on elbow duct pressure drop. In ASHRAE book [5] the following mathematical formulation to express the K_{loss} coefficient is used:

$$K_{\text{loss}} = K_{\text{Reynolds}} K_{\text{elbow}} \tag{3.1}$$

where K_{Reynolds} is a corrective factor calculated as a function of the Reynolds number and K_{elbow} is the effective curve loss coefficient determined as linear interpolation of experimental values. The experimental values in literature review were obtained as a function of cross-section aspect ratio and the elbow angle. Thus, literature suggests there are three influential parameters that determine elbow pressure drop:

- Elbow angle (θ);
- Shape ratio ($S_r = H/W$);
- Reynolds number (Re);

These parameters are further described in figure 3.3:

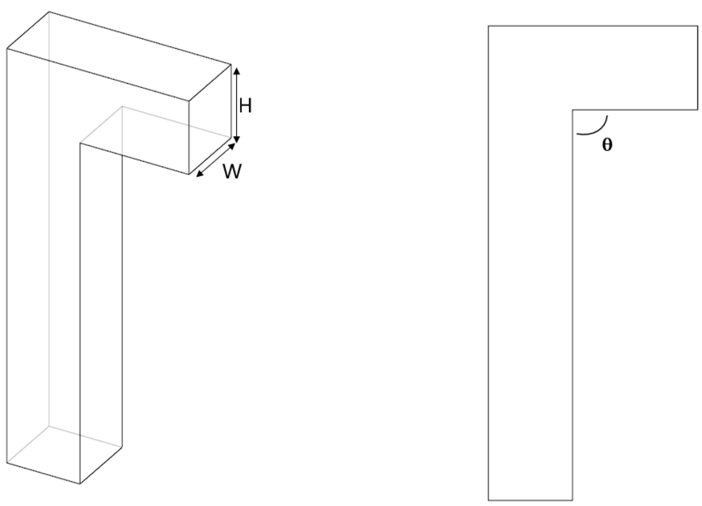

(a) Square elbow ducts with $H = W$

(b) Example with $\theta = 90°$

Figure 3.3: Key geometric parameters for elbow ducts

In this research the effect of the elbow angle (θ) is inspected by analysing only 4 different angle values: 90° - 75° - 60° - 45°.

Instead, the shape ratio or aspect ratio of the cross-section is determined as the ratio between height and base of the duct. This parameter is denoted with S_r. Considering how this parameter is defined, $S_r > 1$ denotes a vertically elongated duct and $S_r < 1$ denotes a horizontally elongated duct, as shown in figure 3.4.

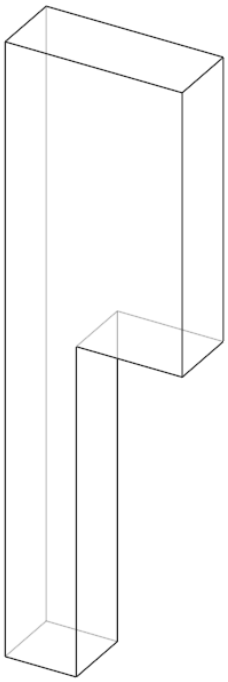

(a) $Sr = 4$ vertically elongated duct

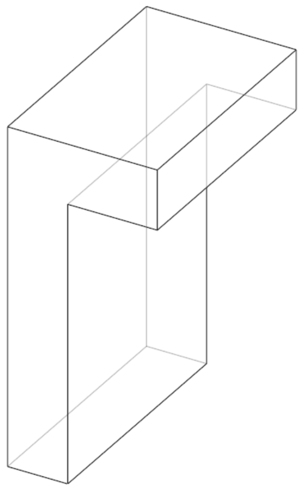

(b) $Sr = 0.25$ horizontally elongated duct

Figure 3.4: Maximum and minimum shape ratio (S_r) values

Differently from the other parameters, the Reynolds number in this research is ignored, because, at high Reynolds regime, variations of it does not affect pressure drop. Therefore, it is reasonable to assume that at typical intake ducts Reynolds values its effect on pressure drop is negligible.

The analysis was performed over a narrower range of S_r and θ values if compared to literature data. The maximum and minimum S_r and θ values are shown in table 3.3:

Table 3.3: Maximum and minimum S_r and θ values for elbow ducts study

Parameter	Minimum value [mm]	Maximum value [mm]
S_r	0.25	4
θ	45°	90°

3.2.2 Mesh and Parametric CFD simulation Setup

An unstructured polyhedral mesh was developed in ANSYS Fluent Meshing by using ANSYS Watertight Mesh Workflow. The obtained mesh is shown in figure 3.5.

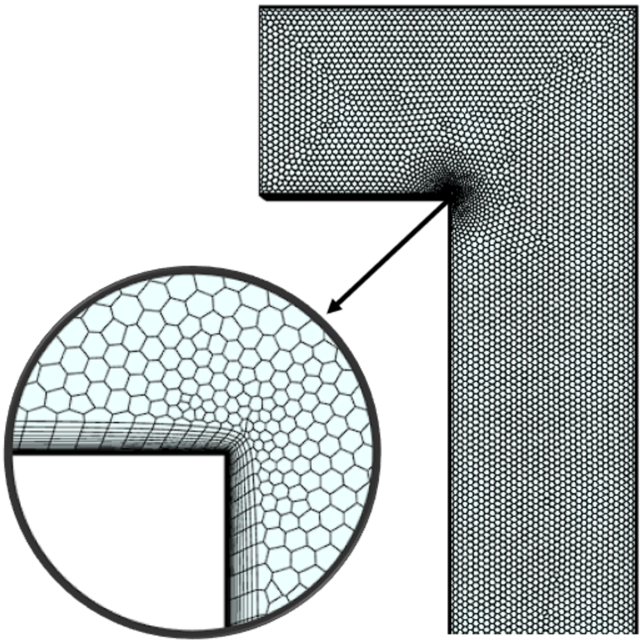

Figure 3.5: Polyhedral unstructured mesh for elbow ducts

The mesh parameters are detailed in table 3.4.

Table 3.4: Mesh parameters for elbow duct study

Edge sizing	Domain sizing	First element thickness	Inflation elements
10mm	100mm	0.035mm	30

For this analysis the K - ω SST model was used. So, an $y^+ \approx 1$ was targeted on all the walls of the computational domain.

3.2.3 Comparison between Numerical and ASHRAE results

In this section a comparison between the CFD parametric analysis performed on elbow ducts and the ASHRAE data is provided.

First, the ASHRAE results are shown in figure 3.6. The trend of the K_{loss} coefficient as a function of the parameters is easily detectable. Indeed, it is evident that the K_{loss} coefficient has lower values for lower angles and vertically elongated ducts. In addition to that, even the K_{Reynolds} trend is shown even though the Reynolds number are not interesting for gas turbine ducts applications.

3-6 Elbow, Mitered, Rectangular (Idelchik et al. 1986, Diagram 6-5)

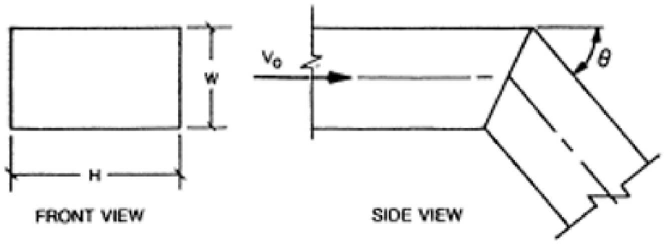

$C_o = K_{Re} C'_o$

θ, degrees	C'_o H/W 0.25	0.5	0.75	1.0	1.5	2.0	3.0	4.0	5.0	6.0	8.0
20	0.08	0.08	0.08	0.07	0.07	0.07	0.06	0.06	0.05	0.05	0.05
30	0.18	0.17	0.17	0.16	0.15	0.15	0.13	0.13	0.12	0.12	0.11
45	0.38	0.37	0.36	0.34	0.33	0.31	0.28	0.27	0.26	0.25	0.24
60	0.60	0.59	0.57	0.55	0.52	0.49	0.46	0.43	0.41	0.39	0.38
75	0.89	0.87	0.84	0.81	0.77	0.73	0.67	0.63	0.61	0.58	0.57
90	1.3	1.3	1.2	1.2	1.1	1.1	0.98	0.92	0.89	0.85	0.83

Reynolds Number Corrections Factors

$Re \times 10^{-4}$	1	2	3	4	6	8	10	≥14
K_{Re}	1.40	1.26	1.19	1.14	1.09	1.06	1.04	1.0

Figure 3.6: ASHRAE data for elbow ducts

As in the CFD simulations the Reynolds number effect was ignored, the results only include S_r and θ dependence. The results are shown in figure 3.7 where on the x-axis there is the shape ratio S_r and on the y-axis there is the K_{loss} coefficient. Each of the scatter group is related to one value of θ.

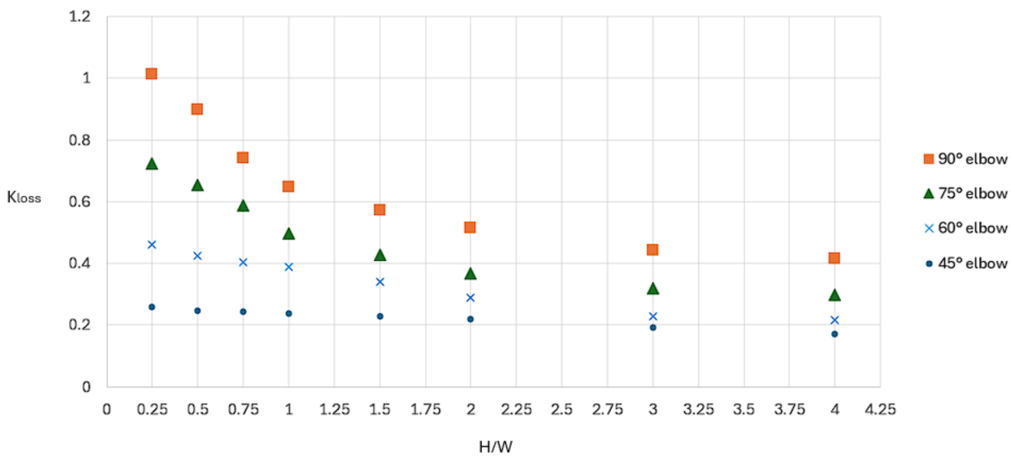

Figure 3.7: CFD results for elbow ducts

The mathematical model was developed only for 90° elbows since they are the most common intake duct fitting, and it consists of a simple logarithmic function defined as follows:

$$K_{\text{loss}} = \beta_1 \cdot ln(S_r) + \beta_2 \tag{3.2}$$

The model accuracy is high since the R^2 value is $R^2 = 0.9771$.

For better clarity even the graphical comparison between the numerical and the experimental data is provided in figure 3.8. As discussed previously, it is evident that the different Reynolds number range leads to a lower K_{loss} coefficient for elbow ducts in gas turbine intake systems compared to the literature.

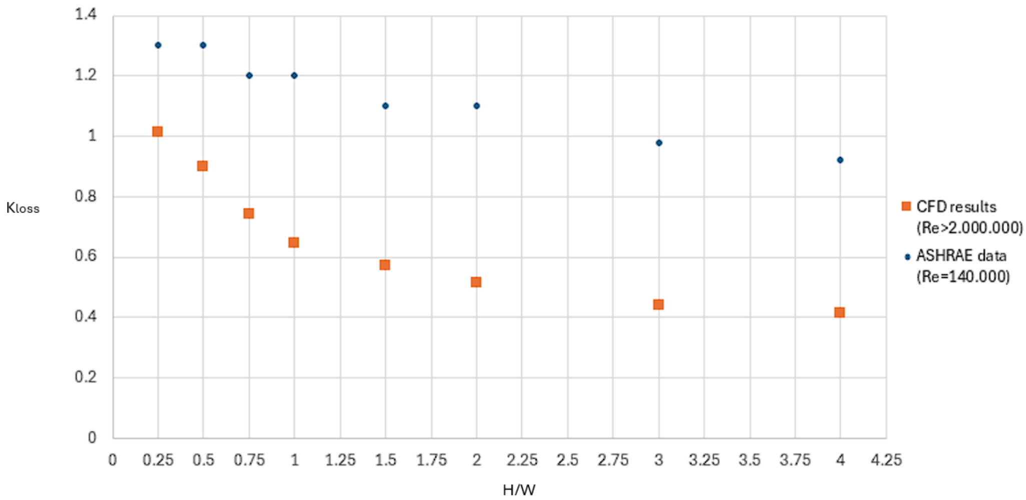

Figure 3.8: Comparison between CFD and ASHRAE data for elbow ducts

3.3 Convergent elbow transition

Convergent elbow transition is a typical gas turbine intake fitting used for very compact systems. Indeed, only one component adapts the filter house gas path to the typical dimensions of the silencer gas path and guarantees the passage from an horizontal duct to a vertical one. An example of a convergent elbow transition is provided in figure 3.9.

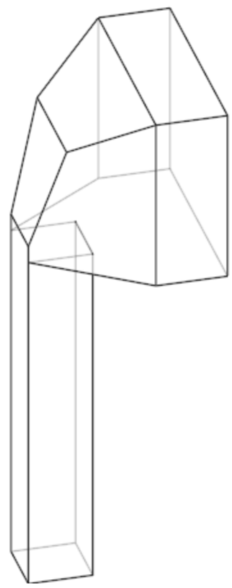

Figure 3.9: Convergent elbow transition

3.3.1 Investigated parameters and design points

As described before, to create a proper mathematical model is necessary to choose the key geometric parameters. In this case, since the fitting does not exist in literature, the parameters were chosen by studying technical drawings. After an accurate study where the typical differences between the intake arrangements were detected, the following parameters were detected:

- H that is the transition inlet height;
- R that is the outlet radius only on the edge perpendicular to the main flow direction;

It is worth noting that the other gas path dimension, the one orthogonal to the main flow direction, was neglected due to the low variability of this parameter between the arrangements that were analysed. To understand how these parameters affect the geometry of the intake transition is better to refer at figures 3.10a and 3.10b.

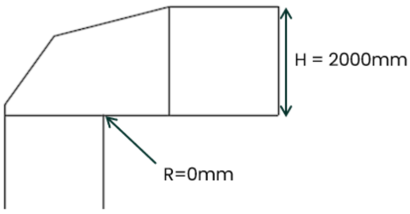

(a) Minimum R and H values

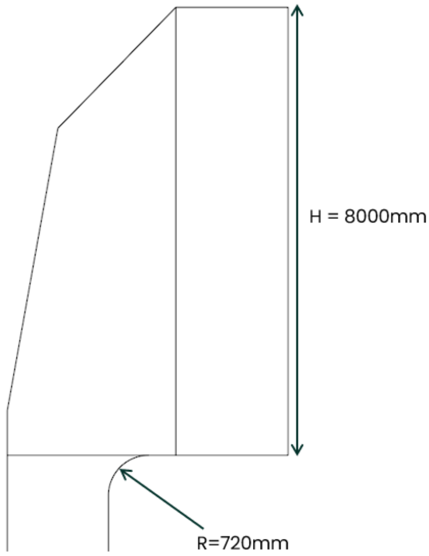

(b) Maximum R and H values

Figure 3.10: Key parameters for convergent elbow transitions

In these images the boundary values of the parameters are specified, as this information points out which are the limits of the mathematical model developed. Clearly, having $R = 0mm$ means that there is a sharp edge at the fitting outlet. Since CFD simulations were performed only inside the range depicted in 3.5, each value extrapolated outside of this range must be validated. The boundary values were chosen starting from an assessment of the existing configurations by aiming to cover all of them.

Table 3.5: Maximum and minimum R and H values for convergent elbow transitions

Parameter	Minimum value [mm]	Maximum value [mm]
R	0	720
H	1000	8000

3.3.2 Mesh and parametric CFD simulation setup

The mesh consists of an unstructured polyhedral mesh and was developed in ANSYS Fluent Meshing by using ANSYS Watertight Mesh Workflow. The obtained mesh is displayed in figure 3.11.

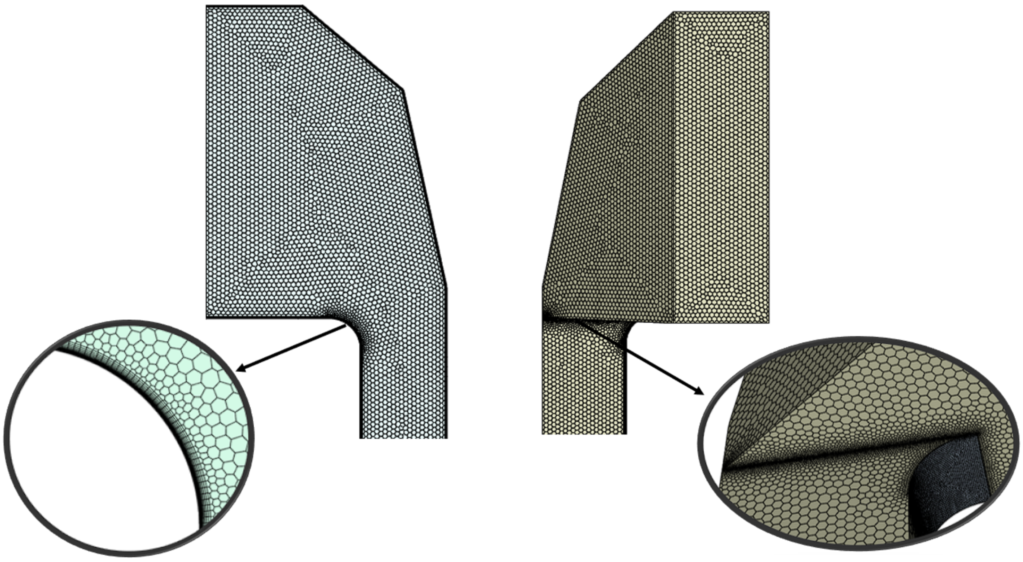

(a) Internal mesh with focus on boundary layer inflation on the filleted edge

(b) External mesh with focus on edge refinement

Figure 3.11: Convergent elbow transition mesh

It is evident that mesh refinements were performed on the edges and on the fillet to obtain a higher mesh quality. The mesh parameters used for this parametric analysis are specified in table 3.6.

Table 3.6: Mesh parameters for convergent elbow transition

Edge sizing	Face sizing	Domain sizing	First element thickness	Inflation elements
8mm	20mm	100mm	0.035mm	30

Even in this case, the purpose was to target an y^+ value of approximately 1 in all the computational domain. Indeed, the turbulence model used for the analysis is the BSL Reynolds Stress Model that uses an omega wall resolved approach.

3.3.3 Numerical results and mathematical model

In this section since no experimental data exists, only the numerical data are discussed without comparing or validating them. However, it is easy to predict the behaviour of the K_{loss} coefficient of this fitting by doing some physical considerations.

First, predicting how the K_{loss} coefficient behaves as a function of the radius R is quite easy. As the radius (R) increases the velocity around the fillet gets lower and the separation point moves downstream. Having a larger radius is clearly beneficial in terms of pressure drop as it avoids flow detachment.

The behaviour of the K_{loss} coefficient as a function of height (H) is less intuitive but still easy to understand. Indeed, in transition with high H values the amount of air that passes above the edge perpendicular to the flow direction is lower. Thus, considering that the air passing above that edge separates, these configurations are characterized by smaller separation zones and consequently by smaller pressure drop values.

Another easy consideration on the K_{loss} coefficient of this fitting is that the value is expected to be lower to the one of 90° elbows without a converging gas path. Indeed, as discussed previously, converging sections implies lower entropy generation. On the other hand, the K_{loss} coefficient is expected to be higher to the one of convergent elbows.

In figure 3.12 the flow path lines for 2 different configurations are shown. The flow separation appears more evident in the configuration indicated as most dissipative that is characterized by low H values and low R values. Since the separation is large, it is important to study how the other fittings behave when are positioned downstream to a convergent elbow transition, and this is the reason why this fitting is also studied in chapter 5.

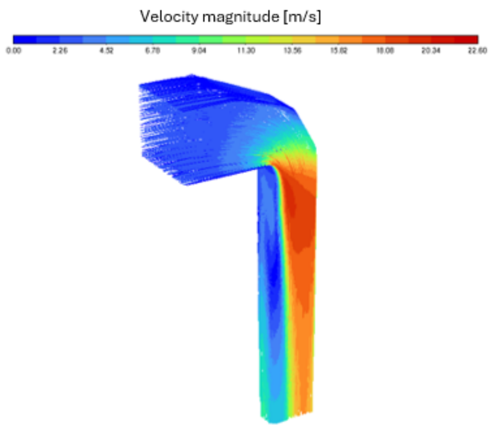

(a) $H = 2500\,\text{mm},\ R = 0\,\text{mm}$

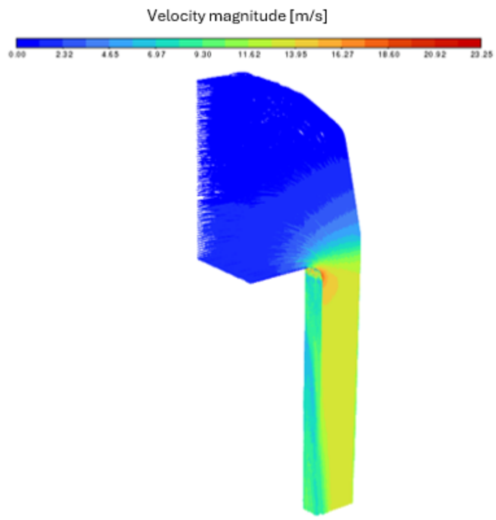

(b) $H = 6500\,\text{mm},\ R = 640\,\text{mm}$

Figure 3.12: Velocity magnitude coloured path lines for least and most dissipative convergent elbow transition configurations

The numerical data were post-processed in Octave and a general law that correlate the K_{loss} coefficient to R and H was developed. The mathematical model consists of a 9 parameters scalar power-law function and was defined as follows:

$$
\begin{aligned}
K_{loss}(R,H) = \beta_1 &+ \beta_2(R+\beta_9)^{-1} + \beta_3 H^{-1} + \beta_4(R+\beta_9)^{-2} \\
&+ \beta_5(R+\beta_9)^{-1}H^{-1} + \beta_6 H^{-2} + \beta_7(R+\beta_9)^{-2}H^{-1} \\
&+ \beta_8(R+\beta_9)^{-1}H^{-2}
\end{aligned}
\tag{3.3}
$$

The parameters were calibrated to optimize the fitting by lowering as much as possible the R^2 and $RMSE$ values. The 3D graph of this scalar function is the one shown in figure 3.13:

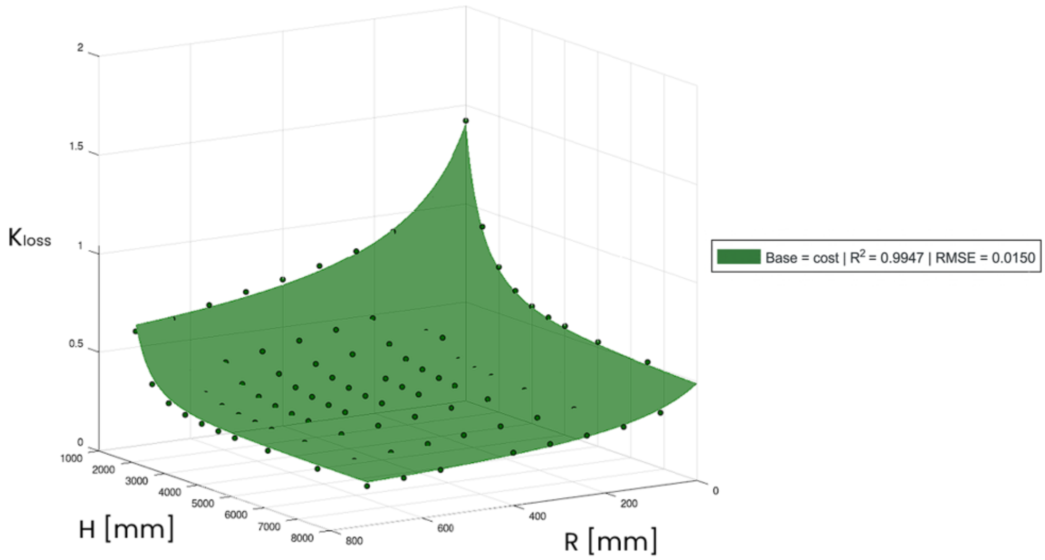

Figure 3.13: K_{loss} coefficient for convergent elbow silencers as a function of R and H

The effect described in words before is clearly shown in the graph since the most dissipative configurations are the ones with low H values and low R values.

3.4 Pyramidal convergent transition

The pyramidal convergent transition is a typical gas turbine intake fitting that is needed to adapt the filter house gas path to the typical dimensions of the ducts that brings air to the axial compressor. A fitting example is provided in figure 3.14.

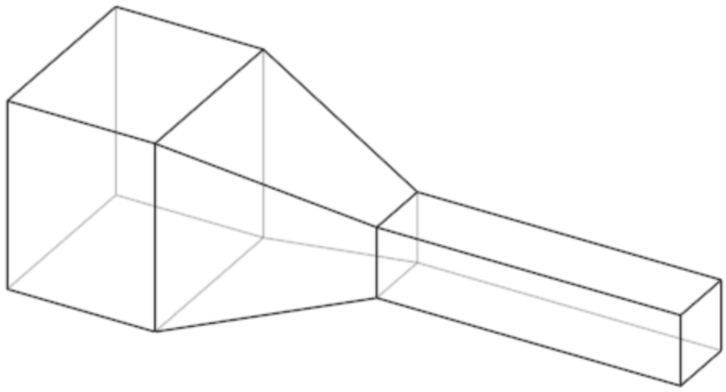

Figure 3.14: Pyramidal convergent transition

3.4.1 Investigated parameters and design points

To create a proper mathematical model is necessary to choose the geometric parameters that have strong impact on pressure drop. Since this fitting is common and it was already studied in the past, the parameters are derived from the following Idelchik formulation [2]:

$$\begin{aligned} K_{\text{loss}}(Ar,\theta) = &(-0.0125Ar^4 + 0.0224Ar^3 - 0.00723Ar^2 + 0.00444Ar - 0.00745) \\ &\times (\theta^3 - 2\pi\theta^2 - 10\theta) \end{aligned} \tag{3.4}$$

Where the parameters are A_r and θ, that are taken as shown in the images 3.15a and 3.15b:

- A_r is the ratio between inlet area and outlet area $A_r = \frac{A_{\text{inlet}}}{A_{\text{outlet}}} < 1$;
- θ is the maximum transition angle between the one calculated from top view and the one calculated from side view;

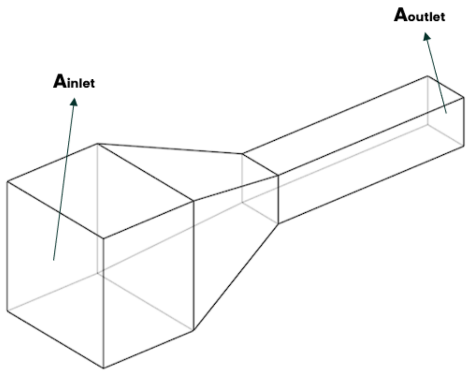

(a) Ar

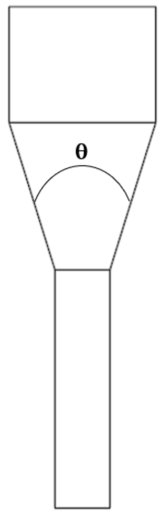

(b) θ

Figure 3.15: Key parameters for pyramidal convergent transition

Rather than investigating a wide range for these two parameters, the primary objective of this analysis is to confirm the behaviour previously observed for elbow ducts. Therefore, the numerical pressure drop is expected to be lower than the experimental value. For this study, only a limited number of A_r values were examined, while keeping the θ value constant.

3.4.2 Parametric CFD simulation setup

In this section the meshing process is discussed. For this analysis a structured hexahedral mesh was built using ANSYS Mechanical Meshing. The procedure consists of enforcing an equal number of divisions for the reciprocal edges. The obtained mesh is shown in figure 3.16.

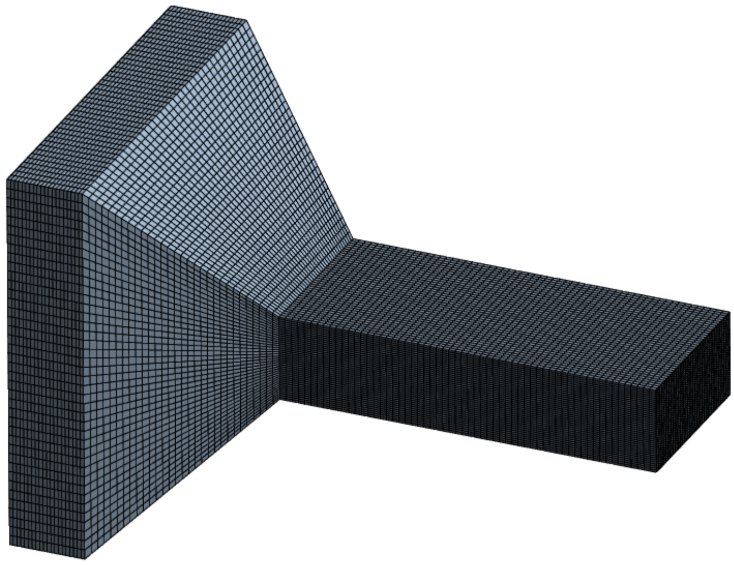

Figure 3.16: Hexahedral structured mesh for pyramidal convergent transition

As the number of divisions is provided, the element dimensions are variable since the geometry varies. The number of divisions was provided to target high mesh quality. The inflation parameters are detailed in table: 3.7.

Table 3.7: Mesh parameters for convergent pyramidal transition analysis

First element thickness	Inflation elements
0.02mm	35

Obviously, even in this case the purpose was to target an y^+ value of approximately 1 in all the computational domain since the turbulence model used for the analysis is the BSL Reynolds Stress Model that uses a wall resolved approach.

3.4.3 Numerical and ASHRAE results

In this section a comparison between the numerical results and the results obtained through the Idelchik formula 3.4 is performed. As shown while discussing elbow ducts, the Reynolds number has an influence on the K_{loss} coefficient value. Therefore, the analytical results are expected to be generally lower than the empirical ones.

In addition to that, the K_{loss} coefficient for this fitting is typically low since convergent transitions exhibit a positive pressure gradient, that is good for flow reattachment and guarantee low entropy and laminar flow even at very high Reynolds numbers. As shown in figure 3.17 the flow separation only occurs in corners, and the flow reattaches only a few meters downstream the transition outlet.

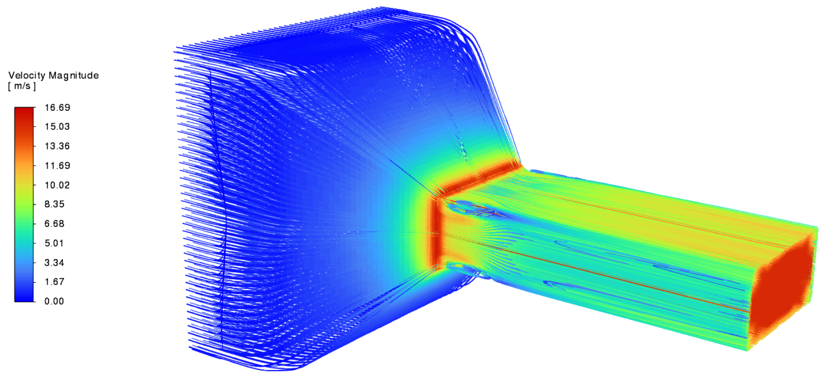

Figure 3.17: Pyramidal convergent transition path lines coloured by velocity magnitude

It is worth noting that no interdependence analyses were performed by coupling this component to silencers. Indeed, since the separation is not large, it is reasonable to assume that the flow entering a silencer positioned downstream of the pyramidal transition is almost uniform, even at short distances. Consequently, the pressure drop of the entire system is merely considered as the sum of the two contributions.

The results of the parametric analysis are detailed in graph 3.18

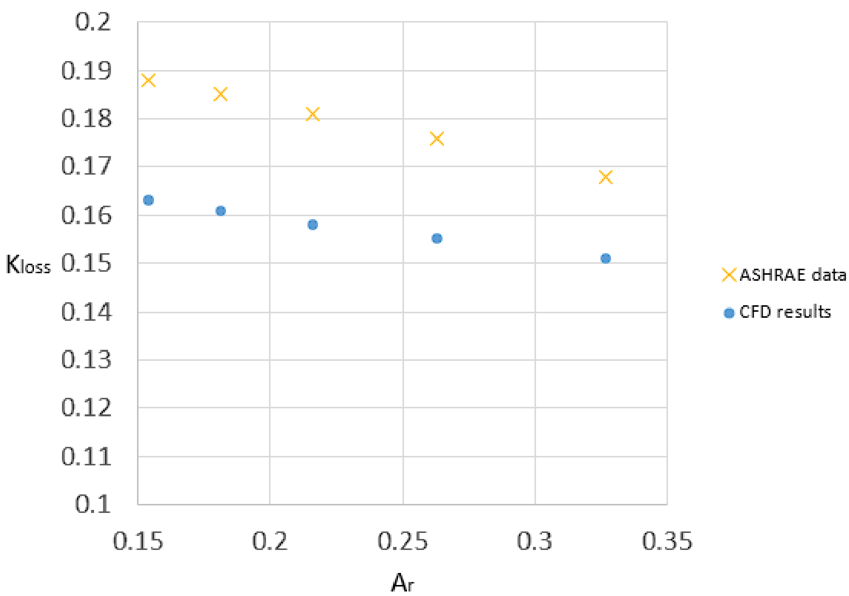

Figure 3.18: Analytical and experimental values of the K_{loss} coefficient for pyramidal convergent transitions

It is evident that the exact same behaviour described previously for elbow ducts is detected also for pyramidal convergent transitions. Therefore, the K_{loss} coefficient related to these fittings is calculated through a similar version of the Idelchik formula that features different coefficients.

3.5 Modular components: fixed geometric parameters

In gas turbine intake arrangements, there are some components that are characterized by non-variable geometric parameters and are used as modular items. Having fixed geometrical parameters implies that a parametric study for these components is not required, and a single CFD simulation is enough to calculate the K_{loss} coefficient.

There are many modular components in gas turbine intake ducts such as curves or silencers with fixed geometry. Only one is presented here as an example, since it was used for results validation in chapter 6. It is denoted as "Modular curve", and it consists of a horizontal elbow with 3 guiding vanes and a vertical elbow with a filleted connection to the intake plenum. This fitting is shown in figure 3.19.

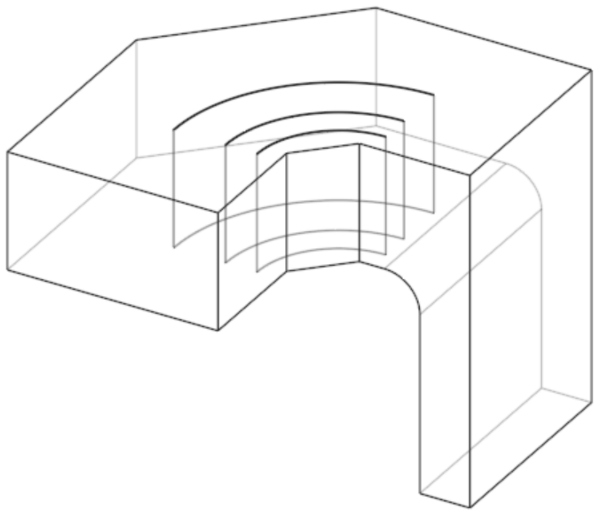

Figure 3.19: Modular curve

Another example of standard components are expansion joints that are a structural separation designed to absorb thermal expansion and contraction, as well as movements caused by loads, vibrations, or seismic activity. Expansion joints are built of rubber or textile materials and are fundamentals to prevent damages to the structure. Clearly, inside intake ducts pressure is lower than ambient external pressure. The pressure difference acts on the expansion joints, so textile ones intrude into the flow generating vortices and disturbing the flow. The behaviour of rubber expansion joints is the opposite, because rubber is stiff enough to avoid intrusion. So, when rubber expansion joints are used, they cause a sudden expansion of the flow path. Expansion joints gave minor contribution to the overall pressure drop of gas turbine intake systems but were modelled to reach greater accuracy. In particular, textile expansion joints were modelled as sudden reduction of area and rubber expansion joints as sudden increment of area, and their K_{loss} coefficient was derived.

Chapter 4

Parallel baffle silencers

4.1 Acoustic and Aerodynamic Performances of parallel baffle Silencers

The intake silencers consist of a duct and a series of internal sound-absorbing panels also called baffles. The design of the silencer baffles depend on the noise level specified in the contract, both in the near field and at the far field. The sound-absorbing panels are made of an outer casing in perforated sheet metal, which may be stainless steel, marine-grade aluminium, or galvanized steel, containing mats of rock wool or other sound-absorbing materials.

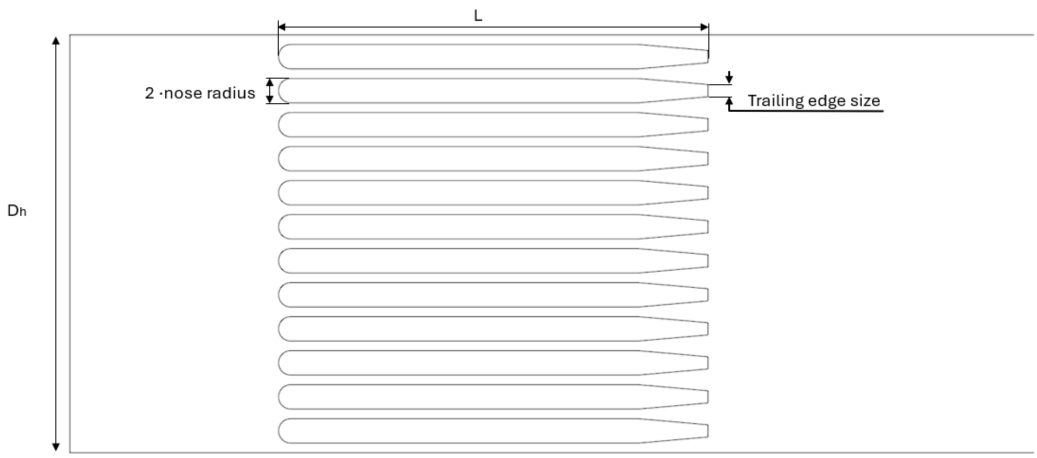

Figure 4.1: Schematic representation of a parallel baffle silencer

Any silencer used in a duct system should fulfil certain criteria to be considered properly designed [6]. Criteria related to diverse fields such as acoustics, aerodynamics, mechanics must be met. The disciplines of interest in this section are:

- Acoustic: silencers must reduce incoming sound by the desired amount. The fundamental parameter is the transmission loss (TL) or absorption (A) which is an intrinsic property of a silencer, defined as the difference between the incident acoustic power and the transmitted acoustic power, measured under standardized laboratory conditions.

- Aerodynamic: silencers must not generate large pressure drops since in industrial gas turbine plants this could cause efficiency losses.

Creating a performative silencer from the acoustic point of view generally entails that the aerodynamic performances of the silencer are not satisfying, so these two disciplines are often conflicting with each other. Therefore, is important to find the right compromise to fulfil the design criteria of each discipline at a satisfactory degree. In this section one of the existing analytical methods to calculate absorption (A) are briefly described to clarify the reasons why aerodynamic and acoustic criteria conflict.

In literature many different computational methods exist to assess the acoustic performances of a parallel baffle silencer, here, only the one proposed by Embleton is presented. In his book a graph is discussed to estimate the total attenuation of a parallel baffle absorber with only a few parameters given. The parameters needed are the baffle width, the spacing between the baffles, their length and the wavelength of sound.

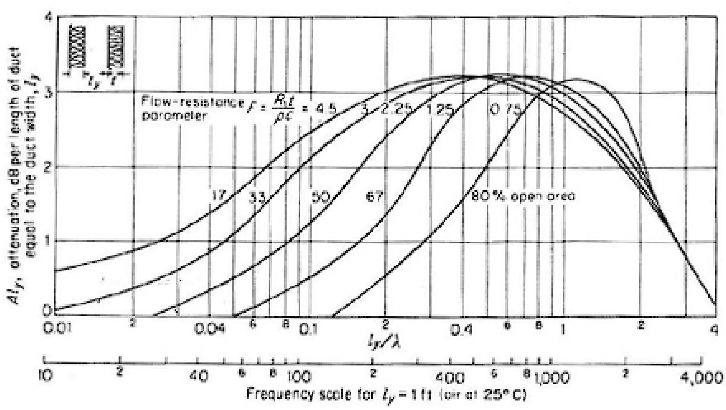

Figure 4.2: Sound absorption as a function of the open area (OA) and the baffle length (L) for different frequencies

Using this graph gives values for the attenuation per length of duct equal to duct width, which can then be converted to total attenuation for the entire length of the baffles. It should be noted that this graph assumes that there is no flow in the duct and that the frequency scale shall be used under the assumption of air at 25 °C. The graph can be used for any gas with known speed of sound and temperature. It is also worth to add that for air, temperature variations cause little differences.

This graph makes it easy to understand how the constructive parameters of parallel baffle silencers influence the acoustic performances. The parameters required for an appropriate interpretation of the graph are:

- Open Area (OA)

- Baffle length (L)

Assessing how the baffles length (L) affects the attenuation (A) is easy since A scales linearly with L, as on the y-axis of the graph there is the attenuation A for a length equal to l_y. Therefore, it is always a good choice to increase L whether more attenuation is requested.

To identify the effect of the open area OA is useful to consider duct width equal to 1ft, in this way on the x-axis there is the sound frequency in Hz. To have a proper attenuation at very low frequencies, for example 100Hz, it is necessary to use low values of OA. When $\frac{l_y}{\lambda} < 0.1$ is preferable to use another prediction method as the results become unreliable. For these frequencies Embleton proposes using an equation by Sabine who empirically found that attenuation in ducts for low frequencies can be expressed as:

$$A = 12.6(\alpha_{sab})^{1.4}\frac{P}{39.37 \cdot OA} \tag{4.1}$$

Also in this equation is shown that absorption is inversely proportional to open area.

As is seen in the graph the attenuation starts to rapidly drop at higher frequencies. Embleton explains this as being caused by a “beaming effect” as high frequency sound simply passes in between the baffles, avoiding the absorptive material.

It’s also worth adding that when gas flows in the same direction as the sound waves, the resulting attenuation will be lowered due to the sound having less time to be absorbed by the baffles. When the direction of the flow is in the opposite direction the total attenuation is instead increased. Embleton presents an equation for how the effect of flow can be estimated given the speed of the flowing gas.

$$A = A_0\left(\frac{1+\gamma|M|}{1+M}\right) \tag{4.2}$$

Therefore, considering that the Mach number (Ma) is negative inside intake parallel baffle silencers, these devices generally show lower acoustic performances when compared to exhaust ones.

4.2 Investigated geometrical parameters

As discussed before, silencer design must be a compromise between aerodynamic and acoustic performances. To get better acoustic performances it is necessary to have baffles characterized by greater length and precise width. Varying these parameters can lead to better acoustic performances but it often occurs in higher pressure drop.

To create a mathematical model used for silencer pressure drop prediction the influential geometrical parameters need to be determined. After some reviews and analyses the following parameters were detected:

- Area ratio (Ar)
- Baffle length (L)
- Silencer baffle shape and taper ratio (T_r)
- Reynolds number (Re)
- Ratio of the length of the side orthogonal to baffles to baffles number (N_r)

The Area ratio (Ar) is defined as the ratio between the obstructed area and the free gas path area, as shown by the following formulation:

$$A_r = \frac{N_{\text{baffles}} \cdot W_{\text{baffles}}}{L_{\perp}} \tag{4.3}$$

where:

- A_r is the dimensionless geometric parameter;
- N_{baffles} is the number of baffles;
- W_{baffles} is the width of each baffle;
- $L_{\perp}$ is the dimension of the gas path side perpendicular to the panels.

The Area ratio (A_r) can also be calculated starting from the open area that is used to evaluate the acoustic performances as follows:

$$A_r = 1 - OA \tag{4.4}$$

The baffle length (L) is the overall length of the panel in the flow direction comprehensive of the nose radius and the tail.

To mitigate the effect on pressure drop, when the design and cost boundaries permit it, a more streamlined and aerodynamic shape can be used. These shapes are characterized by different tail shapes, and the mathematical parameter introduced to account for them is the taper ratio T_r that is defined as follows:

$$T_r = \frac{2 \cdot \text{nose radius}}{\text{trailing edge size}} \tag{4.5}$$

Therefore, the taper ratio essentially defines how thicker the leading edge of the panel is when compared with the trailing edge. Considering this definition, it is evident that a more streamlined shape entails higher T_r values. There are many different shapes that are used for baffles, the ones inspected using T_r are commonly denoted as "tapered-end silencers" but also "double-bullnose silencers are widely diffused. The different shapes investigated in this research are presented in image 4.3

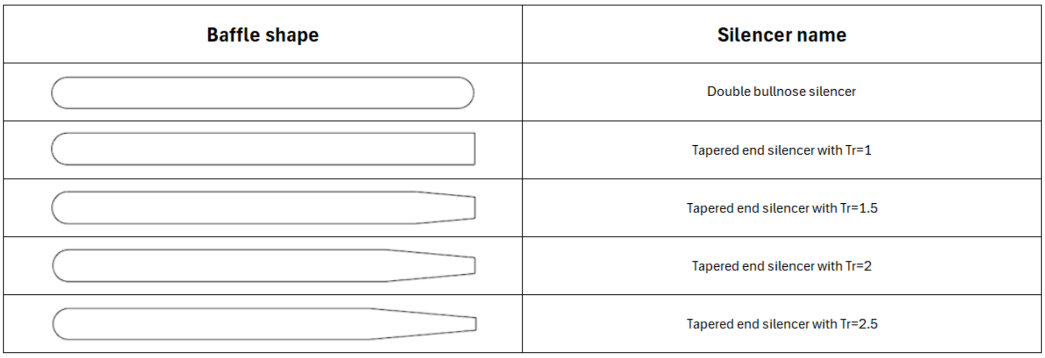

Figure 4.3: Different baffle shapes

Tapered end silencer tails are designed using a constant value of the taper angle that is small enough to avoid flow detachment.

Obviously, the Reynolds number (Re) influences the overall pressure drop of a parallel baffle silencer. Reynolds number values for gas turbine intake arrangements are very high, so the same observations made in the last chapter are also valid now. Therefore, even large variations of Re does not affect pressure drop values. This aspect will be further investigated in subsection 4.3.1.

The last important parameter is the ratio of the length of the side orthogonal to baffles to baffle number, that is denoted using N_r and is calculated as follows:

$$N_r = \frac{L_\perp}{N_{\text{baffles}}} \tag{4.6}$$

In the next analysis, the fact that pressure losses are related to N_r instead of simply being related to N_{baffles} is explained.

4.3 Parallel baffle silencer mathematical model for pressure drop calculation

In this section all the analyses performed to define a mathematical model and the methodology used for silencer K_{loss} coefficient calculation are explained. First a brief description of the CFD simulation setup is provided. In a second moment, the sensitivity of the K_{loss} coefficient to the previously discussed parameters is investigated.

4.3.1 Mesh and CFD simulation setup

In order to study parallel baffle silencers, 2D CFD simulations were chosen to reduce the computational expense of a single design point. This choice was driven by different considerations, such as the fact that on silencers a very large dataset was created to account for all the parameters of influence. The 2D assumption ignores the effect of the walls in the direction orthogonal to the baffles. Brief CFD tests to account for difference between 3D and 2D results were performed and the deviation in terms of pressure losses was negligible.

The meshing operations were performed using ANSYS Mechanical Meshing and are based on multi-zone meshing that permits to obtain a semi-structured mesh. The goal was to obtain an $y^+ \approx 1$ on the entire computational domain as the K-ω SST model was used for these simulations. The mesh is identical to the one presented in chapter 2 in figure 2.5b.

The mesh parameters are expressed in table 4.1:

Table 4.1: Mesh parameters for CFD silencer simulations

Baffle sizing	Domain sizing	First element thickness	Inflation elements
7.5 [mm]	20 [mm]	0.01 [mm]	30

4.3.2 Assessment of Reynolds number independence

This analysis has the goal of demonstrating that Reynolds number (Re) variations in the regime of interest does not affect the pressure drop. To do so, 2D CFD analyses were performed to analyse three different Reynolds numbers. In these sets of simulations, the Reynolds number is varied through studying three different silencer characterized by diverse hydraulic diameters. In the meantime, also A_r and L dependence was studied varying these two parameters within the same ranges for each of the three different values of D_h. This specific analysis is performed on double-bullnose silencers, but it is reasonable to assume that the result is general and applicable even to tapered-end ones.

Hydraulic diameters affect the Reynolds number since for rectangular ducts the

Reynolds number (Re) is calculated as follows:

$$Re = \frac{\rho v D_h}{\mu} \tag{4.7}$$

The tested hydraulic diameters, and the consequent Reynolds number are described in table 4.2.

Table 4.2: Hydraulic diameters, baffles number and equivalent Reynolds number of the inspected configurations

D_h	Re	N_{baffles}
2000	$4.13 \cdot 10^6$	8
3500	$7.23 \cdot 10^6$	14
5000	$1.03 \cdot 10^7$	20

It is worth underlining the fact that the baffle number is varied in this analysis to keep a constant value of N_r, indeed:

$$N_r = \frac{L_\perp}{N_{\text{baffles}}} = \frac{2000}{8} = \frac{3500}{14} = \frac{5000}{20} = 250 \tag{4.8}$$

As detailed before the baffle number N_{baffles} does not affect the pressure drop values, instead in subsection 4.3.4 the influence of N_r is explained.

The analyses were performed over a precise range of A_r and L that was more than sufficient for the scope of the analysis. The maximum and minimum A_r and L values are shown in table 4.3:

Table 4.3: Maximum and minimum A_r and L values for silencer simulations

Parameter	Minimum value	Maximum value
Ar	1	0.7
L	1500 [mm]	2700 [mm]

The output of this study are three different interpolating surfaces, one for each Reynolds number value. Each surface is related to one value of hydraulic diameter (D_h) and this means that each surface describes what happens at a specific Reynolds number (Re). These surfaces are the graphs of scalar functions of two variables which are A_r and L. The graphs are shown in figure 4.4:

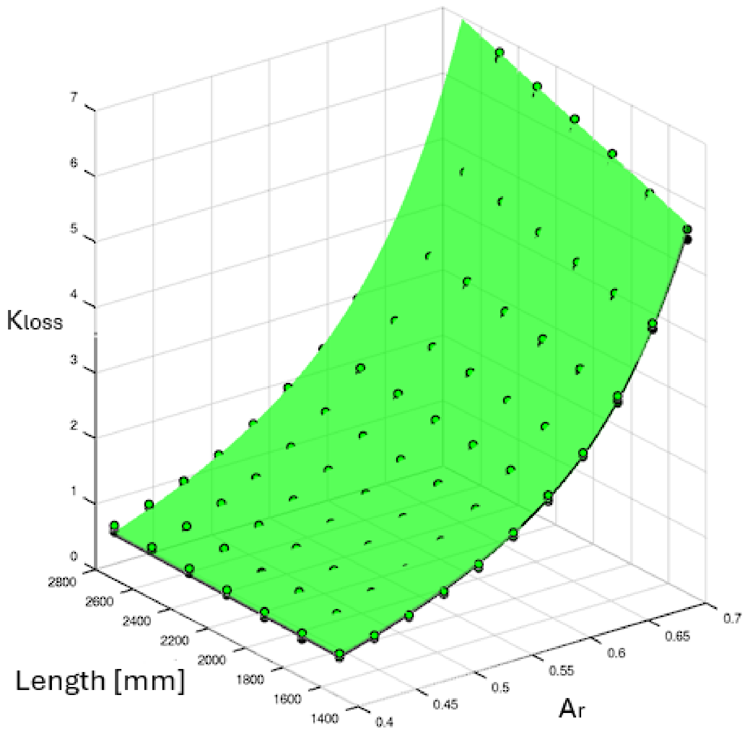

(a) K_{loss} as a function of A_r and L

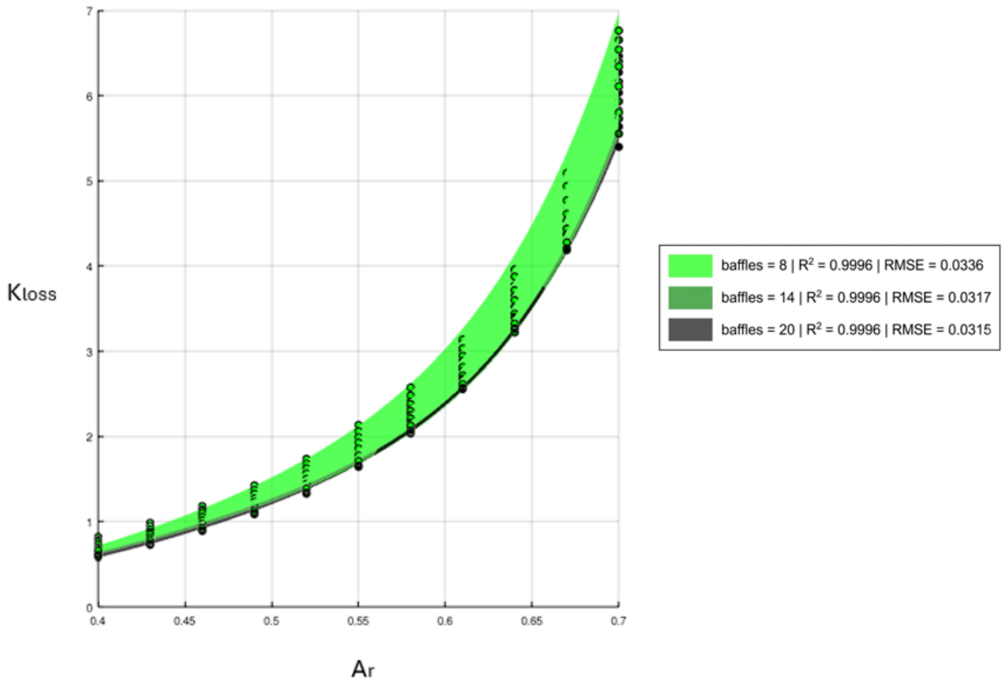

(b) K_{loss} expressed as a function of A_r

Figure 4.4: K_{loss} as a function of A_r and L for 3 groups corresponding to different Reynolds numbers

The scatters on the graphs represent the single CFD simulation output and the surfaces are built by interpolating these values. It is evident that the deviation between one surface to the other is negligible since the scatters, as the different surfaces, are almost overlapping. Therefore, it is reasonable to assume that the Reynolds number does not affect pressure losses in this regime. One interesting aspect to underline is that, in accordance with literature, the K_{loss} coefficient values are slightly lower for higher Reynolds numbers, so for bigger ducts. As even smaller ducts generally grantee a high enough Reynolds number (above 10^6), the analysis was not performed to detect the threshold Reynolds number value at which this behaviour is no longer valid.

4.3.3 K_{loss} coefficient scalar function of two variables: A_r and L

The largest number of analyses on parallel baffle silencers were performed to understand how A_r and L affect the K_{loss} coefficient. The CAD models used for the development of the mathematical model is a 2D parallel baffle silencer with 8 panels and $L_\perp = D_h = 2000$ [mm]. Using these parameters entails that this model is developed for $N_r = 250$.

It is evident that the losses caused by the length of the baffles are related to friction, therefore pressure drop is going to scale linearly with the length of the baffles L. This is consistent with Darcy-Weisbach formula 1.17, that is used to calculate the loss of energy or pressure in a pipe due to friction.

As said before, for gas turbine intake ducts, as the flow velocity is low and the hydraulic diameters are significant if compared to duct lengths, it is possible to assume that friction losses are negligible. However, this condition decays when considering parallel baffle silencers, since the flow accelerates inside them and hydraulic diameters are no longer large enough.

On the other hand, it is difficult to predict which mathematical dependence there is between pressure drop and the parameter A_r. For this reason, the design points were chosen to cover a very wide range of A_r values and this caused to have many design points to simulate. This was done to develop a mathematical model reliable enough while doing data extrapolations out of the sample domain. The model robustness is described in paragraph 4.3.6 that is focused on a data extrapolation test of the mathematical model. That test consists of evaluating how closely the pressure drop values predicted by the analytical model match the corresponding CFD results when the simulated points lie outside the sample domain on which the model was calibrated.

As described before, the analysis has been performed over a large A_r range but a quite narrow L range if compared to the existing and possible silencer dimensions. A wider L range would have been useless since K_{loss} scales linearly with it and few design points are enough to describe this behaviour. The maximum and minimum A_r and L values are shown in table 4.4:

Table 4.4: Maximum and minimum A_r and L values for Reynolds number independence study

Parameter	Minimum value	Maximum value
A_r	0.28	0.85
L	1500 [mm]	2900 [mm]

Several mathematical models were tested to interpolate the CFD results, but the final choice was a model based on exponential formulation linking the K_{loss} coefficient to A_r. Indeed, even though exponential models are difficult to calibrate, they ensure the absence of inflection points providing higher accuracy once data extrapolation is performed. To capture the K_{loss} coefficient variation along the A_r and L domain, even high-degree polynomials could be used as they are easier to calibrate but they can exhibit multiple inflection points. These inflection points give the model unpredictable behaviour.

The model developed is described by the following mathematical formulation that relies on 13 parameters:

$$K_{\text{loss}}(Ar, L) = \beta_1\, e^{\beta_2 Ar^{\beta_3} + \beta_4 Ar^{\beta_5} + \beta_6} + \beta_7\, e^{\beta_8 Ar^{\beta_9} + \beta_{10} Ar^{\beta_{11}} + \beta_{12}} \cdot L + \beta_{13} \tag{4.9}$$

The resulting interpolation is shown in the graphs 4.5 and the legend also reports R^2 and $RMSE$ values:

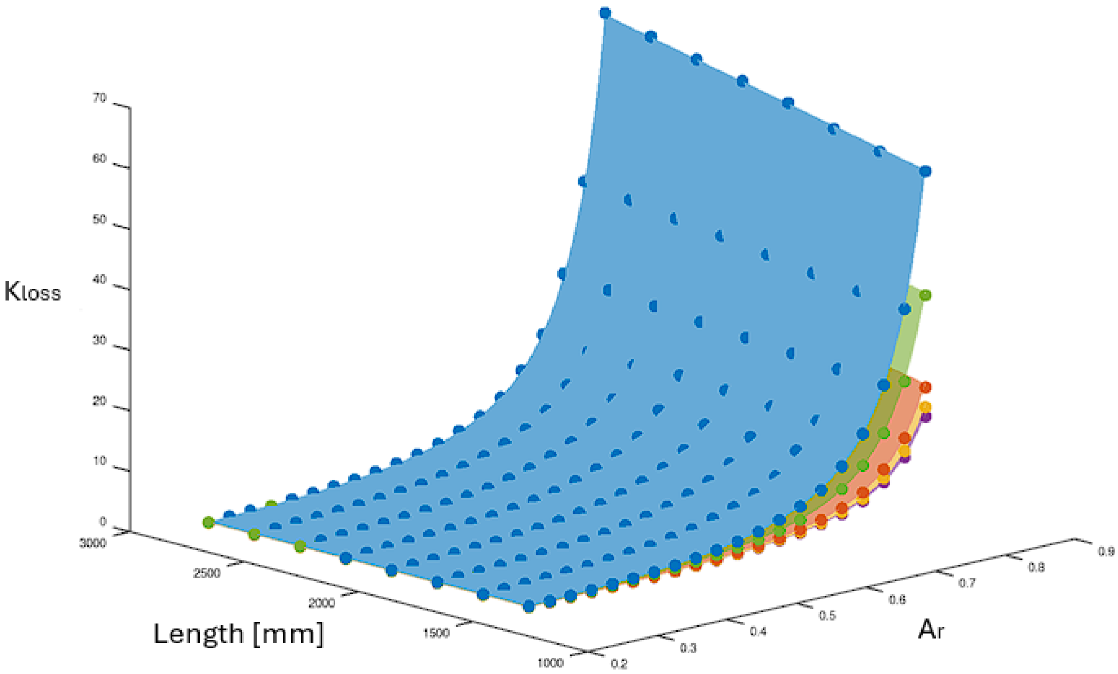

(a) K_{loss} as a function of A_r and L

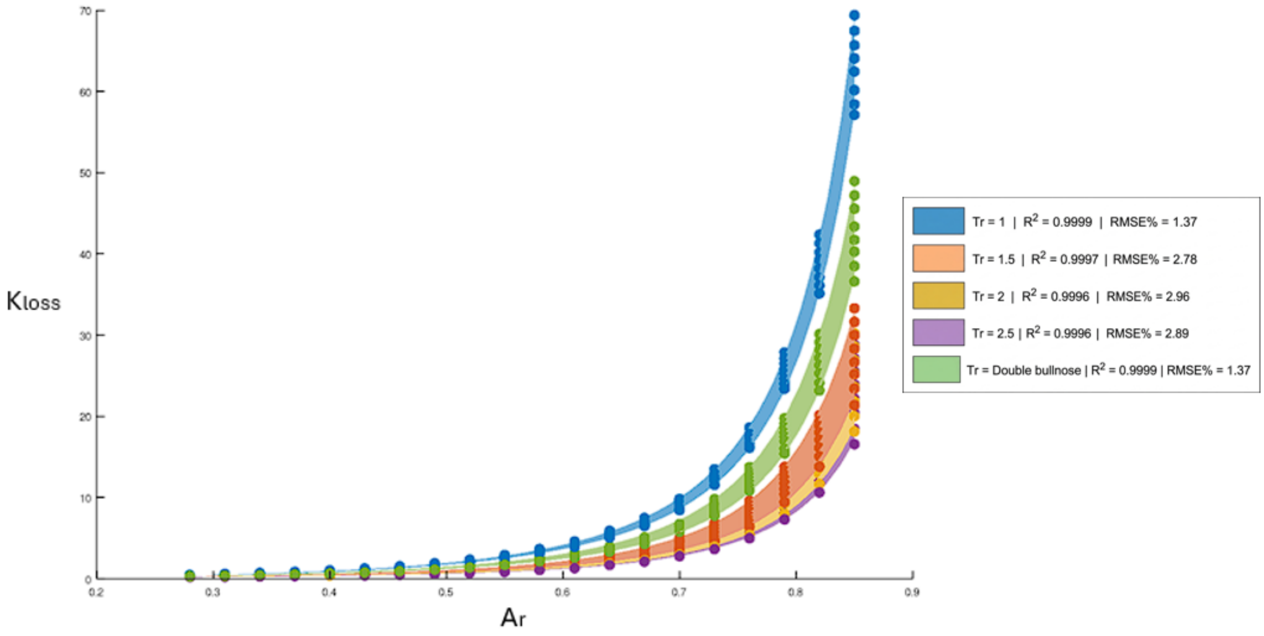

(b) K_{loss} as a function of A_r

Figure 4.5: K_{loss} as a function of A_r and L for five different panel shapes

Plotting these interpolating surfaces on the same graph allows for some qualitative analyses. As expected, the value of the K_{loss} coefficient scales linearly with L, but the parameters that strongly affect K_{loss} are T_r and A_r.

It is worth further investigating from the quantitative point of view how baffle shape variations influence pressure losses. To make this analysis, a fixed length was chosen: $L = 2200$ [mm]. For this specific value of L, the K_{loss} trend as a function of A_r is shown on the following graph:

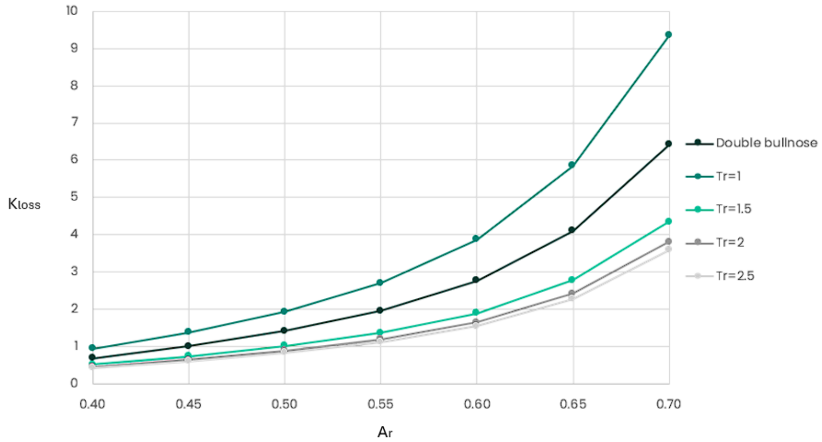

Figure 4.6: K_{loss} as a function of A_r for different panel shapes with fixed panel length $L = 2200$ [mm]

To evaluate the shape effect, the double-bullnose silencers are used as a reference. Thus, the percentage deviation of the K_{loss} coefficient from double-bullnose silencers to tapered-end ones is calculated as follows:

$$\text{Deviation } \% = \frac{K_{\text{tapered-end}} - K_{\text{double-bullnose}}}{K_{\text{double-bullnose}}} \cdot 100 \tag{4.10}$$

The results are summed up in graph 4.7 and table 4.5:

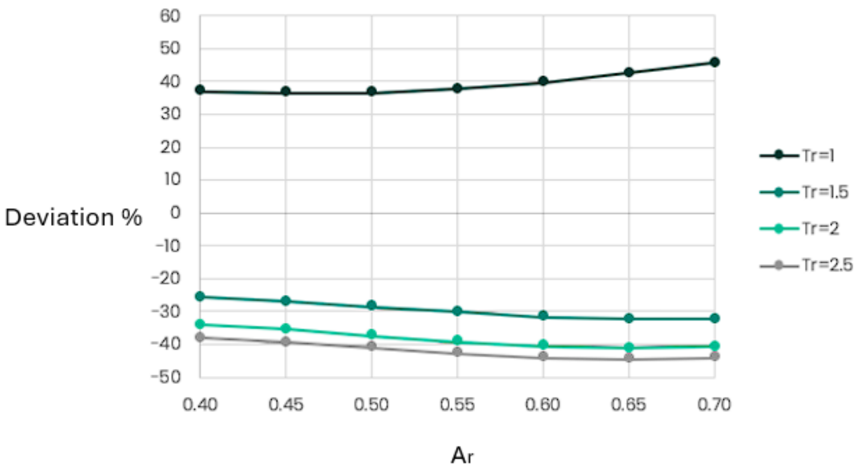

Figure 4.7: Percentage deviation of the K_{loss} coefficient for tapered-end silencers relative to double-bullnose configurations expressed as an A_r function

Table 4.5: Percentage deviation of K_{loss} coefficient over A_r for different panel shapes

A_r	Dev% for $T_r = 1$	Dev% for $T_r = 1.5$	Dev% for $T_r = 2$	Dev% for $T_r = 2.5$
0.4	36.20	-24.97	-33.03	-36.80
0.45	35.56	-25.99	-34.27	-37.90
0.5	35.40	-27.26	-35.75	-39.20
0.55	36.09	-28.66	-37.26	-40.54
0.6	37.90	-29.91	-38.48	-41.60
0.65	40.70	-30.66	-39.00	-42.05
0.7	43.84	-30.72	-38.68	-41.77

Therefore, using a silencer with baffles characterized by $T_r = 1$ is harmful for the aerodynamic performances, but could happen if inside the ducts there is not enough available space along the flow direction. On the other hand, using other types of tapered-end silencers is clearly beneficial for the aerodynamic performances, as pressure drop decreases by $25\% \div 42\%$. It is also worth to note that as the taper ratio T_r increases from $T_r = 1.5$ to $T_r = 2$ the K_{loss} coefficient decreases by nearly 8%, instead, passing from $T_r = 2$ to $T_r = 2.5$ generates a pressure drop decrease of nearly 3%. Therefore, pressure drop does not scale linearly with T_r and the influence of the taper ratio T_r becomes progressively weaker at higher values.

4.3.4 Corrective coefficient K_{corr} introduced to describe N_r influence

As stated before, the number of baffles is not the parameter that directly affects the K_{loss} coefficient. In fact, as seen while discussing the Reynolds number dependence, varying the baffles number N_{baffles} from 8 to 20 while linearly varying the gas path dimension does not affect the pressure drop.

After some tests, the ratio of the length of the gas path side orthogonal to baffles and the baffles number (N_r) was detected as the influential parameter. To account for the effect of N_r, a corrective coefficient K_{corr} was defined. Using this coefficient extends the scalar function discussed before to a wider range of silencers.

The analysis was performed keeping constant values for gas path side length and baffle length which are $L_\perp = 2000$ [mm] and $L = 2000$ [mm], respectively. The parameters varied in this analysis are A_r and the baffles number N_{baffles}. Varying the baffles number while keeping a constant value of $L_\perp$ entails a variation of the parameter N_r.

The maximum and minimum values used for the domain parameters of this analysis are detailed in 4.6.

Table 4.6: Maximum and minimum A_r and N_r values for baffle number dependence

Parameter	Minimum value	Maximum value
A_r	0.3	0.8
N_r	166.67	666.67 [mm]

To clarify what is meant by varying N_r, the figures 4.8 are explicative. Essentially, these images show how the different N_r values are obtained by simply varying N_{baffles}, for $A_r = 0.5$, $L = 2000$ [mm], $L_\perp = 2000$ [mm] and $T_r = 2$.

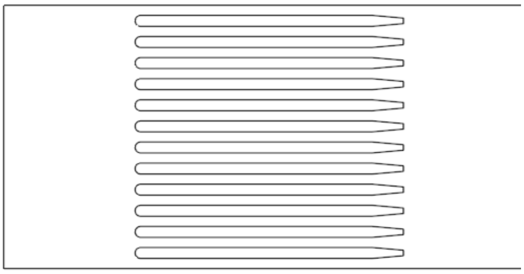

(a) Silencer with $N_r = 166.67$ that is equivalent to 12 baffles for $L_\perp = 2000$ [mm]

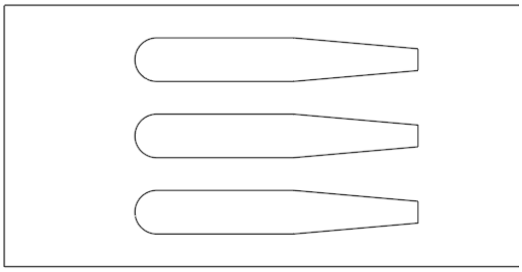

(b) Silencer with $N_r = 666.67$ that is equivalent to 3 baffles for $L_\perp = 2000$ [mm]

Figure 4.8: Maximum and minimum N_r values for silencer analysis

As said before, to account for the N_r dependence, the corrective coefficient K_{corr} is defined as follows:

$$K_{\text{corr}} = \frac{\text{Silencer pressure drop}}{\text{Silencer pressure drop}_{N_r=250}} \tag{4.11}$$

where:

- Silencer pressure drop is the actual pressure drop of the inspected silencer with a value of N_r inside the inspected domain;
- Silencer pressure drop$_{N_r=250}$ is the expected pressure drop value calculated with the formulation presented before, that is the pressure drop value for $N_r = 250$;

Obviously, since the corrective coefficient is defined in this way, its value is equal to $K_{\text{corr}} = 1$ when inspecting a silencer characterized by $N_r = 250$, otherwise it is different and affects the total pressure drop value.

The analysis output is a scalar function of 2 variables that corrects the mathematical model detailed before, as the pressure drop total value is expressed through the $K_{\text{total loss}}$ coefficient that is defined as:

$$K_{\text{total loss}} = K_{\text{corr}} \cdot K_{\text{loss}} \tag{4.12}$$

The mathematical formula used to describe the corrective coefficient K_{corr} is the following one:

$$K(Ar,\, N_r) = \beta_1\, e^{\beta_2 N_r} + \left[\beta_3 (N_r - 250)^2 + \beta_5\right] Ar + \beta_6 \tag{4.13}$$

The interpolating surface obtained by post-processing the CFD results is shown in figure 4.9.

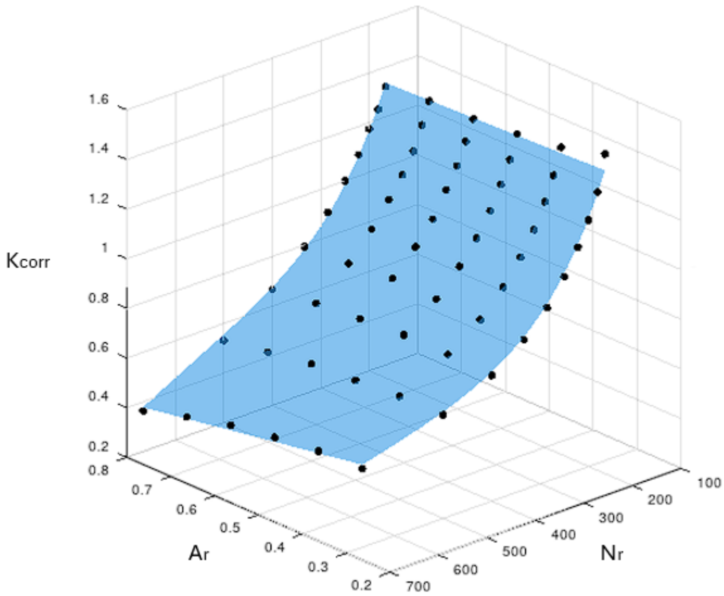

(a) K_{corr} as a function of A_r and N_r

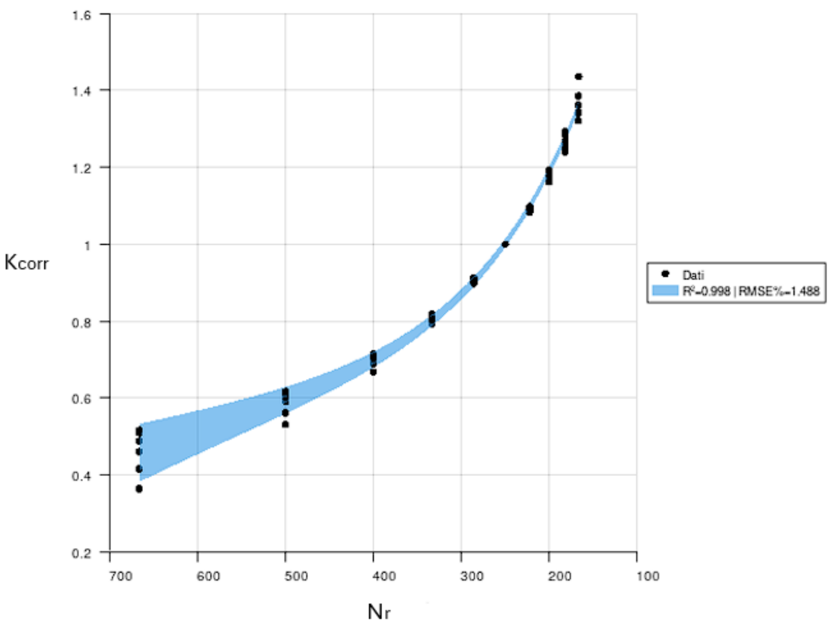

(b) K_{corr} as a function of N_r

Figure 4.9: K_{corr} as a function of A_r and N_r

The graph clearly shows that using silencers with many thinner baffles causes higher pressure drop values than using a low number of thick baffles. On the other hand, A_r does not affect pressure drop except when considering very high or low N_r values. Low precision at the border of the analysis domain is not a big issue since those situations are quite rare.

4.3.5 Validation test of the developed model for data extrapolation

The last analysis performed on parallel baffle silencers is a validation test of the developed model which has the goal of understanding how accurate it is for data extrapolation. Data extrapolation refers to the process of estimating the values of a dependent variable outside the specific range of independent variables used to calibrate the model. To perform this analysis, 2D computational fluid dynamics simulations were performed to compare their results with the ones obtained using the model. The setup of the simulations is identical to the one described before, so no further description is provided.

The analytical model, as discussed previously, was developed covering the entire possible A_r range, as the behaviour of the K_{loss} coefficient as a function of A_r is difficult to predict. The same consideration is made on N_r; indeed, the range of values used to define K_{corr} covers each possible case. On the other hand, the model was developed using a narrow range for the baffle length L. In fact, especially when acoustic criteria are strict, long baffles are necessary to reach higher absorption values. This happens mostly for exhaust ducts, but in some specific cases even for intake ones. Consequently, it is necessary to understand how reliable the developed model is when L values are larger (or smaller) than the values detailed in table 4.4.

In this analysis even the Reynolds number independence was validated, since $L_{\perp}$, which is the gas path side orthogonal to panels, was varied in the range 1500 [mm] $\div$ 6000 [mm]. In the meantime, the baffles number was varied to guarantee $N_r = 250$, so $K_{\text{corr}} = 1$ and no correction is needed. It is worth noting that the model points are related to silencers with $L_{\perp} = 2000$ [mm] and $N_{\text{baffles}} = 8$, while the random points are characterized by random values of these parameters taken within the ranges expressed before.

In table 4.7, the random points characterized by a percentage error between the expected and the actual results above 5% are listed. The results are also presented in descending order of percentage error.

Table 4.7: Maximum percentage error values for the data extrapolation test on the silencer model

Gaspath	Baffles number	T_r	A_r	L	Error %
6000	24	1.5	0.65	750	18.19
2500	10	2.5	0.85	1000	17.23
3000	12	1.5	0.65	750	14.42
3000	12	2.0	0.80	1000	14.23
6000	24	2.0	0.75	4750	11.53
1500	6	1.0	0.35	750	9.94
5000	20	2.5	0.35	4250	9.05
5000	20	2.5	0.65	5000	8.08
2500	10	2.0	0.80	3250	7.51
1500	6	1.0	0.60	4250	6.50
5000	20	2.0	0.60	4750	5.30

The total number of random points used for this analysis was 40 and the average error is 5.10%. It is worth noting that most of the silencers characterized by the highest percentage error are related to baffles with low L values in the order of $L = 750 \div 1000$ [mm]. What causes high percentage errors on these silencers is likely to be one of the two following aspects, or both combined:

- The model deviation from a linear behaviour;
- Unnecessary refinement of the interpolating surfaces;

The first hypothesis is related to a deviation of the model behaviour as a function of L when this parameter assumes low values. To explain how this aspect influences the model behaviour, we must consider that in tapered-end baffles characterized by a small overall length a considerable part of the baffle is not straight. Therefore, the velocity is not uniform and decreases on a consistent part of the baffle and the error in friction losses is not negligible.

The second hypothesis has an evident effect on the model accuracy. Indeed, the best values of R^2 and $RMSE$ are related to $T_r = 1$ as shown in graph 4.5b. This aspect leads to a better refinement of the interpolating surface on the sample points. As a matter of fact, there are no $T_r = 1$ silencers characterized by a percentage error above 10%.

Chapter 5

Study of the interaction between fittings and silencers

5.1 Component interaction and $K_{\text{interdependence}}$ corrective coefficient definition

In all the CFD simulations showed up to this point the inlet flow entering the components has been considered uniform. In real gas turbine intake fittings this is not the usual situation, since as shown in chapter 3, elbows strongly affect the flow velocity distribution generating flow separation. Therefore, it is reasonable to assume that all the components placed downstream of elbows operate in separated flow. This clearly has an impact on the aerodynamic performances of the components placed downstream of the elbows, and this is the topic discussed in this chapter. The general approach used for this study consists of simulating a fitting that generates separated flow, as an elbow, coupled with a silencer positioned downstream of it.

Taking as an example an intake arrangement where a tapered end silencer is positioned downstream of an elbow, the flow velocity distribution looks as the one proposed in figures 5.1. The flow is characterized by a separation bubble that takes up part of the cross-sectional area of the duct. This phenomenon entails that the flow path is narrower and characterized by higher speeds both inside and outside the silencer panels. Clearly, having a much higher flow velocity cause higher pressure losses. The goal of the interdependence analyses is to quantify how aerodynamic performances of silencers deteriorate in these situations.

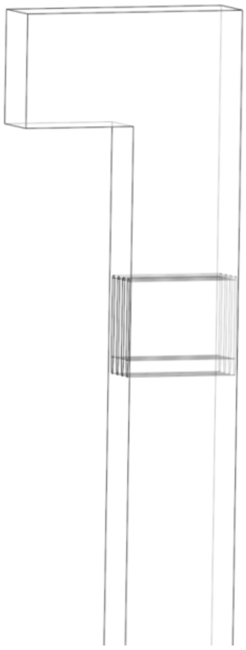

(a) Tested configuration with an elbow coupled with a tapered end silencer

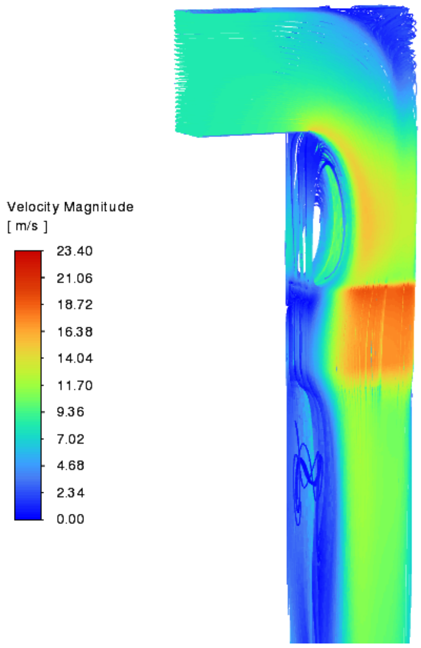

(b) Path lines coloured by velocity magnitude for the tested configuration

Figure 5.1: Effect of inlet flow separation on the flow distribution inside the silencer

Generally, the main variable in this study is the distance D between the fitting outlet and the silencer inlet. The other investigated parameter is the area ratio (A_r) of the silencer, since it is interesting to observe that different silencers exhibit different flow behaviours. The implementation of mathematical models that accurately describe interdependence between the components it is difficult because a lot of variables have an impact on pressure drop. Thus, the model developed consists only in the use of a corrective factor denoted as $K_{\text{interdependence}}$, that acts as a penalization once the silencer is positioned too close to the curve outlet. The $K_{\text{interdependence}}$ parameter is calculated starting from the CFD simulation as follows:

$$K_{\text{interdependence}} = \frac{\Delta P_{\text{calculated}}}{\Delta P_{\text{expected}}} \tag{5.1}$$

where:

- $\Delta P_{\text{calculated}}$ is the pressure drop of the entire arrangement comprehending both, the fitting and the silencer, calculated through a CFD analysis;
- $\Delta P_{\text{expected}}$ is the pressure drop of the silencer calculated through a CFD analysis;

Another possible way to calculate the expected pressure drop of the silencer $\Delta P_{\text{expected}}$ would have been using the mathematical formula detailed in the last chapter. The reason why additional simulations were performed to calculate $\Delta P_{\text{expected}}$ is to reach higher accuracy. Indeed, interdependence CFD simulations are performed on 3D computational domains of complete arrangements. Consequently, these simulations are far more expensive from the computational point of view than the simulations detailed in chapter 4. To reduce the computational expense the K-ϵ model was used, while the silencer mathematical model was developed using k-ω SST model instead. Therefore, to achieve higher precision, the silencers were simulated at first with uniform inlet flow and then, the results were compared to the ones obtained simulating the full arrangements.

Clearly the $K_{\text{interdependence}}$ coefficient acts as a corrective factor used to obtain accurate values of K_{loss} coefficient that is defined as:

$$K_{loss} = \begin{cases} K_{\text{component}} & \text{if } K_{\text{interdependence}} = 1 \\ K_{\text{interdependence}}\, K_{\text{component}} & \text{if } K_{\text{interdependence}} \neq 1 \end{cases} \tag{5.2}$$

Using this definition allows to have correction only when it is necessary.

5.2 Interdependence analyses

As said before, the interdependence analyses are focused mainly on the study of couples of fittings: an elbow and a silencer. The K-ϵ model was selected due to the high computational cost of 3D simulations on complete arrangements, as well as the need for very conservative under-relaxation factors to ensure convergence. This model is inherently based on wall functions, so it operates accurately for the range $y^+ = 30 \div 300$. Since many literature texts suggest using this model within the range $y^+ = 30 \div 100$ the mesh was constructed targeting $y^+ \approx 40$ on the panel walls. Since the flow velocity is higher in the cells adjacent to the panel walls, and the first inflation layer thickness is constant throughout the domain, the generated mesh resulted in y^+ values even below the threshold of $y^+ = 30$. For this reason, scalable wall functions were adopted, as they allow the solver to automatically switch between enhanced wall treatment and standard wall functions depending on the local y^+ value.

As discussed previously, silencers with uniform intake flow were first simulated. Subsequently, the complete configurations were analysed. Both analyses were carried out using identical meshing parameters to ensure comparability of the results. The most relevant mesh parameters are listed in table 5.1.

Table 5.1: Mesh parameters for convergent elbow transition analysis

Edge sizing	Domain sizing	First element thickness	Inflation elements
25 [mm]	120 [mm]	1 [mm]	10

The edge sizing is always provided at the edge where flow separation occurs in the inlet fitting. The mesh details are provided now and are not repeated in the following section of this chapter.

After the single silencer simulations two different arrangements were inspected. These arrangements are then detailed in the following paragraphs:

- 90° elbow and parallel baffle silencers interdependence;
- Convergent elbow transition and parallel baffle silencers interdependence;

These two arrangements were selected, as they correspond to the configurations in which the interaction between components is expected to be the most significant. In these cases, the first component induces flow separation, which affects the performance of the downstream of the component. Although additional arrangements could have been analysed, such as those including a pyramidal transition followed by a silencer, it is reasonable to assume that the flow separation generated by the pyramidal transition is relatively small, and its effect can therefore be considered negligible.

5.2.1 90° elbows and parallel baffle silencers interdependence

This paragraph has the goal of explaining how the parallel baffle silencers are affected by the separated flow generated by 90° elbows at their inlet section. Both the fittings involved in this study were formerly investigated through parametric analyses, and as discussed before, many parameters play an important role on their pressure drop assessment. Only some of the parameters are inspected in this analysis, as $\theta = 90°$, $L = 2500$ [mm] and $T_r = 2$ were fixed to simplify this study. Therefore, the only investigated parameters are:

- Distance D: it is the distance between the elbow outlet and the silencer inlet, so it is defined in the same way as it was on the previous analysis;
- Area ratio A_r: it is the obstructed area percentage of the silencer, and it is investigated to understand how different silencers behave in separated flow;
- Shape ratio S_r: it is the aspect ratio of the cross-section of the duct and is varied to understand how more or less dissipative elbows affect the silencer performances.

These parameters were varied inside the ranges detailed in table 5.2:

Table 5.2: Variation range of the investigated parameters

Distance D[mm]	Area ratio A_r	Shape ratio S_r
$10 \div 4000$	$0.4 \div 0.7$	$0.5 \div 1$

Only two different shape ratios S_r were inspected: $S_r = 1$ and $S_r = 0.5$. Therefore, only perfectly square ducts ($S_r = 1$) and rectangular ducts with the base dimension that is twice the height dimension ($S_r = 0.5$) were inspected in this analysis. This choice was driven by the necessity of reducing the overall computational expense. The CFD simulations were performed with constant mass flow $\dot{m}$, so to have identical flow velocities the cross-sectional area was fixed too at 9 [m^2].

The figures 5.2 show the maximum and minimum D and A_r values used as boundaries of the parametric study for both, $S_r = 1$ and $S_r = 0.5$. The displayed images, consistent with the simulations, show silencers with a fixed length $L = 2600$ [mm].

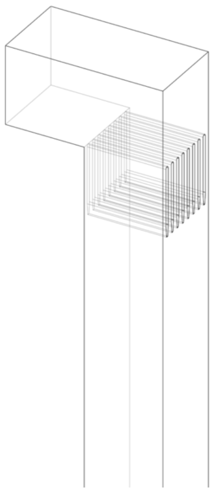

(a) $S_r = 1,\ D = 10\,[\text{mm}],$
$A_r = 1,\ L = 2600\,[\text{mm}]$

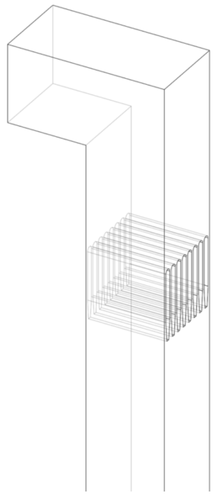

(b) $S_r = 1,\ D = 4000\,[\text{mm}],$
$A_r = 0.7,\ L = 2600\,[\text{mm}]$

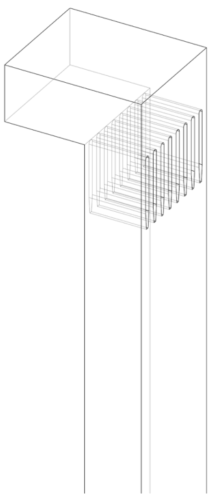

(c) $S_r = 0.5,\ D = 10\,[\text{mm}],$
$A_r = 1,\ L = 2600\,[\text{mm}]$

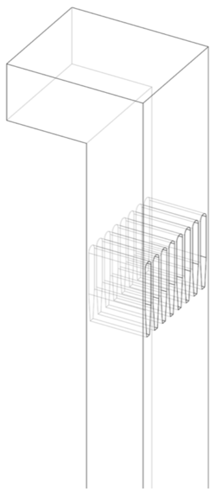

(d) $S_r = 0.5,\ D = 4000\,[\text{mm}],$
$A_r = 0.7,\ L = 2600\,[\text{mm}]$

Figure 5.2: Examples of tested configurations with minimum and maximum parameter values for A_r and S_r

These images are provided to graphically illustrate the boundaries of the parametric study performed in this section.

An immediate comparison of the values of $K_{\text{interdependence}}$ is provided in figure 5.3. Indeed, the first graph shows how $K_{\text{interdependence}}$ varies as a function of A_r and distance D for $S_r = 1$. The second graph shows the identical trends for $S_r = 0.5$. On the x-axis of the graphs there is D expressed, on y-axis $K_{\text{interdependence}}$ and each different curve is obtained for a different value of A_r.

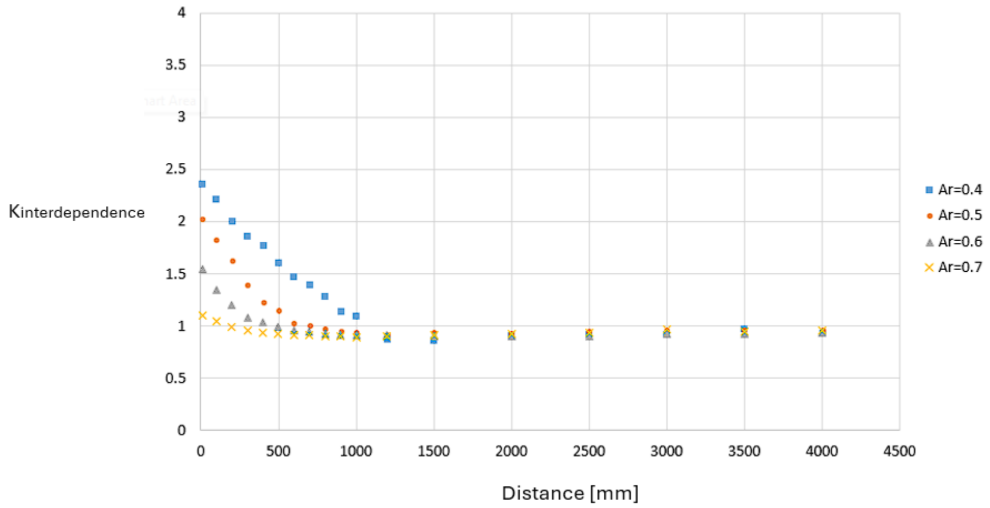

(a) $K_{\text{interdependence}}$ trends for different A_r and D values but fixed $S_r = 1$ value

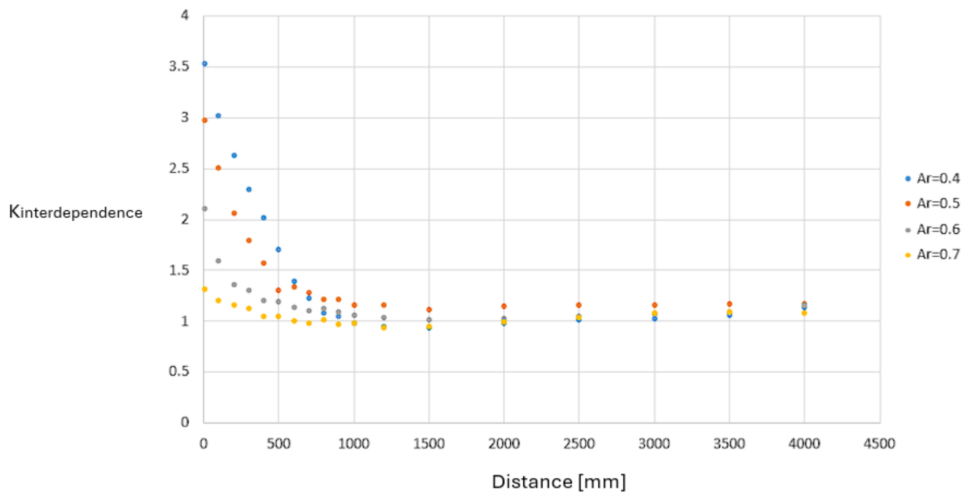

(b) $K_{\text{interdependence}}$ trends for different A_r and D values but fixed $S_r = 0.5$ value

Figure 5.3: $K_{\text{interdependence}}$ trends as a function of S_r, D and A_r

This time the encountered behaviour is different from the one observed in the previous analysis. In this case, reducing the distance between the elbow and the silencer leads to a deterioration in the aerodynamic performance of the silencer. Indeed, as explained before, the flow path becomes narrower and the flow velocity increases entailing an increment in pressure drop as shown in figure 5.4:

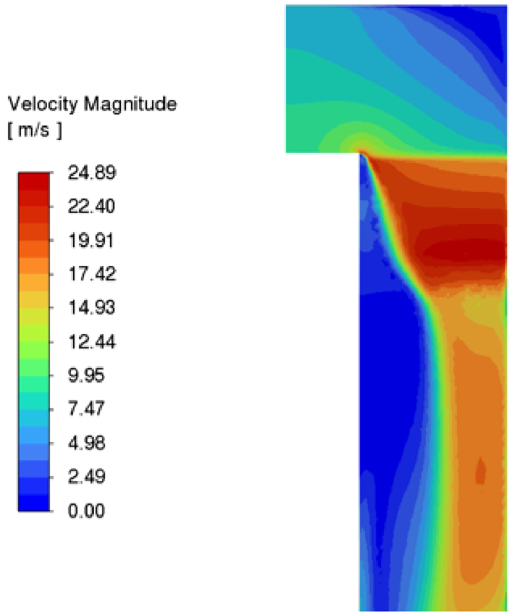

Figure 5.4: Velocity magnitude distribution for an elbow duct coupled with a silencer with $D = 10$ [mm], $S_r = 1$, $A_r = 1$

The silencer shown in this image generate approximately 2.5 times the pressure drop that it would generate operating with uniform inlet flow.

It is also necessary to explain the reasons why silencers that are characterized by high values of obstructed area A_r are less affected by flow detachment. Parallel baffle silencers with high A_r values generate larger pressure losses and strong acceleration of the flow that passes through them. As high-pressure gradients are present in the flow path, flow reattachment is promoted. Indeed, it is possible to witness that the flow enters the silencers characterized by $A_r = 0.7$ almost uniformly, while the ones with $A_r = 1$ experience high flow separation and higher pressure drops.

Another interesting aspect is that, as the elbow becomes more dissipative and generates larger separation bubbles, the $K_{\text{interdependence}}$ coefficient becomes higher. As it is shown in 5.3, 90° elbows with $S_r = 0.5$ combined with silencers cause larger pressure drops and consequently higher values of $K_{\text{interdependence}}$ than the ones generated by 90° elbows with $S_r = 1$. This is clearly due to greater flow separation, which results in a less uniform flow at the silencer inlet.

5.2.2 Convergent elbow transition and parallel baffle silencers interdependence

This paragraph explains briefly how the interaction between a convergent elbow transition and a parallel baffle silencer affects the overall pressure drop. It is useless to describe in detail this situation as the theoretical concepts are identical to the ones explained in the paragraph above.

The investigated parameters in this case are A_r and the distance D. In this case, to reduce the computational time, only $A_r = 0.4$ was investigated by varying the distance between the fittings from 0 [mm] to 4000 [mm]. The graph 5.5 shows a comparison between the $K_{\text{interdependence}}$ values for this couple of fittings and for elbow ducts coupled with silencers.

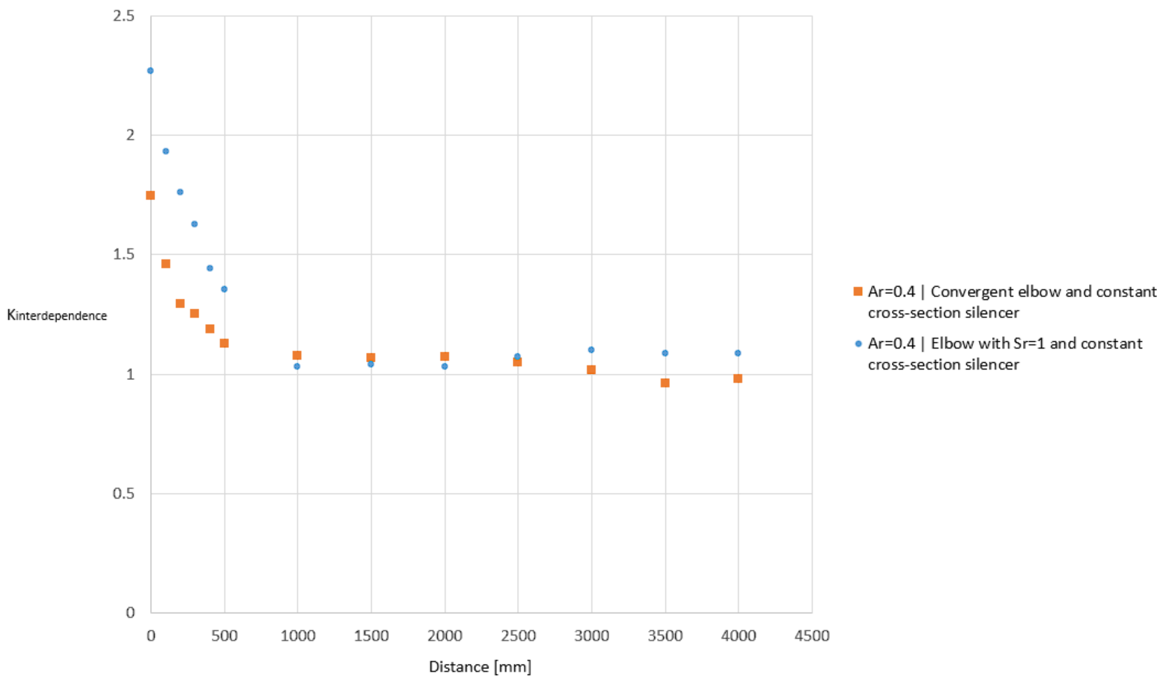

Figure 5.5: $K_{\text{interdependence}}$ variation as a function of D and A_r for convergent elbow transition coupled with silencer and elbow with $S_r = 1$

This behaviour confirms what was explained in the paragraph above. Indeed, convergent elbow transitions are characterized by limited flow separation compared to 90° elbows. In the same way, 90° elbows with $S_r = 1$ generates limited flow separation if compared to 90° elbows with $S_r = 0.5$. As a matter of fact, the silencer positioned downstream of the fitting gets less influenced when the flow separation is limited. This is why $K_{\text{interdependence}}$ for convergent elbows coupled with silencers is lower.

It is worth noting that an arrangement built by coupling a convergent elbow transition and a silencer, not only is it more efficient from the losses point of view, but it also provides benefits in terms of space occupation and weight. In fact, this arrangement compared with a 90° elbow coupled with the same silencer allows the duct dimensions to be adjusted directly from the filter house to the vertical duct where the silencer is located. In this way unnecessary horizontal sections are eliminated. Therefore, this arrangement is a compact and cost-saving solution as less material results in lower costs, but even having a lower footprint makes the whole plant cheaper.

5.3 Model developed for $K_{\text{interdependence}}$ as a function of D and A_{r}

As discussed on the previous paragraphs the number of parameters that plays a role in interdependence studies is high, so developing a proper mathematical law to account for all of them is difficult. In this paragraph the mathematical method to account for interdependence is discussed.

As it is difficult to implement a $K_{\text{interdependence}}$ correction factor for each possible couple of fittings, only one mathematical law was developed for the worst case between the analysed scenarios. The arrangement that generates the larger flow separation and consequently the highest interaction effects, is the 90° elbow with $S_r = 0.5$ coupled with the silencer. The behaviour is detailed in graph 5.3b. To account for different arrangement dimensions the distance could not be expressed in [mm], but it must be expressed as number of hydraulic diameters D_h. The proposed model assumes that the interdependence effect decays at a fixed value of number of hydraulic diameters, that is certainly more accurate than considering a fixed distance in [mm]. This aspect is also shown in graph 5.6, where the $K_{\text{interdependence}}$ trend for $S_r = 1$ and $S_r = 0.5$ with $A_r = 0.4$ is shown. The graph shows clearly that the effect decays approximately at the same value of number of equivalent diameters D_h for both the configurations.

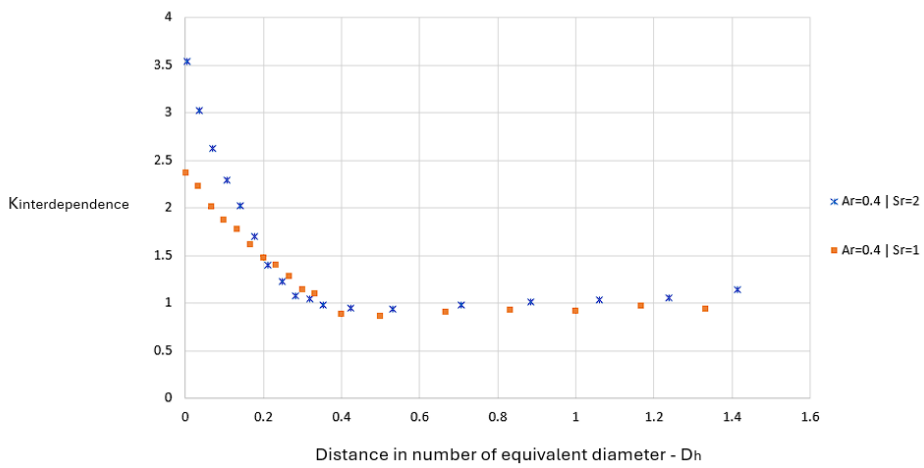

Figure 5.6: $K_{\text{interdependence}}$ as a function of the distance expressed in number of hydraulic diameters D_h for different S_r values but equal A_r value

As discussed before, the $K_{\text{interdependence}}$ coefficient is equal to 1 for high distance values and increases when the silencer inlet is nearer to the curve outlet. The trend exhibited by $K_{\text{interdependence}}$ coefficient once the silencer starts to feel the curve influence is assumed to be linear for simplicity. Always to simplify the mathematical model, a fixed angular coefficient for the linear mathematical model was chosen for all the different A_r values. A_{r} only influences the y-intercept value of the linear mathematical model. Therefore, that describes how component interaction affects pressure drop is:

$$K_{\text{interdependence}} = -\beta_1 D_h + \beta_2 A_{\text{r}}^{-\beta_3} \tag{5.3}$$

where:

- β_1 is the fixed angular coefficient;
- $\beta_2 A_{\text{r}}^{-\beta_3}$ is the y-intercept;
- β_1,β_2,β_3 are positive scalar numbers;

It is worth noting that as A_r increases, the value of the y-intercept decreases in accordance with what was observed in the simulation results. Indeed, silencers with high values of obstructed area are not affected by the presence of an elbow placed upstream of them.

Clearly, the $K_{\text{interdependence}}$ correction is only valid whenever $K_{\text{interdependence}} > 1$, otherwise a value of $K_{\text{interdependence}} = 1$ is assumed. Given the high number of assumptions, this corrective coefficient should be considered as a penalty factor introduced into the pressure drop calculation tool when the silencer is positioned near an elbow.

Chapter 6

Pressure drop calculation tool implementation and results discussion

6.1 Pressure drop calculation tool implementation

The tool consists of an Excel file where all the formulations discussed up to now are implemented. Excel was used to guarantee the tool is easy to use and to create an automated and user-friendly interface.

The tool requires two different types of input parameters that are:

- Air characteristics: volumetric airflow, air temperature, ambient pressure, relative humidity of air;
- Fittings typology and geometric parameters of interest for each fitting;

Giving as input the air parameters detailed above it is useful to calculate the air density that enters directly in the computation of the dynamic pressure. So, the air density is calculated through the following equation:

$$\rho = \frac{p_d}{R_d T} + \frac{p_v}{R_v T} \tag{6.1}$$

where:

- ρ is the air density [kg/m^3]
- p_d is the partial pressure of dry air [Pa]
- p_v is the partial pressure of water vapor [Pa]
- R_d is the specific gas constant for dry air, $R_d = 287.058$ J/(kg $\cdot$ K)
- R_v is the specific gas constant for water vapor, $R_v = 461.523$ J/(kg $\cdot$ K)
- T is the absolute temperature [K]

Clearly, p_d and p_v are calculated as a function of the air parameters.

Fitting typology and geometric parameter data are required as input for all the mathematical formulas developed and explained in Chapters 3, 4, and 5. So, the inlet and outlet gas path dimensions need to be defined accurately to properly calculate $K_{\text{interdependence}}$, $K_{\text{component}}$ and as the product of these two coefficients the $K_{\text{total losses}}$ value.

The pressure drop prediction tool has many different outputs, such as dynamic pressure at each component outlet and even total and static pressure drop related to each item in the intake system. Indeed, once volumetric air flow, density and gas path dimensions are defined it is easy to calculate the ducts area A, the flow velocity $v = \frac{Q}{A}$, and therefore the dynamic pressure P_{dynamic}:

$$P_{\text{dynamic}} = \frac{1}{2}\rho v^2 \tag{6.2}$$

At this point the total pressure drop is calculated as:

$$\Delta P_{\text{total}} = K_{\text{total losses}} \cdot P_{\text{dynamic}} \tag{6.3}$$

The last calculated result in the tool is the static pressure drop ΔP_{static} that is derived from the total pressure drop and calculated as:

$$\Delta P_{\text{static}} = \frac{1}{2}\rho(v_{outlet}^2 - v_{inlet}^2) + \Delta P_{\text{total}} \tag{6.4}$$

Total and static pressure drop results are available for each single fitting and they are expressed both in [Pa] and [mmH_2O].

In figure 6.1 an example of calculation for an invented intake system is provided.

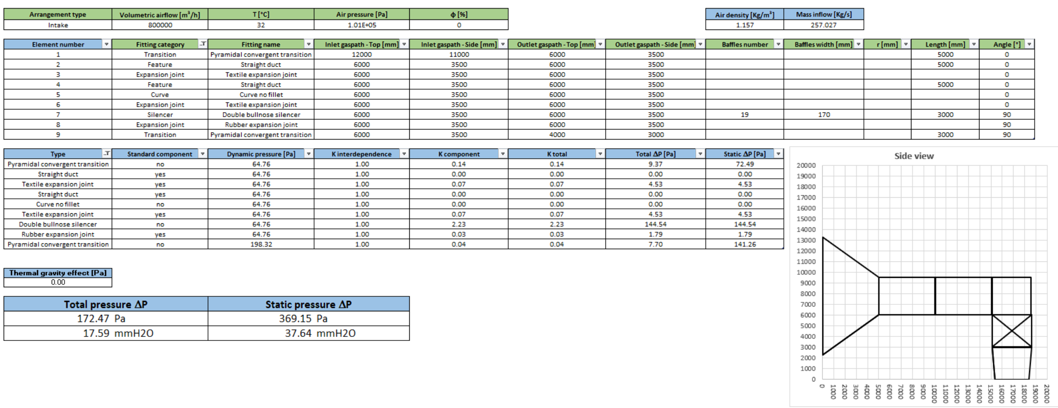

Arrangement type	Volumetric airflow [m³/h]	T [°C]	Air pressure [Pa]	φ [%]	Air density [Kg/m³]	Mass inflow [Kg/s]
Intake	800000	32	1.01E+05	0	1.157	257.027

Element number	Fitting category	Fitting name	Inlet gaspath - Top [mm]	Inlet gaspath - Side [mm]	Outlet gaspath - Top [mm]	Outlet gaspath - Side [mm]	Baffles number	Baffles width [mm]	r [mm]	Length [mm]	Angle [°]
1	Transition	Pyramidal convergent transition	12000	11000	6000	3500				5000	0
2	Feature	Straight duct	6000	3500	6000	3500				5000	0
3	Expansion joint	Textile expansion joint	6000	3500	6000	3500					0
4	Feature	Straight duct	6000	3500	6000	3500				5000	0
5	Curve	Curve no fillet	6000	3500	6000	3500					0
6	Expansion joint	Textile expansion joint	6000	3500	6000	3500					0
7	Silencer	Double bullnose silencer	6000	3500	6000	3500	19	170		3000	90
8	Expansion joint	Rubber expansion joint	6000	3500	6000	3500					90
9	Transition	Pyramidal convergent transition	6000	3500	4000	3000				3000	90

Type	Standard component	Dynamic pressure [Pa]	K interdependence	K component	K total	Total ΔP [Pa]	Static ΔP [Pa]
Pyramidal convergent transition	no	64.76	1.00	0.14	0.14	9.37	72.49
Straight duct	yes	64.76	1.00	0.00	0.00	0.00	0.00
Textile expansion joint	yes	64.76	1.00	0.07	0.07	4.53	4.53
Straight duct	yes	64.76	1.00	0.00	0.00	0.00	0.00
Curve no fillet	no	64.76	1.00	0.00	0.00	0.00	0.00
Textile expansion joint	yes	64.76	1.00	0.07	0.07	4.53	4.53
Double bullnose silencer	no	64.76	1.00	2.23	2.23	144.54	144.54
Rubber expansion joint	yes	64.76	1.00	0.03	0.03	1.79	1.79
Pyramidal convergent transition	no	198.32	1.00	0.04	0.04	7.70	141.26

Thermal gravity effect [Pa]
0.00

Total pressure ΔP	Static pressure ΔP
172.47 Pa	369.15 Pa
17.59 mmH2O	37.64 mmH2O

Figure 6.1: Pressure drop prediction tool: user interface

The tool also provides a graph that is compiled runtime while editing the input parameters, so the user has immediate feedback of the configuration he is testing.

6.2 Tool validation through numerical and experimental results comparison

As discussed in chapter 2, from the monitoring application is possible to acquire pressure drop data of the entire intake systems of running gas turbines. The data acquired from the software tool were used as experimental data to validate the mathematical models that were developed. Unfortunately, is often impossible to acquire pressure drop data for one single component. Indeed, no sensors are placed upstream and downstream of one single intake item apart from the filters, that are not considered in this study.

The validation is made as explained in chapter 2, by comparing the software tool pressure drop of the entire inspected domain and the numerical results. As a matter of facts, it is difficult to understand how accurate the pressure drop prediction is for a single component, but it is possible to understand the prediction accuracy on the entire arrangement.

The validation was performed on 2 different arrangements:

- Pyramidal transition coupled with parallel baffle silencer and a modular curve that is flanged to the inlet plenum;
- Convergent elbow transition coupled with a modular silencer;

6.2.1 Validation of the first arrangement: pyramidal transition, parallel baffle silencer and modular curve

The complete arrangement is composed by a pyramidal transition, a silencer with double bullnose panels and the modular curve shown in chapter 3.4. The entire arrangement is presented in figure 6.2.

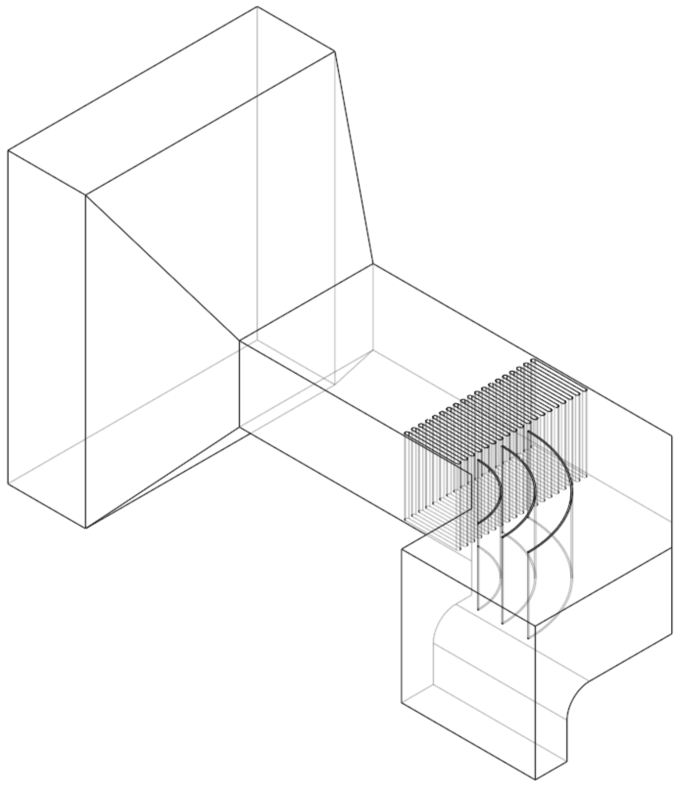

Figure 6.2: 3D model that represents the first validation arrangement

This arrangement is characterized by a Pitot tube placed upstream of the inlet plenum, so the comparison is made on the total pressure losses. Then, the entire configuration is implemented in the tool, and the results are presented in table 6.1:

Table 6.1: Comparison between numerical and experimental results for the first arrangement

Software ΔP [Pa]	Analytical ΔP [Pa]	Percentage error [%]
259.39	242.83	7%

As depicted in the table the overall error between the predicted and the experimental data is within the 10%, the maximum tolerated error in this research. The value 10% was assumed as the maximum tolerated error instead of 5% since many different simplifying assumptions were made in the process:

- The effect of perforated sheet on baffle panels;
- The CAD models used for the parametric analyses do not include the imperfections that characterize real intake ducts, such as flanges, bolts, internal deflectors, and surface roughness;
- The friction effect, that is assumed as a negligible contribution in large ducts;

As the friction effect contribution is likely to be negligible in large ducts, as detailed in chapter 1, the same cannot be said for perforated sheet effect. Indeed, having perforated sheets on baffles surfaces is like having an increased roughness and this clearly generates a pressure drop increment. There are mainly two reasons why the additional contribution to friction losses given by the increment in the surface roughness is not negligible:

- Inside a parallel baffle silencer, the flow is split so the hydraulic diameter (D_h) is reduced;
- As the open area is reduced, the flow velocity increases;

Both these effects tend to increase the friction losses as Darcy-Weisbach equation 1.17 suggests. In addition to these two effects, even the friction factor f increases inside a parallel baffle silencer.

The fact that three different contributions are ignored in the tool entails that the analytical pressure drop underestimates the experimental pressure drop of the simulated arrangements. So, the results shown in table 6.1 are acceptable, since the numerical value is lower than the experimental value. On the other hand, it would have been strange if the obtained results figured out to overestimate the pressure drop value.

Once many different configurations are going to be tested and enough data will be collected, a corrective coefficient to consider for all these effects is going to be defined.

The total pressure losses of this arrangement are divided in different contributions as follows:

Table 6.2: Numerical ΔP for the different components of the first validation arrangement

Component	Analytical ΔP [Pa]	Percentage of total ΔP [%]
Pyramidal convergent transition	14.75	6%
Textile expansion joint	7.04	2.9%
Double bullnose silencer	149.48	61.6%
Textile expansion joint	7.04	2.9%
Standard curve	49.02	20.2%
Rubber expansion joint	15.49	6.4%

The large attention dedicated to silencers is now devoted, since they represent the most dissipative component in gas turbine intake systems apart from the filters. As shown by the data in table 6.2, the expansion joints gave only a minor contribution to the total pressure drop.

6.2.2 Validation of the second arrangement: convergent elbow transition, modular silencer

The other validated configuration is composed by two different components: a convergent elbow transition and a modular silencer. The real intake arrangement is equipped with static pressure ports downstream the filter house and upstream of the inlet plenum. Therefore, the comparison between analytical and experimental results is made on static pressure drop for this configuration.

The issue related to static pressure ports is that they provide a less accurate measurement since static pressure is inherently connected to velocity variations. Knowing where the static pressure ports are placed is fundamental to understand whether all the contributions are taken into consideration.

To understand if other contributions need to be considered, it was necessary to study the entire intake arrangement comprehending not only the transition and the silencer, but even the inlet plenum and the compressor bell mouth. The entire intake system is presented in figure 6.3.

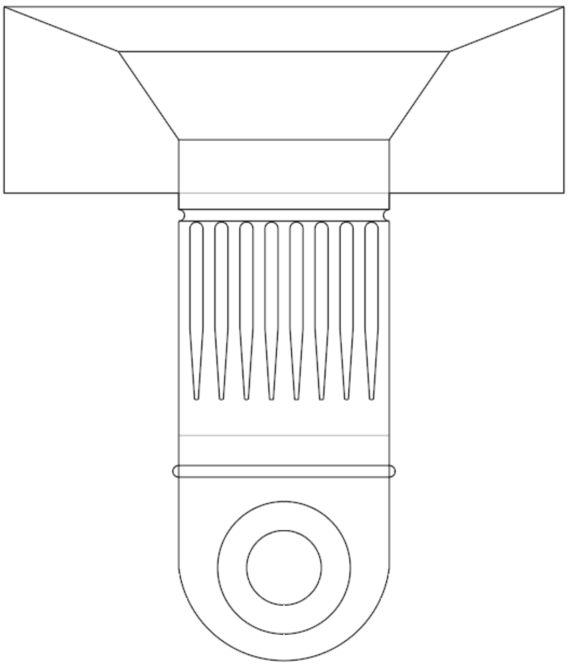

Figure 6.3: Convergent elbow transition and modular silencer with inlet plenum and compressor bell mouth

To assess whether the position of the static pressure ports could influence the monitoring application measurements, a simulation of the complete intake system was performed. The static pressure is plotted in figure 6.4.

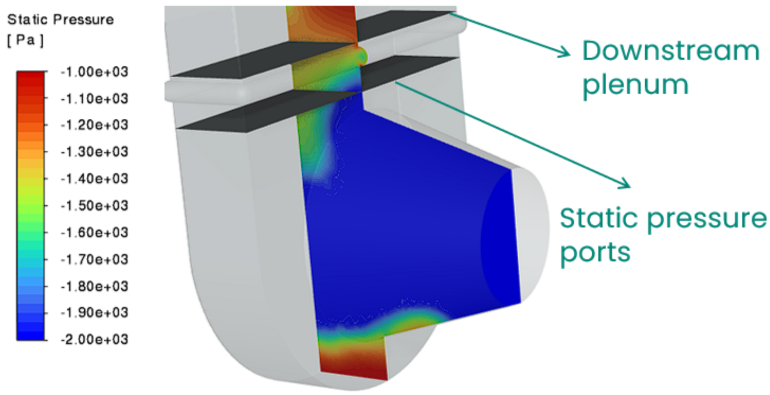

Figure 6.4: Static pressure contour plot in plenum and compressor bell mouth region

The static pressure ports are located at a certain distance from the plenum inlet and they are near to the compressor bell mouth. In this zone the flow undergoes a sudden cross-area contraction. The area reduction brings to an increase in velocity and to a consequent static pressure reduction. In quantitative terms the static pressure drop that the tool does not take into consideration is the difference between the static pressure on the two planes, that is described in detail in table 6.3.

Table 6.3: Velocity magnitude and static pressure difference between the plane downstream the plenum and the static pressure port plane

Plane location	Static pressure [Pa]	Average velocity magnitude [m/s]
Downstream plenum	1150	39.42
Static ports	1271	41.4

Therefore, an addictive contribution of $\Delta P_{\text{static}} = 151[\text{Pa}]$ needs to be added to the numerical prediction made by the computational tool. Considering this additional contribution, the comparison between numerical and experimental values provides the results expressed in table 6.4:

Table 6.4: Comparison between numerical and experimental data for the second validation arrangement

Software ΔP [Pa]	Analytical ΔP [Pa]	Percentage error [%]
644.49	615.17	4.6%

Once again, the developed mathematical models gave results with a percentage error considered acceptable. To achieve a proper validation of the tool, a larger number of configurations needs to be studied.

Chapter 7

Future developments and conclusions

7.1 Future developments

Mainly, two future development paths can be identified, focusing on the following aspects:

1. Studying additional intake components and perform more interdependence analyses;

2. Extending the tool to exhaust ducts;

In the following sections, these additional analyses are described in detail.

7.1.1 Adding more intake components and interdependence analyses

While designing intake ducts many different arrangements can be adopted. As there are many different configurations and fittings, only a part of them were studied in this work and many other components can be added.

For instance, further investigation could focus on the behaviour of one-sided pyramidal convergent transition by correlating the K_{loss} coefficient of this fitting to the standard pyramidal convergent transition coefficient. Another fitting to study is the pyramidal divergent transition as in some spurious calculations his behaviour did not accurately matched literature data.

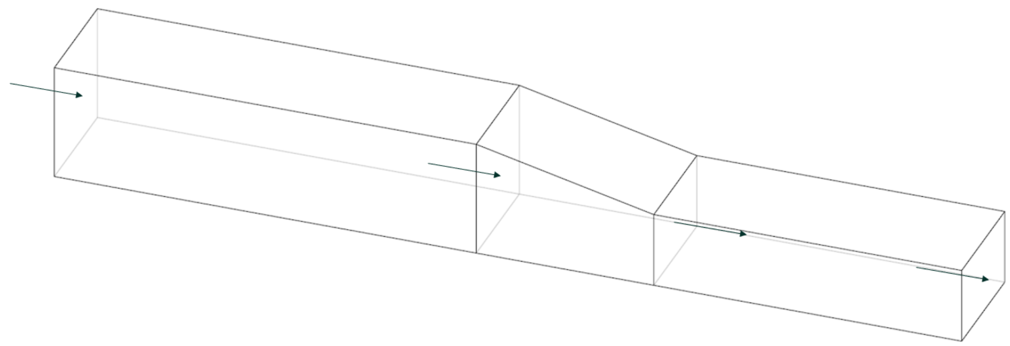

(a) One-sided pyramidal convergent transition

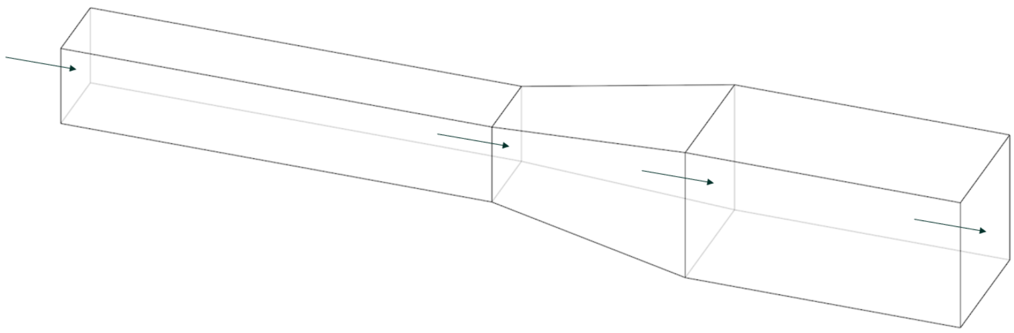

(b) Pyramidal divergent transition

Figure 7.1: Examples of fittings to be added to the pressure drop prediction tool

Pyramidal divergent transitions are largely used in exhaust ducts to enlarge gas path dimensions and assure lower velocities and consequently lower pressure drop values.

Another interesting analysis to perform is based on understanding how to optimize 90° elbow bevel parameters, such as angle and length, since qualitative analyses have been performed on this topic, but no mathematical model was developed. As shown in figure 7.2, the bevel has a beneficial effect on flow detachment and, as a consequence, even a beneficial effect on pressure drop.

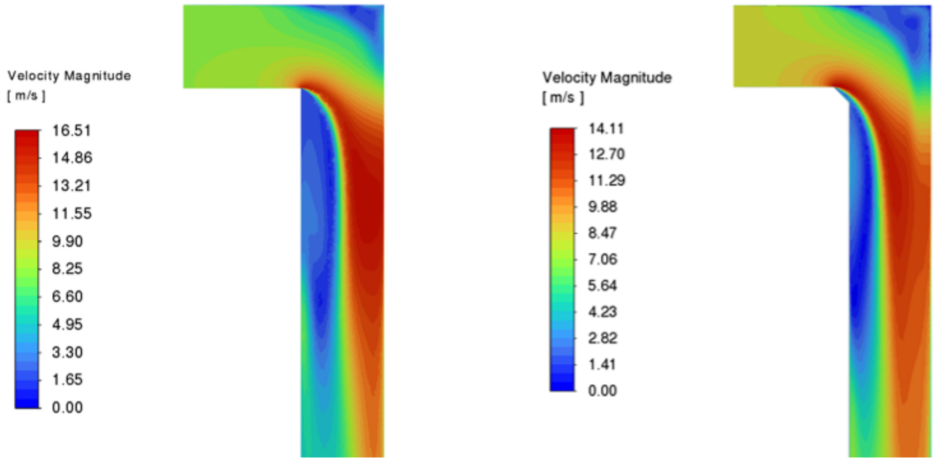

(a) Velocity magnitude contour for 90° elbow without bevel

(b) Velocity magnitude contour for 90° elbow with bevel

Figure 7.2: Separated flow reduction due to the bevel presence

As one of the aspects that a correctly designed intake system must guarantee is to provide uniform flow at the compressor inlet, in some configurations guide vanes are used. These devices guide the flow efficiently across elbows and reduce flow separation, but it would be interesting to understand how they affect pressure drop in intake arrangements.

7.1.2 Tool extension to exhaust ducts

The method used during this project could be extended to the pressure drop assessment in exhaust ducts if some assumptions are validated. In this section only qualitative examples and calculations are provided to discuss whether these assumptions are realistic or not. The main hypotheses needed are:

- Gas composition variation effects due to the presence of combustion residuals are negligible;
- Temperature can be assumed to be constant inside one single fitting;
- Flow is incompressible, so $Mach < 0.3$ condition must be matched;
- Reynolds number does not decrease significantly, ensuring the flow regime remain comparable to intake duct one;

The air-gas mixture in industrial gas turbines is typically lean. Nonetheless the stoichiometric ratio guarantees maximum combustion efficiency and, in the meantime, even maximum flame temperature, a gas turbine cannot operate under these conditions. In fact, the stoichiometric conditions result in gas temperatures that would be unacceptable for the turbine components. Under full-load conditions, the ratio between the total air mass flow rate and the fuel mass flow rate is approximately

2.5 to 3 times the stoichiometric value. However, such a mixture is too lean to sustain efficient and stable combustion. Therefore, the architecture of the combustion chamber is designed to introduce only a portion of the available air into the combustor reaction zone. In the meantime, the remaining portion is used to cool the system and to dilute the combustion products through mixing to levels acceptable for turbine inlet conditions. For instance, considering that the stoichiometric air–methane ratio is approximately 1:17.24, the fuel mass flow rate in a gas turbine is roughly 1/50 of the air mass flow rate and therefore the effect on gas composition and density could be considered negligible.

Gas temperature obviously varies along the entire exhaust system due to heat exchange with the ambient environment. For safety reasons, the external surface temperature of the ducts must not exceed 60°C in areas that may be accessed by personnel. Additionally, to prevent issues related to thermal expansion, even those sections of the exhaust system that are not accessible to personnel must be insulated. Although thermal insulation reduces temperature variations along the system, a gradual decrease in gas temperature still occurs throughout the exhaust line. Nevertheless, it is worth noting that, even if assuming a constant temperature within a single fitting may be a simplification, the developed mathematical formulations remain valid for such components.

It is easy to demonstrate that the flow is incompressible so that $Mach < 0.3$ condition is met in exhaust ducts. This could be done by taking some reference temperatures for intake and exhaust systems:

$T_{\text{intake}} = 15\ [°C]$

$T_{\text{exhaust}} = 550\ [°C]$

From these temperature values is possible to calculate the sound speed in both the conditions:

$$v = \sqrt{\frac{\gamma R T}{M}} \tag{7.1}$$

where v is sound velocity [m/s], γ is air adiabatic index usually assumed to be 1.4, R is the universal gas constant 8.314 $[\frac{J}{molK}]$, T is the absolute temperature expressed in Kelvin [K] and M is the molar mass of air that is approximately 28.97 [g/mol].

Using these data the following sound velocity are obtained:

$v_{15°C} = 343.23$ [m/s]

$v_{550°C} = 575.15$ [m/s]

The hypothesis of incompressible flow is met since the intake and exhaust flow velocities does not exceed the 30 % of the sound speed at the respective temperature values, that are:

$0.3 \cdot v_{15°C} = 102.97$ [m/s]

$0.3 \cdot v_{550°C} = 172.55$ [m/s]

Typical intake and exhaust systems velocities are well below the values calculated above.

The last aspect to discuss is how the Reynolds number gets affected by temperature variations. Here a brief discussion is provided to compare the typical Reynolds number in intake ducts with the ones calculated for exhaust ducts. Thus, the goal of this theoretical analysis is to compare Re_{intake} calculated considering $T = 15°C$ to the $Re_{exhaust}$ calculated at $T = 550°C$.

As the comparison is made on equal sized ducts the same hydraulic diameter D_h and the same area A are used for both intake and exhaust conditions. Changing the temperature does not affect the mass inflow rate $\dot{m}$, but in exhaust systems the total mass inflow rate varies by adding the fuel mass inflow to the air mass inflow. In this case this variation is neglected for the reasons discussed previously, and therefore, the same mass inflow rate $\dot{m}$ is considered for both intake and exhaust ducts. By doing some easy mathematical considerations and addressing with i and e respectively to intake and exhaust parameters, the Reynolds ratio can be calculated as:

$$\frac{Re_i}{Re_e} = \frac{\rho_i v_i D_h}{\mu_i} \cdot \frac{\mu_e}{\rho_e v_e D_h} = \frac{\rho_i \frac{\dot{m}}{\rho_i A} D_h}{\mu_i} \cdot \frac{\mu_e}{\rho_e \frac{\dot{m}}{\rho_e A} D_h} = \frac{\mu_e}{\mu_i} \tag{7.2}$$

So, the Reynolds ratio turns out to be the inverse of the viscosity ratio. The standard viscosity value for $T = 15°C$ is $\mu = 1.78 \times 10^-5$ [Pa · s], and the viscosity value at $T = 550°C$ can be calculated using Sutherland Law:

$$\mu(T) = \mu_0 \left(\frac{T}{T_0}\right)^{3/2} \frac{T_0 + S}{T + S} = 3.68 \times 10^-5 \text{ [Pa} \cdot \text{s]} \tag{7.3}$$

Therefore, it turns out that the Reynolds ratio is:

$$\frac{Re_{\text{intake}}}{Re_{\text{exhaust}}} = \frac{\mu_{\text{exhaust}}}{\mu_{\text{intake}}} = \frac{3.68 \times 10^{-5}}{1.78 \times 10^{-5}} = 2.07 \tag{7.4}$$

It can be assumed that the Reynolds number of the exhaust ducts is half the one of intake ducts. Further investigation on how this aspect affects losses is needed. For this scope the following comparison between the K_{loss} coefficient for $T = 15°C$ and for $T = 550°C$ was performed.

The simulations were performed on silencers with identical geometrical parameters for intake and exhaust systems. The geometric parameters of the silencer used for this analysis are $N_r = 250$, $L = 2000$ [mm], $Tr = 2$ and the only variable parameter is A_r, that was varied in the range $A_r = 0.3 \div 0.8$. The air density is varied considering only temperature variation; thus the fuel addition is ignored. The temperature considered for exhaust and intake ducts are respectively $T_{\text{exhaust}} = 550°C$ and $T_{\text{intake}} = 15°C$.

The results are presented as scatters on graph 7.3 and quantitatively described in table 7.1.

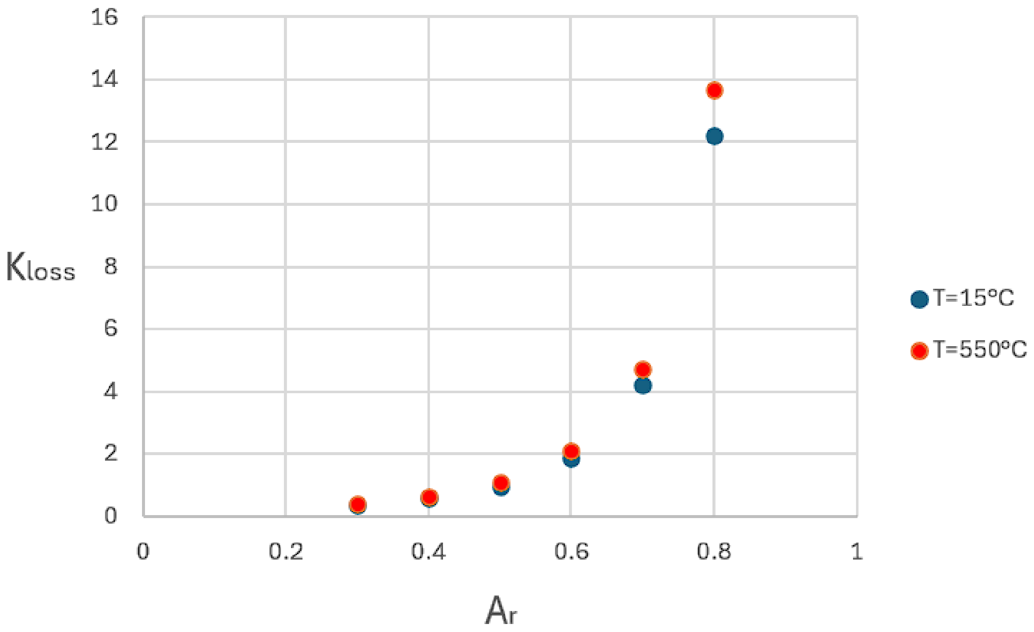

Figure 7.3: K_{loss} coefficient at intake and exhaust conditions

Table 7.1: Percentage error between the K_{loss} coefficient calculated at intake and exhaust conditions

A_r	Percentage deviation [%]
0.3	13.85%
0.4	13.87%
0.5	13.58%
0.6	12.91%
0.7	12.29%
0.8	11.81%

It turns out that the percentage error is not negligible but is constant as A_r varies. Indeed, the analysis shows that the K_{loss} coefficient for exhaust ducts is larger if compared to intake ducts one by approximately the 13%. This effect is related to lower Reynolds number and an increased value of friction losses due to a more viscous flow regime. Further investigation on this aspect is required to understand if a corrective factor is sufficient to account for this difference.

7.2 Conclusions

This thesis aimed to develop pressure drop predictive mathematical models for gas turbine intake fittings to evaluate the total pressure drop of gas turbine intake arrangements. This was achieved through many parametric CFD analysis that were performed to understand how the pressure drop of each fitting is influenced by their design parameters. All the predictive models developed were implemented in an Excel tool to compare the analytical results obtained and the experimental results acquired on a software tool used for real time monitoring of running gas turbines.

The tool had to satisfy three different goals, such as giving an accurate pressure drop prediction, reducing the computational effort by eliminating time-consuming CFD simulation from the daily work and specify how different components interact with each other and how they contribute on the overall pressure drop. The findings of this research demonstrated that high accuracy prediction with a percentage error well below the 10% can be accomplished by using the predictive tool. The pressure drop assessment only needs some minutes and no CAD models, meshing software or CFD analysis are no longer required. Moreover, while using the tool, both the different component contributions and their interaction are described.

However, this study is not without limitations. Indeed, the number of inspected fittings is limited since parametric studies require a lot of time to be performed, therefore, only standard gas turbine intake ducts can be simulated using it. Additionally, the model validation has been performed only on a small number of arrangements, and it could be useful to further validate the developed formulations. Future research should therefore aim to extend the domain of arrangements covered by the tool and even further validate the accuracy of the results.

As explained even in this research, the workflow used is easily extendable to exhaust ducts. Specifically, it would be sufficient to define a function that describes how the temperature varies along the exhaust ducts and verify that the Reynolds number does not drop significantly. If these assumptions are verified, the work detailed in this research would be directly applicable to hot ducts.

In conclusion, this thesis provides a procedure to develop a user-friendly pressure drop predictive tool and all the mathematical models on which it relies. The tool demonstrated that high accuracy and fast prediction can be provided by substituting CFD simulations during the first design phases of gas turbine intake arrangements.

Bibliography

[1] Meherwan P. Boyce. *Gas Turbine Engineering Handbook*, volume 3. Elsevier, Gulf Professional Publishing, 2006.

[2] I. E. Idelchik. *Handbook of Hydraulic Resistance*, volume 3. Gulf Professional Publishing, 1996.

[3] Donald S. Miller. *Internal Flow Systems*, volume 3. BHRA Fluid Engineering, 1978.

[4] Fluent Inc. *ANSYS Fluent User's Guide*, volume 6.1. Fluent Inc, 2003.

[5] Herman F. Behl. *ASHRAE Fundamentals Handbook, chapter 34*, volume 1. ASHRAE, 2001.

[6] D. Bogdanovic. Calculation methods for predicting attenuation of parallel baffle type silencers. Master's thesis, Chalmers University of Technology, Göteborg, Sweden, 2014.